

**EFFICIENCY OF TANDEM
BREAKWATER IN REDUCING WAVE
HEIGHTS AND DAMAGE LEVEL: A
MOSSEL BAY CASE STUDY**

by
Eldré Thesnaar



*Thesis presented in fulfilment of the requirements for the degree of
Master of Engineering (Research) in the Faculty of Engineering at
Stellenbosch University*

Supervisor: Mr Geoff Toms

March 2015

DECLARATION

By submitting this thesis electronically, I declare that the entirety of the work contained therein is my own, original work, that I am the sole author thereof (save to the extent explicitly otherwise stated), that reproduction and publication thereof by Stellenbosch University will not infringe on any third party rights and that I have not previously in its entirety or in part submitted it for obtaining any qualification.

Date:.....

ABSTRACT

In recent years, breakwater design has been governed not only by structural stability, but by cost effectiveness as well. Breakwater designers are constantly trying to find the perfect balance between low-risk design and low-cost design.

The combination of a main rubble mound breakwater and a submerged offshore reef, that are designed to function together, is known as a tandem breakwater. The reef structure is responsible for dissipating some of the energy by causing wave breaking. Thereafter, the area between the reef and the main structure - the tranquillity zone - allows for natural energy dissipation. The combination of the effects of the reef and tranquillity zone results in reduced significant wave heights at the main rubble mound structure, which allows it to be designed with lighter armour units.

This study investigates the application of a tandem breakwater, based on the conditions at the port of Mossel Bay, by achieving the following set of objectives: (1) to determine the influence of the tandem breakwater's submerged reef crest elevation on the damage level of the main rubble mound structure, (2) to determine the relationship between the relative wave attenuation distance and the percentage wave attenuation, and (3) to compare the abovementioned parameters for rock and geotube reefs.

A physical model test series was conducted to gain the data required for achieving the objectives. A rubble mound structure that makes use of dolos armour units, resembling the one at Mossel Bay, was constructed inside a concrete flume equipped with a single-paddle wavemaker. Two reef structure types (rock and geotube) were tested at three crest elevations (below-LAT, LAT and ML), against combinations of two significant wave heights (2.5 m and 3 m) and two peak periods (8 s and 12 s), at one water level (ML) and one offshore reef distance (50 m).

From the model test results, it is evident that the presence of a reef structure significantly affects the wave conditions that reach the main structure. When comparing significant wave heights measured at a prototype distance of 20 m in front of the main breakwater, a reduction of as high as 42% can be observed for a reef structure made from rocks and 54% for a geotube structure. In all cases, the geotube structure causes more wave attenuation due to its lower permeability, which enables it to reflect more wave energy. However, it should be noted that the stability of the geotube reef was not considered during testing.

Generic graphs are presented, that aim to provide guidance in the design process of such a tandem breakwater system. The graphs are produced for a case where dolos armour units are used and might not be exactly the same when a different type of armour unit is used. One graph shows the relationship between the damage reduction at the main breakwater and the relative reef submergence. The other shows the relationship between wave attenuation and the relative wave attenuation distance.

Unfortunately, the implementation of geotube reefs of the nature described in this investigation is not likely in the South African context at present. This, however, does not eliminate the possibility of future applications. As geotextile technology develops and greater operational experience and equipment is gained, tandem breakwaters that incorporate geotube reefs could provide an alternative that is both cost-effective and more environmentally friendly with regards to transport emissions. Until then, tandem breakwaters that incorporate rock reefs may be able to provide a desired alternative design for certain scenarios.

OPSOMMING

In die afgelope jare, word breekwater ontwerp nie net beheer deur strukturele stabiliteit nie, maar ook koste effektiwiteit. Ontwerpers poog alewig om die perfekte balans tussen lae-risiko ontwerp en lae-koste ontwerp na te streef.

Die kombinasie van 'n hoof ruklipgolfbreker en 'n sekondêre onderwater rif breekwater, wat ontwerp is om as 'n eenheid te funksioneer, staan bekend as 'n tandem breekwater. Die rif struktuur is verantwoordelik vir die verlies van 'n gedeelte van die golf energie deur golf breking te veroorsaak. Daarna veroorsaak die area tussen die rif en die hoof struktuur – die kalmeringsone – verdere natuurlike energie verlies. Die gekombineerde effek van die rif en kalmeringsone veroorsaak dat kleiner branders die hoof breekwater bereik, wat toelaat dat dit ontwerp kan word met kleiner pantser eenhede.

Dié studie ondersoek die toepassing van 'n tandem breekwater, gebaseer op die kondisies by die Mosselbaai hawe, deur die volgende doelwitte te bewerkstellig: (1) om die invloed van die onderwater rif kruinhoogte op die vlak van skade aan die hoof breekwater te bepaal, (2) om die verhouding tussen die relatiewe golfhoogte-verminderings-afstand en die golfhoogte vermindering te bepaal, en (3) om die bogenoemde parameters vir rots en geo-buis riwwe te vergelyk.

'n Fisiese model toets reeks is uitgevoer sodat die benodigde data ingesamel kan word om die doelwitte te bereik. 'n Rotsvul breekwater wat gebruik maak van dolos pantser eenhede, soortgelyk aan dié by Mosselbaai, is gebou in 'n beton kanaal wat toegerus is met 'n enkel-spaan golfmasjien. Twee tipes riwwe (rots en geo-buis) is getoets met drie kruin hoogtes (onder-LAG, LAG en GV), teen kombinasies van twee beduidende golfhoogtes (2.5 m en 3 m) en twee spitsperiodes (8 s en 12 s), by een watervlak (GV) en een sekondêre breekwater afstand (50 m).

Uit die model toets resultate is dit duidelik dat die teenwoordigheid van 'n rif struktuur, die golfkondisies wat die hoof breekwater bereik, beduidend beïnvloed. Wanneer beduidende golfhoogtes, gemeet op 'n prototipe afstand van 20 m voor die hoof breekwater, vergelyk word, word 'n vermindering van so hoog as 42% waargeneem vir 'n rif bestaande uit rots en 54% vir 'n rif bestaande uit geo-buise. In alle gevalle veroorsaak die geo-buis struktuur meer golfhoogte vermindering, as gevolg van sy laer deurlaatbaarheid, wat dit in staat stel om meer golfenergie te reflekteer. Die stabiliteit van die geo-buis struktuur is egter nie in ag geneem tydens die toetse nie.

Generiese grafieke word weergegee, met die doel om leiding te gee tydens die ontwerpsproses van só 'n tandem breekwater struktuur. Die grafieke hou verband met die geval waar dolos pantser eenhede gebruik word, en mag verskil vir ander tipes pantser eenhede. Een van die grafieke dui die verhouding tussen skadevermindering aan die hoof breekwater en die relatiewe posisie van die onderwater rif se kruinhoogte aan. Die ander grafiek dui die verhouding tussen die golfhoogte vermindering en die relatiewe golfhoogte-verminderings-afstand aan.

Huidiglik is die toepassing van die tipe geo-buis riwwe soos beskryf in hierdie ondersoek, ongelukkig onwaarskynlik in die Suid-Afrikaanse konteks. Dit skakel egter nie die moontlikheid van toekomstige toepassings van dié aard uit nie. Soos geo-tekstiel tegnologie ontwikkel en meer operasionele ervaring en toerusting bekom word, kan die effektiewe implementasie van geo-buis riwwe 'n alternatief bied wat beide koste effektief en omgewingsvriendelik is met betrekking tot die vrystelling van uitlaatgasse tydens die vervoer van materiale. Tot dan, kan tandem breekwaters wat van rots riwwe gebruik maak, moontlik die gewenste alternatiewe ontwerp bied vir sekere situasies.

ACKNOWLEDGEMENTS

The author wishes to express his gratitude towards the following persons that played an important role during the course of the project:

Mr G Toms: for his supervision and guidance throughout the project.

Mr K Tulsi (CSIR): for allowing the use of the modelling facility at the CSIR, as well as providing recommendations regarding the physical model set-up.

Mr J Kieviet (CSIR): for his willingness to assist, answer questions and share ideas regarding the project.

Mr M Rossouw and Mrs U von Saint Ange (CSIR): for providing wave- and bathymetric data regarding Mossel Bay.

Mr G Davids, Mr W Prins, Mr R Jappie and Mr R Solomons (CSIR): for their assistance during the construction and set-up of the physical model.

Mr K Jankowitz and Ms Z Goba (TNPA): for providing various sets of information contributing to a greater insight into the workings of the port of Mossel Bay, as well as the opportunity to visit the port and view the breakwater.

Mr F Theron (Murray & Roberts): for the opportunity to meet and discuss certain practical aspects of breakwater and reef construction.

Mr D Hall and Mr T Milner (Stefanutti Stocks Marine): for providing detailed information about breakwater and reef construction with specific emphasis on the related costs.

Danish Hydraulics Institute (DHI Group): for providing the MIKE 21 software used in this study to the University of Stellenbosch, free of charge.

Mr P Roux, Mr C Muller and Ms L Eigelaar: for sharing ideas regarding the project, as well as providing assistance whenever needed.

TABLE OF CONTENTS

Declaration	i
Abstract	ii
Opsomming	iii
Acknowledgements	iv
Table of Contents	v
List of Figures	vii
List of Tables.....	x
Nomenclature	xi
Chapter 1: Introduction	1
1.1 Background	1
1.2 Objectives.....	2
1.3 Brief Chapter Overview	2
Chapter 2: Literature Review	4
2.1 General	4
2.2 History of Modern Breakwater Structures	4
2.3 Development of the Tandem Breakwater.....	6
2.4 Breakwater Repair Methods.....	7
2.5 Wave Transmission Over Submerged Structures.....	11
2.6 Geotextiles.....	14
2.7 Case Studies	18
2.7.1 Narrowneck Reef.....	18
2.7.2 Boscombe Reef.....	21
2.7.3 Cable Station Reef.....	22
2.7.4 Hammond Tandem Breakwater.....	23
Chapter 3: Methodology.....	26
3.1 General	26
3.2 Study Approach.....	26
3.3 Port of Mossel Bay	27
Chapter 4: Numerical Wave Modelling	30
4.1 General	30
4.2 Model Selection.....	30
4.3 Model Set-up	32
4.3.1 Bathymetry	32
4.3.2 Model Inputs.....	34
4.3.3 Model Outputs.....	35
4.3.4 Model Runs	36
4.4 Summary	46
Chapter 5: Physical Modelling.....	47

5.1 General	47
5.2 Model Facility and Equipment	47
5.2.1 2D Concrete Flume	47
5.2.2 WaveMaker	48
5.2.3 Wave Measurement System	48
5.2.4 Camera.....	49
5.3 Rubble Mound Breakwater.....	50
5.3.1 Bathymetry	50
5.3.2 Design Wave Height	51
5.3.3 Armour Unit Selection and Size.....	56
5.3.4 Model Scaling.....	57
5.3.5 Material Selection and Grading.....	60
5.3.6 Breakwater Dimensions	60
5.3.7 Construction	62
5.4 Reef Breakwater.....	63
5.4.1 Rock Reef Structure	63
5.4.2 Geotube Reef Structure	65
5.5 Test Series	67
5.5.1 Test Schedule	67
5.5.2 Wave Calibration.....	68
5.5.3 Rock Reef Crest Reduction	68
5.5.4 Breakwater Damage Results.....	70
5.5.5 Wave Attenuation Results	73
5.6 Application of Results	79
5.6.1 Reduction of Design Wave Height.....	79
5.6.2 Reduction of Armour Unit Size.....	81
5.6.3 Cost of Construction.....	81
5.7 Summary	84
Chapter 6: Findings, Conclusions and Recommendations	85
6.1 Physical Model Findings	85
6.2 Conclusions	86
6.3 Recommendations on Future Work.....	86
Bibliography	87
Appendices	I
Appendix A: Procedure for Determining Mass Density of Model Armour Units	II
Appendix B: Rock Grading Curves.....	V
Appendix C: Physical Model Construction.....	VII
Appendix D: Damage Analysis Images	X

LIST OF FIGURES

Figure 2.1: Breakwater at Cherbourg (Constable, 1824)	4
Figure 2.2: Evolution of Breakwater Structures (Tanimoto & Goda, 1992)	5
Figure 2.3: Typical Berm Breakwater and Equilibrium Profile (Juhl, 1995)	6
Figure 2.4: Evolution of Tandem Breakwater (Cox & Clark, 1992).....	7
Figure 2.5: Rubble Mound Breakwater Failure Modes - Adapted from BSI (2003)	8
Figure 2.6: Breakwater Rehabilitation Method 1 (Mol et al., 1984)	10
Figure 2.7: Breakwater Rehabilitation Method 2 (Mol et al., 1984)	10
Figure 2.8: Breakwater Rehabilitation Method 3 (Mol et al., 1984)	11
Figure 2.9: Breakwater Rehabilitation Method 4 (Mol et al., 1984)	11
Figure 2.10: Parameters Influencing Wave Transmission Coefficient (van der Meer et al., 2005)	12
Figure 2.11: Comparison Between Measured and Predicted Transmission Coefficient (Tomasicchio & d'Alessandro, 2013)	14
Figure 2.12: Continuous Geotube Folding Method (van Zijl et al., 2006).....	16
Figure 2.13: Displacements of Geocontainers Relative to Barge (Bezuijen et al., 2004)	17
Figure 2.14: Standard Deviation of Relative Displacement of Geocontainers (Bezuijen et al., 2004) .	17
Figure 2.15: Location of Narrowneck Reef (Google Inc., 2014)	19
Figure 2.16: Aerial View of Narrowneck Reef (Jackson & Hornsey, 2003)	20
Figure 2.17: Placement Accuracy of 150 mm (Jackson & Hornsey, 2003)	21
Figure 2.18: Location of Boscombe Artificial Reef (Google Inc., 2014).....	21
Figure 2.19: Aerial View of Boscombe Reef (Rendle & Davidson, 2012).....	22
Figure 2.20: Location of Cable Station Artificial Reef (Google Inc., 2014).....	23
Figure 2.21: Plan View of Cable Station Reef (Johnson, 2009)	23
Figure 2.22: Location of Hammond Tandem Breakwater (Google Inc., 2014)	24
Figure 2.23: Tandem Breakwater at Hammond Marina (Cox & Clark, 1992).....	24
Figure 2.24: Aerial View of Hammond's Tandem Breakwater (Google Inc., 2014).....	25
Figure 3.1: Location of Port of Mossel Bay (Google Inc., 2014).....	28
Figure 3.2: Layout of the Port of Mossel Bay – Adapted From TNPA (2014a)	28
Figure 3.3: Water Depths Around Mossel Bay Breakwater Relative to CD - Adapted From TNPA (2014b)	29
Figure 3.4: View Along Mossel Bay Breakwater (Looking South-East).....	29
Figure 3.5: Damaged Portions of the Overtopping Wall at Various Points Along the Breakwater	29
Figure 4.1: Scatter Data Plot of Mossel Bay	32
Figure 4.2: Mossel Bay Mesh.....	33
Figure 4.3: Numerical Model Bathymetry	33
Figure 4.4: Numerical Model Boundary Layers.....	34
Figure 4.5: Position of Breakwater Output Point in Numerical Model.....	35
Figure 4.6: Position of Breakwater Output Point Relative to Breakwater (Google Inc., 2014)	36
Figure 4.7: Overview of Wave Height and Period Distribution Around South African Coast as Predicted with NCEP Model (Rossouw & Theron, 2009)	37
Figure 4.8: Significant Wave Heights Around Mossel Bay (4m 8s SSW).....	39
Figure 4.9: Significant Wave Heights Inside Mossel Bay (4m 12s SSW)	39
Figure 4.10: Significant Wave Heights Around Mossel Bay (6m 8s SSW).....	40
Figure 4.11: Significant Wave Heights Inside Mossel Bay (6m 12s SSW)	40
Figure 4.12: Significant Wave Heights Around Mossel Bay (8m 8s SSW).....	41
Figure 4.13: Significant Wave Heights Inside Mossel Bay (8m 12s SSW)	41
Figure 4.14: Significant Wave Heights Around Mossel Bay (4m 8s e)	42
Figure 4.15: Significant Wave Heights Inside Mossel Bay (4m 12s E).....	42
Figure 4.16: Significant Wave Heights Around Mossel Bay (6m 8s E)	43
Figure 4.17: Significant Wave Heights Inside Mossel Bay (6m 12s E).....	43
Figure 4.18: Significant Wave Heights Around Mossel Bay (8m 8s E)	44
Figure 4.19: Significant Wave Heights Inside Mossel Bay (8m 12s E).....	44
Figure 4.20: Comparison of Significant Wave Heights of 8s Wave	45

Figure 4.21: Comparison of Significant Wave Heights of 12s Wave	45
Figure 5.1: 2D Concrete Flume	47
Figure 5.2: Single-paddle Wavemaker (left) and Control Room (Right)	48
Figure 5.3: Capacitance Probe Array	48
Figure 5.4: Waterproof GoPro® Camera Casing	49
Figure 5.5: Existing Slope in Concrete Flume (Drawing Not To Scale, Model Dimensions Given)....	50
Figure 5.6: Mossel Bay Waverider Data (May 2009 - April 2010) (CSIR, 2014)	51
Figure 5.7: Position of CSIR Waverider Inside Mossel Bay (Google Inc., 2014)	51
Figure 5.8: Shallow Water Significant Wave Heights on Uniform Sloping Foreshore (CIRIA CUR CETMEF, 2007)	53
Figure 5.9: Extreme Value Analysis	55
Figure 5.10: Dolos Unit Used in the Model	59
Figure 5.11: Mossel Bay Breakwater Section from 1967 (TNPA, 1967)	61
Figure 5.12: Cross-section of Model Rubble Mound Breakwater (Dimensions in Metres Prototype). 62	
Figure 5.13: Long Section Through Concrete Flume - No Reef Structure (Drawing Not To Scale, Model Dimensions Given)	62
Figure 5.14: Completed Main Rubble Mound Breakwater in Flume	63
Figure 5.15: Cross-section of Model Rock Reef Breakwater (Dimensions in Metres Prototype)	64
Figure 5.16: Long-section Through Concrete Flume - Rock Reef Structure (Drawing Not To Scale, Model Dimensions Given)	65
Figure 5.17: Formwork Used While Filling Model Geotubes.....	65
Figure 5.18: Cross-section of Model Geotube Reef Breakwater (Dimensions in Metres Prototype) ...	66
Figure 5.19: Construction of Geotube Reef Breakwater	66
Figure 5.20: Long-section Through Concrete Flume - Geotube Reef Structure (Drawing Not To Scale, Model Dimensions Given)	66
Figure 5.21: Initial and Equilibrium Profile of Rock Reef.....	69
Figure 5.22: Before (Left) and After (Right) Images of Armour Layer Showing Extracted Units.....	70
Figure 5.23: Before (Left) and After (Right) Images Used in the Damage Analysis.....	71
Figure 5.24: Effect of Relative Reef Submergence on Damage Reduction	73
Figure 5.25: Effect of Relative Wave Attenuation Distance on Wave Height Attenuation	76
Figure 5.26: Comparison of Present and Previous Studies with regards to Wave Attenuation (Cox & Clark, 1992; Roa & Shirlal, 2003)	77
Figure 5.27: Measured vs Predicted Transmission Coefficients	78
Figure A.1: Water Container Filled Up To 1000ml	II
Figure A.2: Dolos Unit Placed Inside Container With Initial Water Level Mark	II
Figure A.3: Filling of Container Up To Second Water Level Mark	III
Figure A.4: Measuring the Mass of Dolos Unit	IV
Figure B.1: Core Layer Rock Grading Curve	V
Figure B.2: Under Layer Rock Grading Curve	V
Figure B.3: Toe Layer Rock Grading Curve	VI
Figure B.4: Submerged Rock Reef Grading Curve.....	VI
Figure C.1: Cutting of Breakwater Templates (Left) and Core Construction (Right).....	VII
Figure C.2: Spraypainted Under Layer Before (Left) and After (Right) Installation.....	VII
Figure C.3: Spraypainted Armour Layer.....	VIII
Figure C.4: Overtopping Wall Attached to Angle Iron	VIII
Figure C.5: Submerged Reef Cross-section Profiles (left) and Construction (Right)	IX
Figure D.1: Before (Left) and After (Right) Images of Test TS01_1	X
Figure D.2: Before (Left) and After (Right) Images of Test TS01_2	X
Figure D.3: Before (Left) and After (Right) Images of Test TS02_1	X
Figure D.4: Before (Left) and After (Right) Images of Test TS02_2	XI
Figure D.5: Before (Left) and After (Right) Images of Test TS03_1	XI
Figure D.6: Before (Left) and After (Right) Images of Test TS03_2	XI

Figure D.7: Before (Left) and After (Right) Images of Test TS04_1	XII
Figure D.8: Before (Left) and After (Right) Images of Test TS04_2	XII
Figure D.9: Before (Left) and After (Right) Images of Test TS05_1	XII
Figure D.10: Before (Left) and After (Right) Images of Test TS05_2	XIII
Figure D.11: Before (Left) and After (Right) Images of Test TS06_1	XIII
Figure D.12: Before (Left) and After (Right) Images of Test TS06_2	XIII
Figure D.13: Before (Left) and After (Right) Images of Test TS07_1	XIV
Figure D.14: Before (Left) and After (Right) Images of Test TS07_2	XIV
Figure D.15: Before (Left) and After (Right) Images of Test TS08_1	XIV
Figure D.16: Before (Left) and After (Right) Images of Test TS08_2	XV
Figure D.17: Before (Left) and After (Right) Images of Test TS09_1	XV
Figure D.18: Before (Left) and After (Right) Images of Test TS09_2	XV
Figure D.19: Before (Left) and After (Right) Images of Test TS10_1	XVI
Figure D.20: Before (Left) and After (Right) Images of Test TS10_2	XVI
Figure D.21: Before (Left) and After (Right) Images of Test TS11_1	XVI
Figure D.22: Before (Left) and After (Right) Images of Test TS11_2	XVII

LIST OF TABLES

Table 2.1: Classification of Armour Layer Damage (Mol et al., 1984)	9
Table 4.1: Numerical Model Wave Runs	38
Table 5.1: Maximum Depth-limited Significant Wave Height at Toe of Structure	54
Table 5.2: Calculated Armour Unit Mass Using Burcharth & Liu Equation	57
Table 5.3: Similitude Ratios for Froude Similarity (Hughes, 1995)	59
Table 5.4: M_{50} , NLL and NUL for Each Breakwater Layer.....	60
Table 5.5: Mossel Bay Tidal Information (in metres) (SANHO, 2013).....	61
Table 5.6: Test Schedule	67
Table 5.7: Incident Significant Wave Heights of Calibrated Waves.....	68
Table 5.8: Rock Reef Crest Reduction and Effective Crest Elevation	69
Table 5.9: Damage Encountered in Test Series (As Built Crest Elevation for Rock Reefs Shown Between Brackets).....	72
Table 5.10: Repeatability of Damage Tests	72
Table 5.11: Wave Attenuation in Test Series (As Built Crest Elevation for Rock Reefs Shown Between Brackets).....	74
Table 5.12: Repeatability of Wave Attenuation Tests.....	75
Table 5.13: Measured vs Predicted Transmission Coeffocoents (As Built Crest Elevation for Rock Reefs Shown Between Brackets)	78
Table 5.14: Reduced Design Hs for Rock Reef	80
Table 5.15: Reduced Design Hs for Geotube Reef	80
Table 5.16: Total Cost of Single Rubble Mound Breakwater (Stefanutti Stocks Marine, 2015).....	82
Table 5.17: Cost per 5.64 Ton Dolos Unit (Stefanutti Stocks Marine, 2015).....	82
Table 5.18: Cost of Tandem Breakwater System (Stefanutti Stocks Marine, 2015).....	82
Table 5.19: Cost of Reef per Cubic Metre (Stefanutti Stocks Marine, 2015)	83
Table A.1: Delta Volume Measurements	III

NOMENCLATURE

AMS	Annual Maximum Series
B	Berm/Crest width
B_{eff}	Effective crest width
CD	Chart Datum
CSIR	Council for Scientific and Industrial Research
D	Damage number
d_c	Depth of crest submergence
D_{eff}	Nominal stone diameter
DGPS	Differential Global Positioning System
DHI	Danish Hydraulics Institute
D_n	Nominal diameter of armour unit
D_{n50}	Nominal diameter of rock
DWA	Dynamic Wave Absorption
EVA	Extreme Value Analysis
g	Gravitational acceleration (9.81 m/s^2)
h	Water depth
h_c	Height of structure (distance from seabed to crest)
HAT	Highest Astronomical Tide
H_i	Incident significant wave height
H_{max}	Maximum wave height
H_{m0}	Significant spectral wave height
H_s	Significant wave height
H_{s0}	Deep water significant wave height
H_t	Transmitted significant wave height
JONSWAP	JOint North Sea WAve Project
K_h	Contribution of waves passing through structure to energy of transmitted waves
K_t	Transmission coefficient
$(K_t)_{\text{all}}$	Transmission coefficient for energy through and over structure

$(K_t)_{over}$	Transmission coefficient for energy over structure
$(K_t)_{thru}$	Transmission coefficient for energy through structure
L	Length/Wavelength
LAT	Lowest Astronomical Tide
LWOST	Low Water of Ordinary Spring Tide
L_0	Deep water wave length
M	Armour unit mass
m	Front slope of structure
MHWN	Mean High Water Neaps
MHWS	Mean High Water Springs
ML	Mean Level
MLWN	Mean Low Water Neaps
MLWS	Mean Low Water Springs
MWD	Mean Wave Direction
M_{50}	Median armour unit mass
N	Action density function
NLL	Nominal lower limit
NUL	Nominal upper limit
N_x	Scale ratio
N_z	Number of waves
P	Wave measurement probe (e.g. P5 represents probe number 5)
PDS	Partial Duration Series
r	Dolos waist ratio
R_c	Freeboard
$R_{c,o}$	Limit of non-dimensional run-up
Rec	Berm recession
RRS	Relative reef submergence
S	Source term for energy balance equation
s	Wave steepness

SANHO	South African Navy Hydrographic Office
S_{bot}	Dissipation due to bottom friction
S_{ds}	Dissipation of wave energy due to white-capping
S_{in}	Momentum transfer of wind energy to wave generation
S_{nl}	Energy transfer due to non-linear wave-wave interaction
S_{surf}	Dissipation due to depth-induced breaking
SWAN	Simulating WAVes Nearshore
SWL	Still Water Level
t	Time
T_m	Mean period
TNPA	Transnet National Ports Authority
T_p	Peak period
V	Velocity
\bar{v}	Propagation velocity of wave group in 4D space
WAD	Relative wave attenuation distance
X	Distance between breakwaters
\bar{x}	Cartesian coordinates
α	Slope angle
ξ_m	Iribarren number
θ	Direction of wave propagation
ρ	Mass or fluid density
ρ_a	Mass density of armour unit
ρ_w	Mass density of water
σ	Relative angular frequency ($2\pi f$)
$\varphi_{n=2}$	Packing density of double armour layer
∇	4D differential operator

CHAPTER 1: INTRODUCTION

1.1 BACKGROUND

During the design stages of a breakwater there are several factors that have to be considered, one of which is the design storm condition. The severity of the design storm is usually chosen by studying the history of storm patterns in the waters surrounding the proposed breakwater location, and then taking a calculated risk.

When selecting a storm condition, the more severe it is, the bigger the rock and armour units have to be, resulting in a higher cost, but also less risk of breakwater failure. On the other hand, if a less severe storm condition is used as design storm, the cost will be lower due to the smaller rock and armour units required, but then the chance of breakwater failure is higher, and thus more risk.

In the event that a bigger-than-design storm occurs, the breakwater may be damaged. The severity of the damage will depend on how much bigger the storm is in relation to the design storm condition. The restoration of a damaged breakwater is often a costly and time consuming activity.

A breakwater which has been partly damaged by a previous bigger-than-design storm has weak spots that can easily be damaged further. Therefore, the period immediately after breakwater damage occurs is very critical. In this period the cost of restoring the breakwater can accumulate at a rapid pace if the necessary measures to prevent further damage are not undertaken quickly. However, to perform such an emergency breakwater repair with short notice, is challenging and not to mention, costly.

It is obviously desirable that all damage at the breakwater be prevented. Unfortunately, this is not always possible without a great increase in expenditure towards the breakwater. Therefore, it is sometimes opted to prevent additional damage rather than prevent all damage.

Preventing all damage relies on having a fundamental breakwater design that is able to withstand the extreme wave conditions, while preventing additional damage makes use of temporary solutions to increase the durability of the structure for a limited period. For both cases there exist various techniques which can be applied.

One strategy is to simply increase the size of the armour rock or units. Bigger sizes of the individual units that make up the armour layer result in a breakwater that can withstand more severe conditions. For a breakwater consisting of an armour layer made of rock, it quickly becomes difficult to find sufficiently large rocks. If rock quarries are not located close to the construction site, the transportation cost also has to be taken into account. Thus, concrete armour units are normally preferred. These units can be cast at the site or at another nearby site. If need be, the density of the concrete that is used for the units can be increased to increase the unit's mass or produce a smaller equivalent unit. All the while, the costs associated with these solutions should be considered.

Knowing that it is the interaction between the wave energy and the primary armour layer of the breakwater that mainly determines the extent of the damage (if any) that is caused to the breakwater, it is possible to find an additional solution. This entails finding a way to reduce the size of the waves reaching the breakwater. Detached breakwaters are often used to reduce the size of waves reaching an exposed shoreline and provide erosion protection. These detached breakwaters are normally submerged structures, although in some cases they may also be low-crested, i.e. stick out just above the waterline. A similar approach may be applied to the design of a rubble mound breakwater.

The combination of a main rubble mound breakwater and a submerged offshore reef that are designed to function together is known as a tandem breakwater. A wave that becomes too steep when passing over the reef will break and some of the total energy will be lost. The area between the reef and the main structure - the tranquillity zone - allows for natural energy dissipation. Thus, this tandem breakwater system results in smaller waves reaching the main structure, which means that it may be designed with smaller armour units. Based on a limited study, this design is said to provide a least cost solution for some applications (Cox & Clark, 1992).

Further investigation into this subject may prove useful for future applications of such a system as either a temporary or permanent solution. Conventionally, these reef structures are constructed from rock. However, the success of geotextile applications in the coastal environment in recent years could possibly be extended further by using it as part of a tandem structure. Sand-filled geotextile bags are especially useful in areas where rock material is limited. Also, using geotextile material has the advantage of being more environmentally friendly with regards to transport emissions.

1.2 OBJECTIVES

This study aims to provide further insight into the use of tandem breakwaters as temporary or permanent alternative to conventional rubble mound breakwaters. The investigation is focused primarily on the application of a tandem breakwater system at the port of Mossel Bay, which makes use of dolos armour units, but it is also intended to be more general, so that its findings can be relevant to other potential tandem breakwater applications. The specific objectives are as follows:

- To determine the influence of the tandem breakwater's submerged reef crest elevation on the damage level of the main rubble mound structure
- To determine the relationship between the relative wave attenuation distance (a non-dimensional parameter which is related to the tranquillity zone length, the peak period of the incident waves, and the depth of crest submergence) and the percentage wave attenuation
- To compare the abovementioned parameters for rock and geotube reefs

The provision of comprehensive design guidelines lies outside the scope of this study. However, some generic, non-dimensional relationships are provided to aid in future designs.

1.3 BRIEF CHAPTER OVERVIEW

This report consists of a total of six chapters. In the next chapter, Chapter 2, a review of current literature is provided for relevant subjects. The topics of the literature review include the history of modern breakwaters, the development of the tandem breakwater, breakwater repair methods, wave transmission over submerged structures, and geotextiles. A number of case studies are also considered.

A description of the methodological approach is given in chapter 3. This includes the rationale behind the selection of the model types, as well as a description of the site conditions for the case study under consideration.

Chapter 4 provides information on the numerical wave modelling that was done to determine the depth-limited significant wave height at the toe of the Mossel Bay breakwater for various deep water wave conditions.

In chapter 5, the physical modelling process is discussed in detail. It starts off with a description of the test facility, then moves on to the design and construction of the model, before discussing the test

schedule and results. The chapter concludes with a discussion on how to apply the findings in future projects, with the use of some examples.

The final chapter is dedicated to a discussion of the results of the physical model. Recommendations regarding future work on the subject are also made.

CHAPTER 2: LITERATURE REVIEW

2.1 GENERAL

This section aims to bring greater insight to subjects that are relevant to the investigation. The first discussion is on the history of breakwaters of the modern era. This includes information of the first breakwater and how it evolved into the various types of breakwater designs that are found today. Thereafter, the concept of a tandem breakwater system is described. Various breakwater repair methods that apply specifically to rubble mound structures are mentioned. Thereafter, the transmission of waves over submerged structures is discussed. Then, geotextiles and its applications in coastal engineering are discussed, before considering a number of relevant case studies.

2.2 HISTORY OF MODERN BREAKWATER STRUCTURES

Ancient ports of the world have been traced back to the ages of Egypt and Mycenae, and it is believed that the first port in the world was built in Egypt (Tanimoto & Goda, 1992). However, the breakwater of Cherbourg in France is considered to be the first modern breakwater. It started out as little more than a pile of rocks to provide sheltered waters behind it. The construction of this structure was completed just before the end of the 18th century (Constable, 1824).

In 1830, construction started to improve the breakwater structure at Cherbourg. A concrete topping was added on top of the rubble and a superstructure made from masonry was constructed upon it. This undertaking was finally completed in 1853 (Vernon-Harcourt, 1885). An illustration of the layout of the breakwater at Cherbourg is shown in figure 2.1.

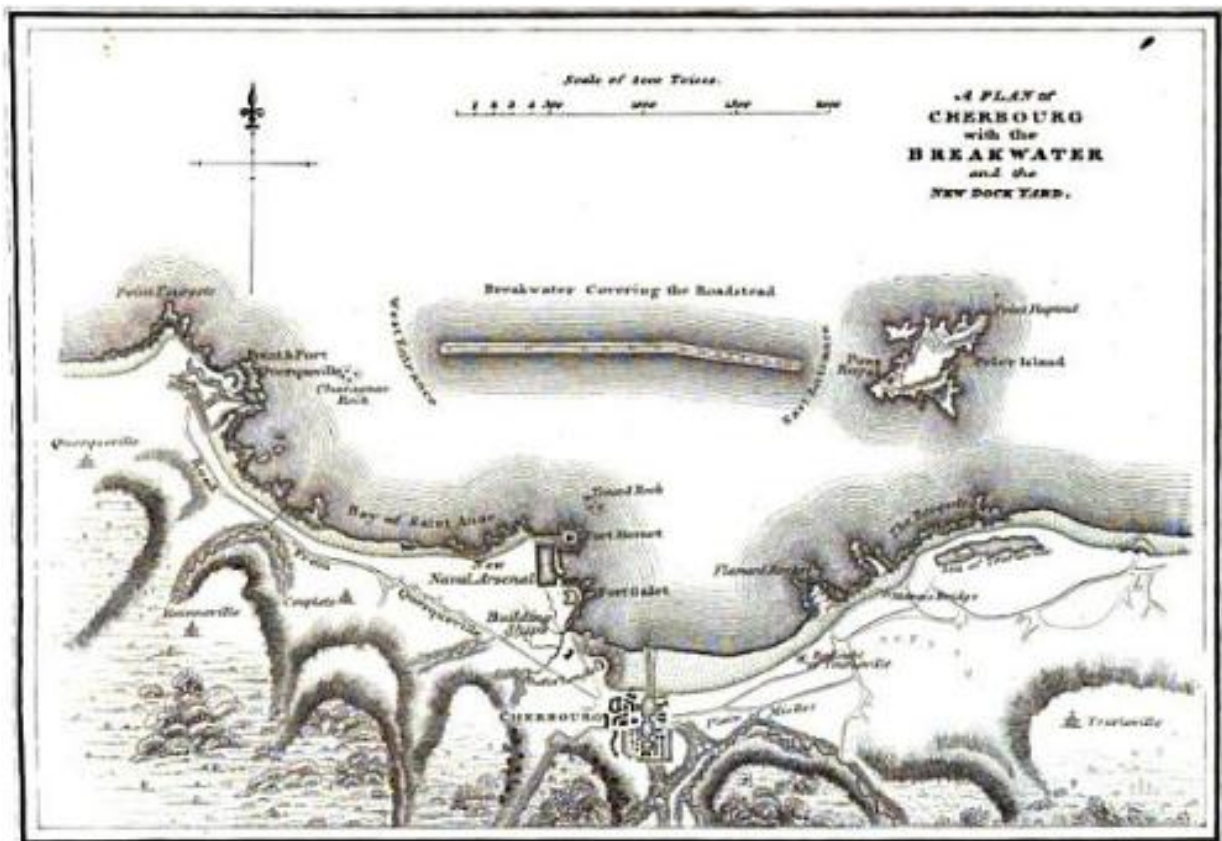


FIGURE 2.1: BREAKWATER AT CHERBOURG (CONSTABLE, 1824)

As time passed and experience on wave-structure interaction was gained, the appearance of breakwater structures has undergone natural changes. These changes can be ascribed to the development of structure stability against wave action or the strive towards producing cost effective solutions in recent years (Roa & Shirlal, 2003).

Figure 2.2 shows the evolution of modern breakwater structures. In it can be seen that there were various paths of development. The primitive structures that were constructed solely out of rock can be seen to develop into structures with concrete armour layers and even into caisson structures that consist of an outer shell made of concrete and filled with rock or sand material (Tanimoto & Goda, 1992).

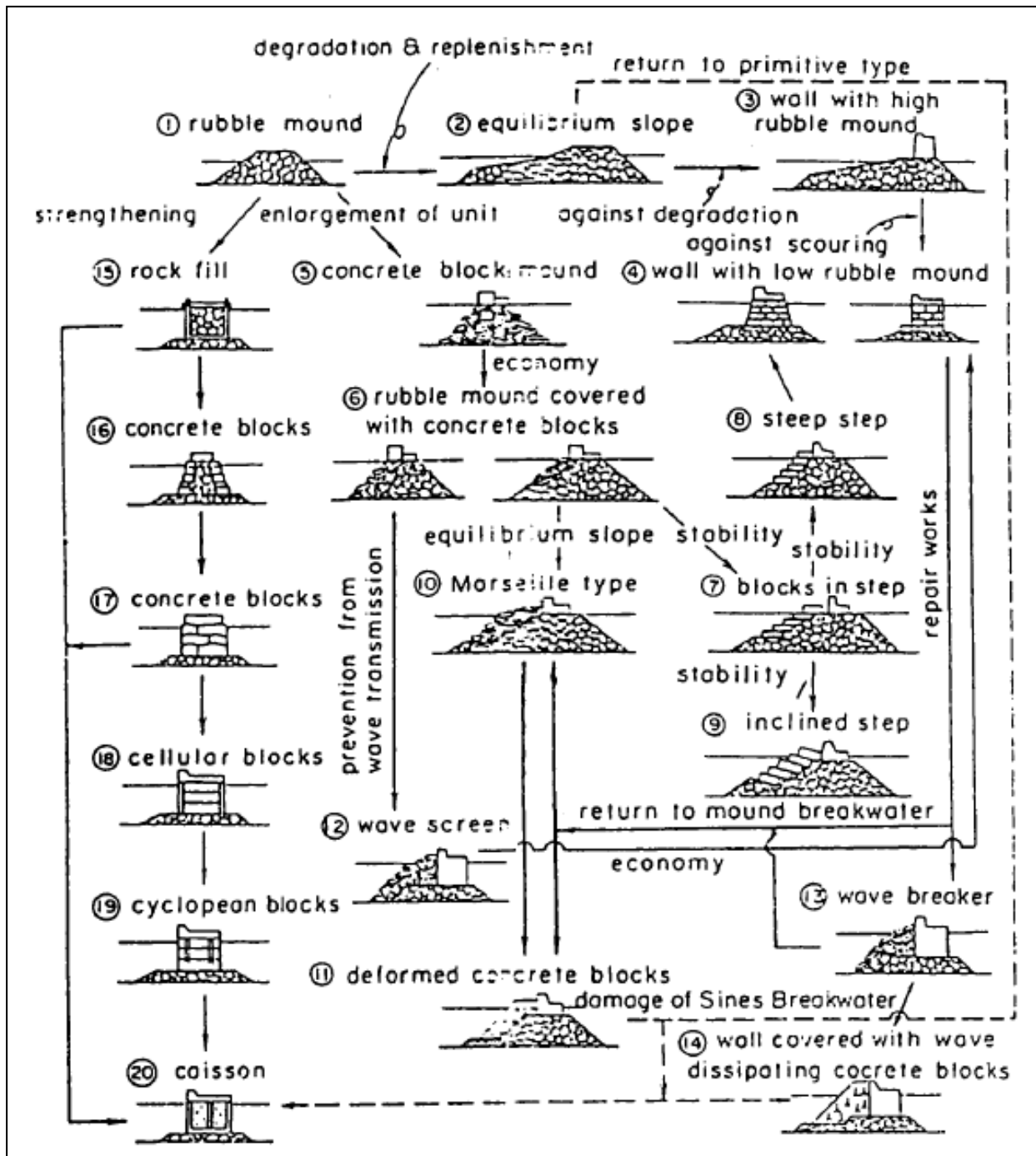


FIGURE 2.2: EVOLUTION OF BREAKWATER STRUCTURES (TANIMOTO & GODA, 1992)

2.3 DEVELOPMENT OF THE TANDEM BREAKWATER

To understand the development of the tandem breakwater system, it is required to first understand the berm breakwater system, because the one flows from the other. The concept of a berm breakwater design is as a result of an observation made during work done by Danel in 1952 (Cox & Clark, 1992). This observation was that damage to the area around the waterline tends to be the reason for rubble mound breakwater failure. The interaction of waves on the slope of the structure results in material being displaced from higher on the structure to form a gentler slope. Material is deposited on the lower portion of the seaward slope until the structure reaches an equilibrium profile that resembles the shape of an 'S' (Juhl, 1995). A typical berm breakwater and its equilibrium profile can be seen in figure 2.3.

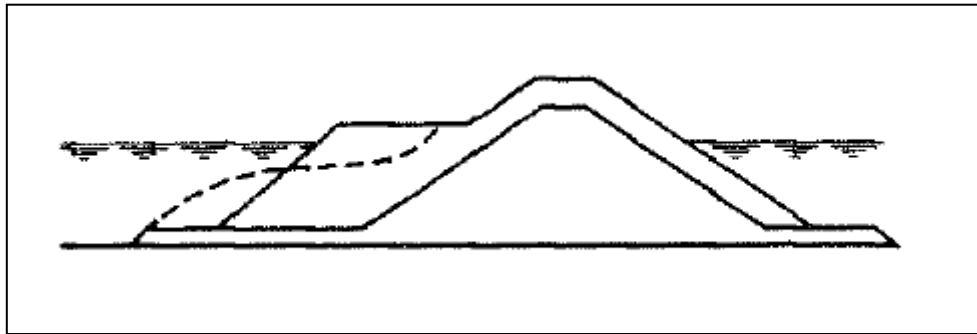


FIGURE 2.3: TYPICAL BERM BREAKWATER AND EQUILIBRIUM PROFILE (JUHL, 1995)

Unlike the conventional rubble mound breakwater, which is designed to be statically stable, the berm breakwater is designed with the specific intention that the front slope may be shaped into a flatter and more stable S-profile (van Gent, 1993).

When waves approach such a berm breakwater, the front portion of the berm causes the waves to start breaking. This removes some of the wave energy. The waves that are not broken by the front portion propagate over the rest of the berm until it reaches the main slope of the breakwater. At that point, the remaining wave energy is removed (Juhl & Jensen, 1995).

In previous studies it was found that the stability of a berm breakwater is influenced by the level of the berm relative to the water surface, the width of the berm, the wave steepness, and the slope angle of the breakwater (van Gent 2013). The failure of a berm breakwater is generally defined by $Rec > B$, where Rec is the recession of the berm and B is the width of the berm (PIANC, 2003). The recession of the berm is defined as the horizontal distance between the seaward side of the berm and the point at which no more damage to the berm is present (van Gent, 2013).

In certain cases it was found that the area between the point where berm damage stops and the main upper slope of the breakwater plays little part in the stability of the structure (Roa & Shirlal, 2003). One such a case was the breakwater that was designed for the marina located in Hammond, Indiana (Cox & Clark, 1992). The depth-limited nature of the wave breaking in the area made it possible to move forward the front part of the berm, where recession takes place, and remove the remaining berm material without compromising the integrity of the structure (Cox, 1992).

The removal of the material in the abovementioned area results in a breakwater system consisting of a detached submerged reef and a conventional rubble mound breakwater, separated by an energy dissipation zone. This system is referred to as a tandem breakwater. Figure 2.4 shows the evolution of the tandem breakwater system as reported by Cox & Clark (1992).

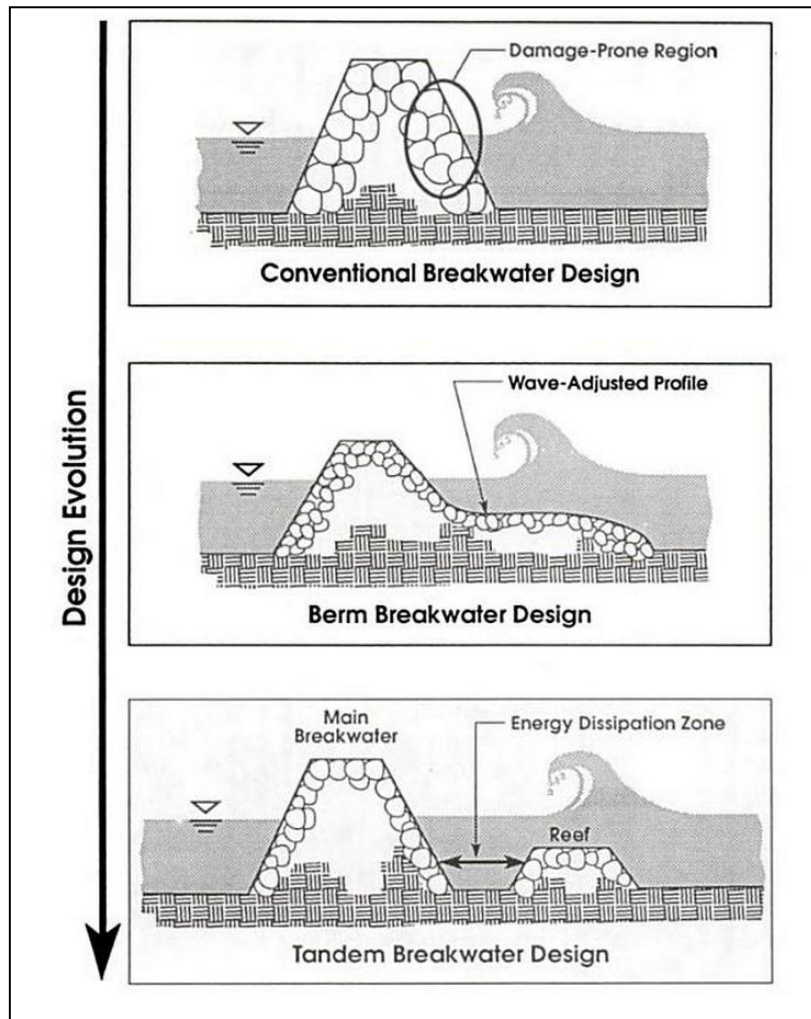


FIGURE 2.4: EVOLUTION OF TANDEM BREAKWATER (COX & CLARK, 1992)

2.4 BREAKWATER REPAIR METHODS

Breakwaters can be designed to serve a variety of purposes. These purposes range from preventing shoreline erosion to providing tranquil water conditions in which vessels can be moored (U.S. Army Corps of Engineers, 2002). To provide these conditions, the breakwater is required to absorb the energy from the constantly attacking waves. When designing such a structure, there is always a certain amount of uncertainty with regards to the wave conditions that will occur. The more severe the design storm condition is, the less risk of this condition being exceeded, but the higher the cost of breakwater construction. The converse is also true: less severe design storm means lower cost, but higher risk.

In the event of the occurrence of a bigger-than-design storm, the breakwater may be damaged. Excessive damage leads to breakwater failure (U.S. Army Corps of Engineers, 2002). There exist various modes of failure for rubble mound breakwaters, several of which can be related to the Iribarren number (Bruun, 1979). The Iribarren number is a useful parameter that describes wave action on a slope. It is often used to describe wave breaking and is defined by the following equation (van der Meer, 1993):

$$\xi_m = \frac{\tan \alpha}{\left(\frac{2\pi H_s}{gT_m^2} \right)^{0.5}}$$

2-1

where

- ξ_m = Iribarren number
- $\tan \alpha$ = slope
- H_s = significant wave height
- g = gravitational acceleration (9.81 m/s^2)
- T_m = mean wave period

Figure 2.5 indicates the 9 most common failure modes of rubble mound breakwaters. These range from the loss or damage of armour units, to cap movement, to toe erosion, to sea bed scour.

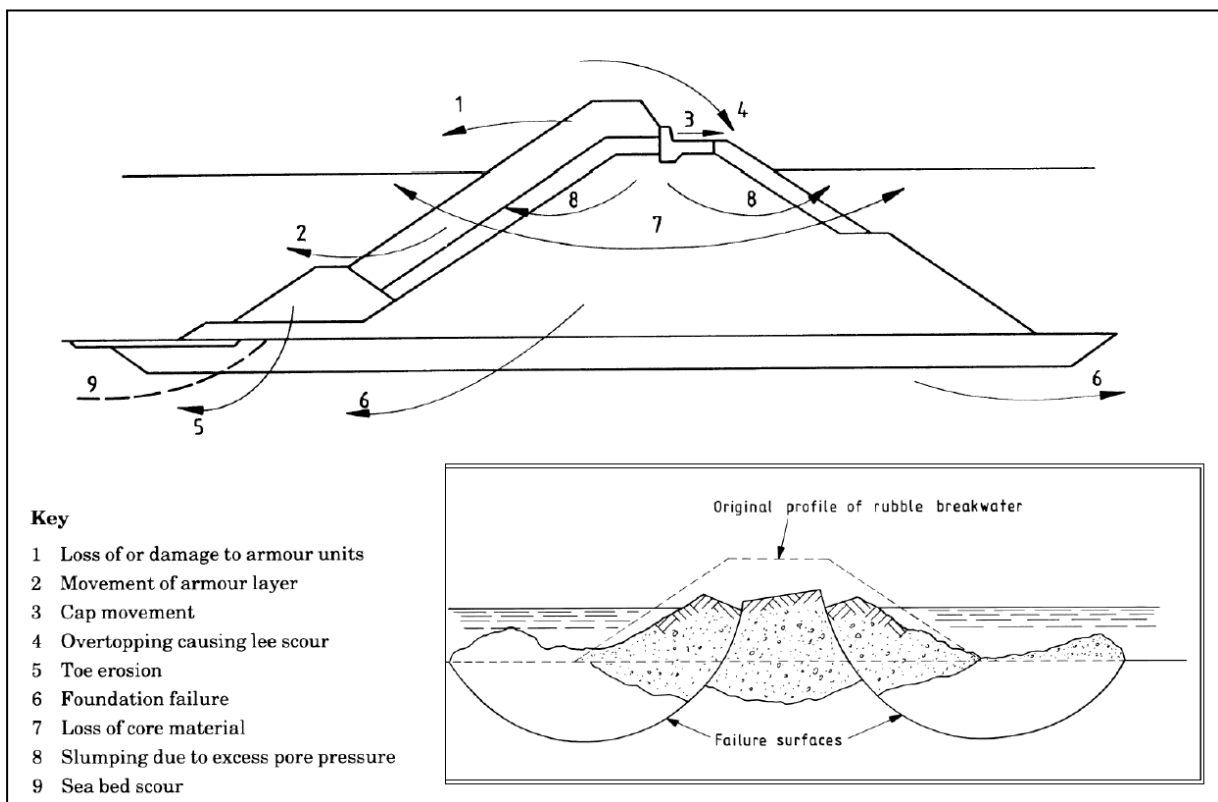


FIGURE 2.5: RUBBLE MOUND BREAKWATER FAILURE MODES - ADAPTED FROM BSI (2003)

Regular monitoring of breakwaters, especially after severe storm events, is required in order to identify damaged areas before the overall stability of the breakwater is jeopardised (Phelp, 2005). A host of breakwater monitoring techniques exist, which includes visual inspections, diver inspections, photographic monitoring, crane and ball surveys, seismic surveys, sonar surveys, and multibeam surveys (Tulsi & Phelp, 2009).

Once breakwater damage has been identified, it is necessary to assess the severity of the damage, and from there determine what would be the most viable method of rehabilitation, if any.

Determining the optimum method with which to restore a damaged breakwater depends on several factors, including (Mol et al., 1984):

- the cause of failure (inadequate design, unsatisfactory construction, or extreme environmental conditions)
- the degree and nature of the damage
- the geometry of the structure
- the local topography
- the availability of construction material and equipment
- the acceptable level of risk to port operations or other facilities
- future requirements for port expansion or other construction works
- financial resources, cash-flow details and requirements on local and foreign elements of rehabilitation costs

There also exists the option of not taking any action in restoring the breakwater. This option is called the ‘zero-condition’. However, it should be noted that if it is decided to not take any action, the further deterioration of the breakwater is highly probable, not to mention the added financial implication due to restrictions in port operations and possible damage to other facilities within the area (Mol et al., 1984).

Whenever breakwater damage has been identified, the zero-condition has to be investigated to establish the capacity of the damaged breakwater, predict the pattern of future deterioration, and assess the maintenance requirements (Mol et al., 1984). If the zero-condition is determined to be an inadequate solution, possible rehabilitation solutions are designed and investigated. The feasibility of restoration methods is related to the causes of failure and the extent of damage (Bruun, 1979). Table 2.1 shows a basic classification of damage as a result of hydraulic instability of the armour system.

TABLE 2.1: CLASSIFICATION OF ARMOUR LAYER DAMAGE (MOL ET AL., 1984)

Classification of Damage	Percentage of Displaced Units	Description of Damage
(i) Minor	0 – 3 %	A few individual units of top layer displaced, but no gaps in top layer larger than 4 units, bottom layer intact.
(ii) Moderate	3 – 5 %	No gaps in top layer larger than 6 units, slight displacements of bottom layers only.
(iii) Major	5 – 30 %	Top layer removed over large area, bottom layer over not more than 2 units.
(iv) Total	Over 30 %	Armour and under layers removed over large area, exposure of core material.

The following are four conventional methods of breakwater rehabilitation, and are discussed hereafter:

- Method 1: Replacement of units
- Method 2: Replacement of armour system
- Method 3: Reconstruction of rubble mound
- Method 4: Provision of sheltering against Critical Wave Condition

The method of replacing damaged units can be used when damage of either type (i) or (ii) occurs, as shown in table 2.1. This method should only be used if the event that caused the damage is similar to the design condition for the breakwater (Mol et al., 1984). It is also important that the units that are used are of the same size and type as the original units.

Method 1 is not as costly as the other methods, because it is only the damage parts of the breakwater that are restored. This also results in a shorter rehabilitation period. Figure 2.6 gives a representation of this method.

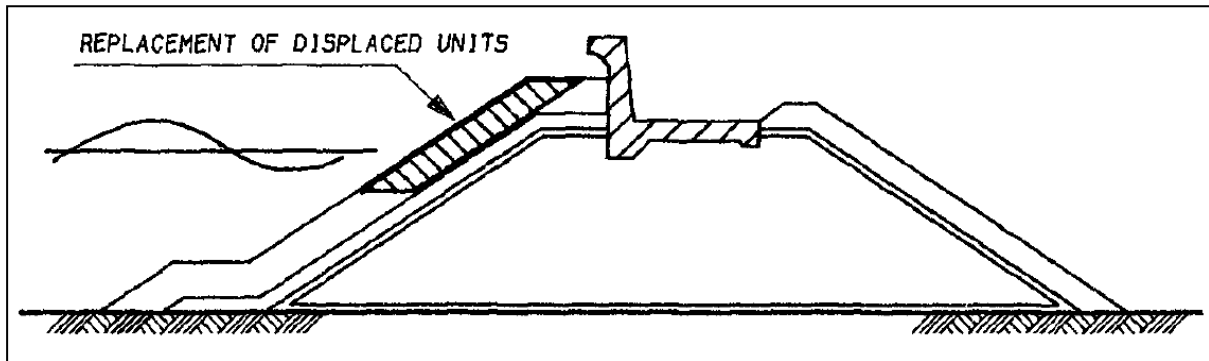


FIGURE 2.6: BREAKWATER REHABILITATION METHOD 1 (MOL ET AL., 1984)

Unlike the first method, which only requires the removal of the damaged armour units, Method 2 replaces all the units with units of a different type. This, of course, means a higher cost, as well as a longer rehabilitation period. Although this is not always the best solution, it may become feasible if the anticipated future maintenance costs of the original armour system outweigh the cost of replacing the primary armour layer with a more adequate one (Mol et al., 1984). A representation of this method is shown in figure 2.7.

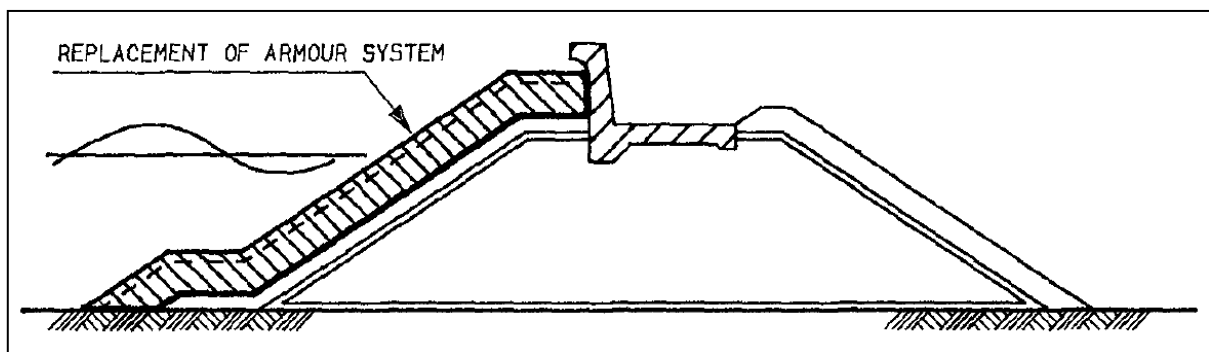


FIGURE 2.7: BREAKWATER REHABILITATION METHOD 2 (MOL ET AL., 1984)

The third method is a complete overhaul of the structure. It requires the removal of the armour layer, as well as the under layers, after which the core material is re-compacted to a suitable density. A new filter layer is then placed on top of the core material, before replacing the under layers and primary armour layer. Although the use of new armour units is preferred, it is not always necessary. To save on cost, original units that are not damaged can be reused (Mol et al., 1984).

This method is favoured when geotechnical instability is suspected, for example when slopes are close to being too steep in relation to the internal friction of the core, under layers or sub-soil (Mol et al., 1984). Figure 2.8 gives a representation of this method.

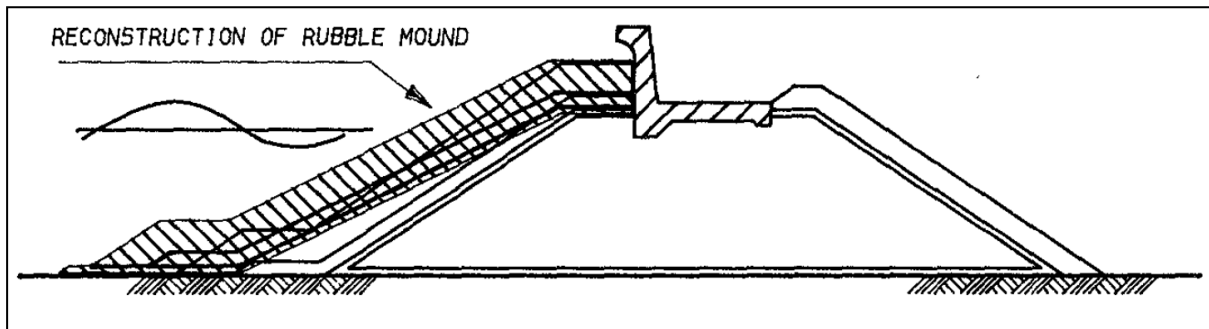


FIGURE 2.8: BREAKWATER REHABILITATION METHOD 3 (MOL ET AL., 1984)

The fourth method involves the construction of an additional structure to provide sheltering against critical wave conditions that attack the structure. There are two alternatives: an underwater berm attached to the breakwater, or a detached submerged breakwater in front of the main breakwater. Both types are designed to dissipate some of the energy from oncoming waves, resulting in smaller waves attacking the main breakwater (Mol et al., 1984). A representation of the berm structure attached to the main breakwater is given in figure 2.9.

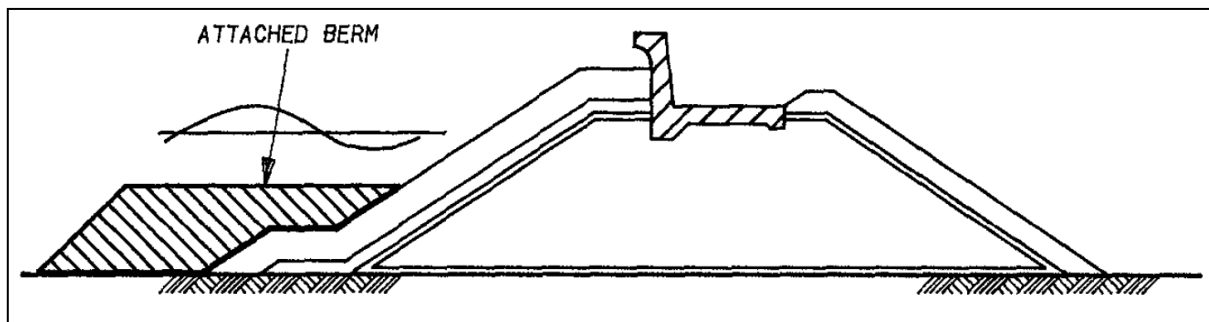


FIGURE 2.9: BREAKWATER REHABILITATION METHOD 4 (MOL ET AL., 1984)

It is evident from the abovementioned rehabilitation methods that even the most basic solutions to repairing breakwater damage are very time consuming. Extended periods of time usually pass before actual reconstruction can begin. This rehabilitation period is critical, as the breakwater is most vulnerable (U.S. Army Corps of Engineers, 2002).

2.5 WAVE TRANSMISSION OVER SUBMERGED STRUCTURES

In recent years, the conceptual design of coastal defence structures has involved more than just the consideration of physical factors. Certain non-physical factors such as the environmental and aesthetic value of the nearshore landscape have also become important aspects to consider (Makris & Memos, 2007). This has played a part in the development of low-crested and submerged structures that offer the benefit of low visual impact (Tomasicchio & d'Alessandro, 2013).

A commonly used measure of the performance of such structures is the transmission coefficient. This coefficient provides the anticipated decrease in wave height due to the presence of the structure under consideration. The primary parameter that impacts the transmission coefficient is the freeboard of the structure, i.e. the distance between the water level and the crest level of the structure (Makris & Memos, 2007). A mathematical description of the transmission coefficient is given as (van der Meer & Daemen, 1994):

$$K_t = H_t/H_i \quad 2-2$$

where

K_t = transmission coefficient

H_t = transmitted wave

H_i = incident wave

Several parameters effect the value of the transmission coefficient, including the crest width of the breakwater (B), the freeboard (R_c), the water depth (h), the height of the structure (h_c), the front slope of the structure (m), the nominal rock diameter of the armour slope (D_{n50}), the incident significant wave height at the toe of the structure (H_i), the local wavelength (L), the peak period (T_p), the Iribarren number (ξ_m), and the wave steepness (s) (Makris & Memos, 2007). Figure 2.10 gives a graphical representation of these parameters.

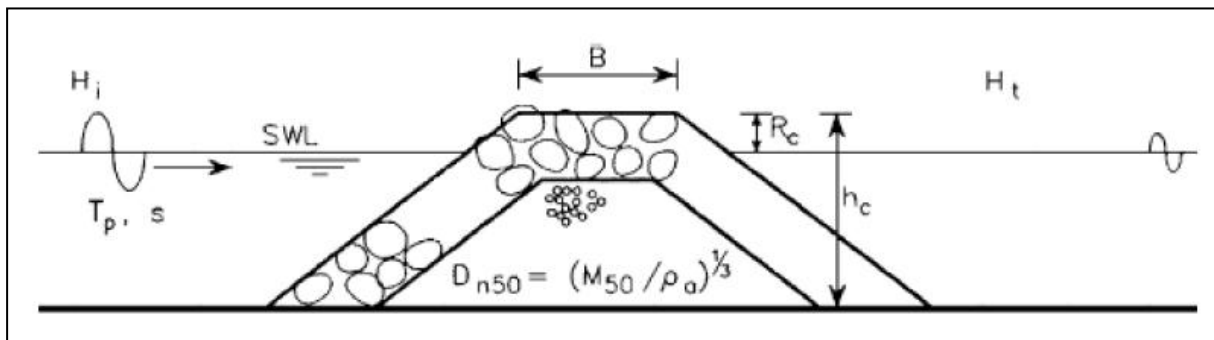


FIGURE 2.10: PARAMETERS INFLUENCING WAVE TRANSMISSION COEFFICIENT (VAN DER MEER ET AL., 2005)

Extensive research has been done on the topic of transmission coefficients by various authors, including Seelig (1980), van der Meer (1990), d'Angremond et al. (1996), Seabrook & Hall (1998), Hirose et al. (2002), van der Meer et al. (2005), Buccino & Calabrese (2007), and Goda & Ahrens (2008). Several of the abovementioned authors have proposed empirical formulae for the wave transmission coefficient based on regression analysis of physical model data (Tomasicchio & d'Alessandro, 2013).

The latest formulae for predicting transmission coefficients are based on an extensive database consisting of 33 separate data sets of experimental studies conducted with regards to transmission over low-crested/submerged structures (Tomasicchio & d'Alessandro, 2013). The formulae are similar to those proposed by Goda & Ahrens (2008), although certain coefficients have been re-calibrated to better fit the improved set of data.

The re-calibrated formulae provide better prediction than the original formulae, especially for K_t values smaller than 0.4, where the original formulae overestimates slightly (Tomasicchio & d'Alessandro, 2013).

The proposed wave transmission coefficient is defined as a combination of the transmittance over and through the low-crested structure and is as described by the following set of equations (Tomasicchio & d'Alessandro, 2013):

$$(K_t)_{all} = \min \left\{ 1.0; \sqrt{(K_t)_{over}^2 + K_h^2 (K_t)_{thru}^2} \right\} \quad 2-3$$

$$K_h = \min \left\{ 0.8; h_c / (h + H_i) \right\} \quad 2-4$$

$$(K_t)_{over} = \max \left\{ 0.0; 1 - \exp \left(a \left(\frac{R_c}{H_i} - R_{c,o} \right) \right) \right\} \quad 2-5$$

$$a = 0.248 \exp \left(-0.384 \ln \left(\frac{B_{eff}}{L_0} \right) \right) \quad 2-6$$

$$R_{c,o} = 1.0 \quad : D_{eff} = 0$$

$$R_{c,o} = \max \left\{ 0.6; \min \left\{ 0.8; H_i / D_{eff} \right\} \right\} \quad : D_{eff} > 0 \quad 2-7$$

$$(K_t)_{thru} = \frac{1}{\left[1 + C \left(H_i / L \right)^{0.5} \right]^2} \quad 2-8$$

$$C = 3.45 \left(\frac{B_{eff}}{D_{eff}} \right)^{0.65} \quad 2-9$$

In the above equations, $(K_t)_{all}$ refers to the transmission coefficient for a combination of the transmission coefficient for energy passing over the structure $(K_t)_{over}$ and the transmission coefficient for energy passing through the structure $(K_t)_{thru}$. K_h describes the contribution of waves passing through the structure to the energy of transmitted waves. $R_{c,o}$ represents an approximate limit of non-dimensional run-up. B_{eff} is effective crest width of the structure and D_{eff} is the nominal stone diameter (Tomasicchio & d'Alessandro, 2013). For impermeable structures, D_{eff} and $(K_t)_{thru}$ are both equal to zero. The effective crest width, B_{eff} , varies according to the nature of the structure and is calculated as follows (Goda & Ahrens, 2008):

- emerged breakwaters: $B_{eff} = \text{width at still water level (SWL)}$
- zero freeboard: $B_{eff} = (9 \times \text{crest width} + \text{bottom width})/10$
- submerged breakwaters: $B_{eff} = (4 \times \text{crest width} + \text{bottom width})/5$

Figure 2.11 shows the comparison of the transmission coefficient measured in model experiments and the transmission coefficient as predicted by the abovementioned formulae. It has a correlation coefficient of 0.902 (Tomasicchio & d'Alessandro, 2013). Before re-calibration of the formulae, the correlation coefficient was 0.831 (Goda & Ahrens, 2008).

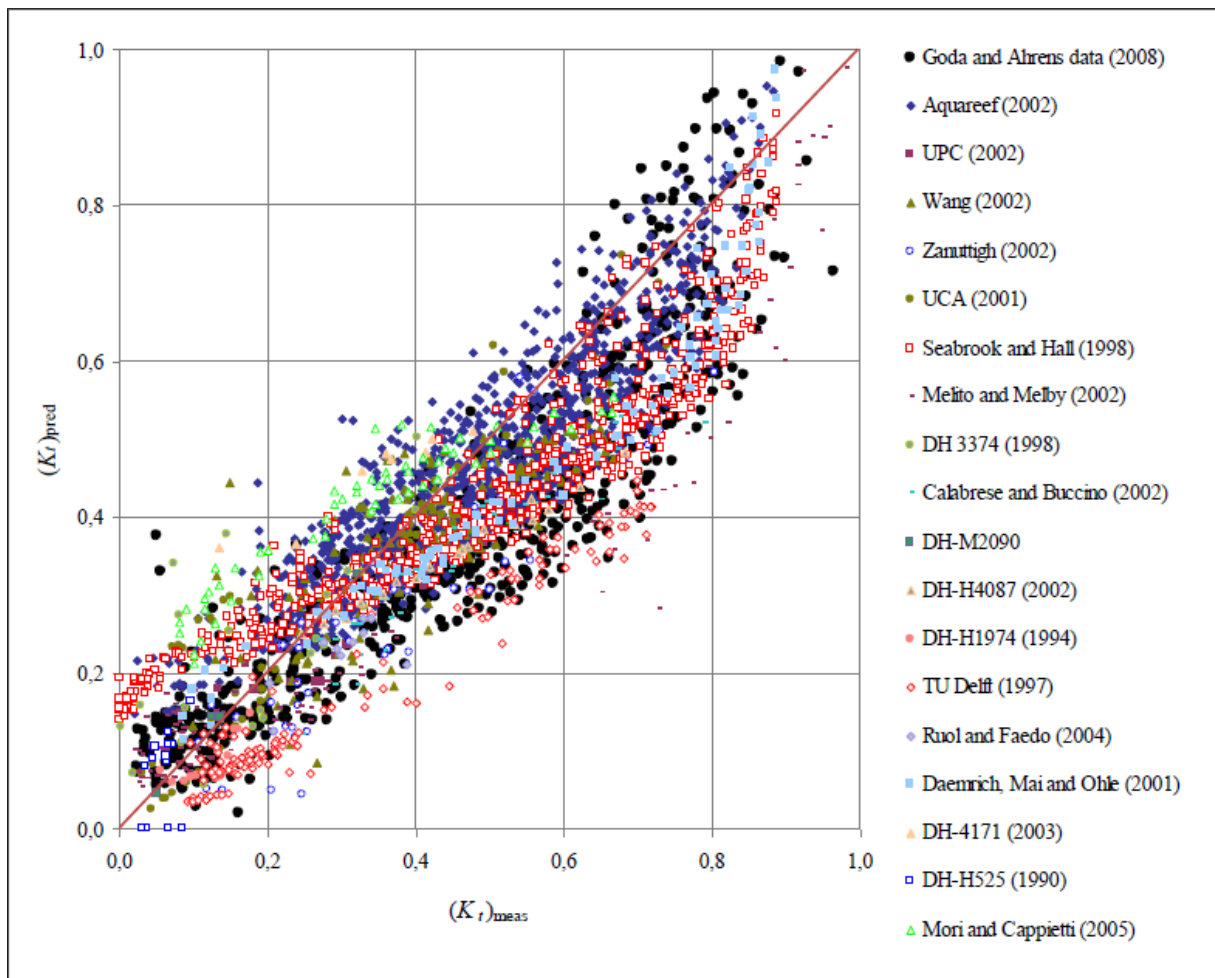


FIGURE 2.11: COMPARISON BETWEEN MEASURED AND PREDICTED TRANSMISSION COEFFICIENT (TOMASICCHIO & D'ALESSANDRO, 2013)

2.6 GEOTEXTILES

This section is dedicated to geotextile materials and its application in coastal engineering. First, a description of the various types of geotextile material is given. Then, the placement accuracy of geotubes in the coastal environment is investigated.

During the 1960s, the first applications of geotextiles in civil construction projects took place throughout Europe and USA for drainage and separation purposes in road construction. Since then, the technology surrounding geotextile materials has developed to such an extent that basically every new civil construction project that is undertaken will involve the use of some type of geotextile material (Hornsey, 2009).

The geotextile material allows water to pass through it, but retains sand or other granular materials. This characteristic of the material resulted in the creation of geotextile sandbags. The semi-permeable nature of the geotextile material allows for easy placing and filling of the sandbags (Bezuijen & Pilarczyk, 2012).

Various coastal erosion problems have been solved by using geotextile sandbags as protective measure against wave attack. The earliest of which was the use of a woven monofilament fabric to protect a shoreline property in Florida in the early 1960s (Mitra, 2013). This was the defining case which opened the door for geotextile applications in coastal engineering.

Geotextiles that are used in coastal protection structures are subject to much more severe conditions than geotextiles that are used for road construction purposes. In the harsh oceanic environment, geotextiles are exposed to a variety of forces that include abrasion from armour rock and marine sediment, large dynamic flow conditions due to tidal and wave action, UV rays from the sun, debris in the water, as well as potential acts of vandalism (Kriel, 2012). These factors result in geotubes having a relatively short lifetime compared to conventional coastal protection structures, which mostly consist of various sizes of rock (Weerakoon et al., 2003). However, improvements in the technology of geotubes have led to better design options that provide various forms of protection for geotextile containers. One such an example is TenCate's 'Debris Shield' product, which provides additional protection against UV rays, abrasion and vandalism (TenCate, 2011).

In order to gain a better understanding of the durability of geotextiles, more prototype data is still required, as the majority of geotextile applications in coastal engineering are only now reaching maturity. The time in which a geotextile's strength reduces by 10% is considered to be the service lifetime thereof (PIANC, 2011).

The majority of geotube applications in the coastal environment are done either on land or in shallow water. Numerous projects involving the installation of geotubes have been undertaken, producing satisfactory results (Pilarczyk, 2003).

The preferred technique when placing geotubes is to hydraulically fill the sandbag, as this technique greatly reduces turbidity in the area (Fowler et al., 2002). The placement of the sandbag on land is not difficult, as there is no need to compete with the forces of the ocean. The placing of geotubes in relatively shallow water is more difficult, but not impossible (Theron, 2014).

To hydraulically fill a geotube, a slurry mixture of water and sand is pumped into the bags. As more sand enters the geotubes, water is forced out to make room for the sand. Special care should be taken when filling geotubes, as they can easily collapse if the slurry's water-sand mixture is not carefully controlled. The flow tempo and pressure from the pumps that are used is also very sensitive. Another operational problem with installing geotubes is that they tend to start moving about during the filling operation. Still, with the right equipment, successful installation is possible (Theron, 2014).

Using sand-filled geotubes, as opposed to rock, reduces cost, as there is no need for rock quarrying or rock transportation costs. Geotubes are also a more environmentally friendly option, because emissions due to transport of construction material are reduced (Oh & Shin, 2006).

Unlike placing geotubes in shallow water, placing them in deeper water is a discipline that still requires improvement. This is probably due to the fact that the number of applications in shallow water far outnumbers those in deep water. The reason for this is that as you move farther away from the shoreline, into deeper water, the environmental conditions become much harsher (van Zijl et al., 2006). In deeper water it is necessary to contend with bigger waves and stronger currents. These added difficulties hamper the ability to place geotubes with the same degree of accuracy as in shallow water. Nevertheless, techniques for installing geotubes in deeper water have been developed, albeit not perfected (Bezuijen et al., 2002).

One such a technique is to make use of a split-hull barge to place a group of geocontainers. While geotubes are prefabricated and then filled once placed in position, geocontainers are filled and stitched

on site. The barge is lined with the geotextile material and then mechanically filled with sand at a berth. Thereafter, the sides and ends of the geotextile material are brought together and sewn shut. The barge then sails to the required location and opens the split hull to release the geocontainer (Bezuijen et al., 2004).

In reality it is not possible to fill the geotextile containers up to 100%. While geotubes can be hydraulically filled to come quite close to that, it is not possible for geocontainers to be filled in a similar fashion. The filling of a geocontainer is limited by the opening of the barge's hull, which it has to be able to pass through when dumping. The flexible geotextile material allows sufficient deformation of the container's shape to pass through the opening in the hull, so long as the container is not over-filled (Bezuijen et al., 2004).

Another method is to make use of a continuous geotube. It is essentially the same as the normal geotubes, except that it is much longer. The simultaneous filling and stitching of such a long geotube is a problem. Therefore, the method of placement and filling of a continuous geotube had to be altered. It was decided that the geotube be manufactured beforehand, and that the only sewing to be done on site would be to seal the end of the geotube after filling (van Zijl et al., 2006).

A specific method of folding the geotube has been developed, which allows the geotube to be filled from one end while placing it on the seabed. The first step in the folding method is to fold two parallel sides toward each other, leaving a gap between them. After this, the two perpendicular sides are folded in a similar manner to the first step. The process is repeated until the whole length of the geotube is folded, leaving a square hole in the middle by which to fill the geotube. Figure 2.12 shows the method of folding the continuous geotube (van Zijl et al., 2006).

The placement of the continuous geotube is done from a pontoon. A clamp system has been developed to keep the geotextile material stable while placing it. After testing different designs, it was decided that a clamp system located on the outside of the geotube will be most advantageous. Two clamps will be used, one on each side of the filling hole, as well as a tensioner system to allow for a continuous release process. The clamp system is also responsible for the transfer of forces to the pontoon during installation. During this placement, the geotube is partly supported by a slide, which is attached to the pontoon (van Zijl et al., 2006).

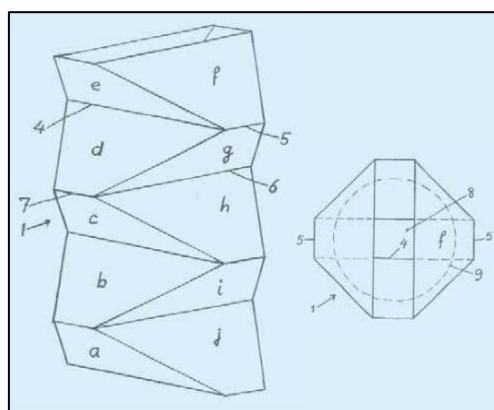


FIGURE 2.12: CONTINUOUS GEOTUBE FOLDING METHOD (VAN ZIJL ET AL., 2006)

Field tests have been performed for the releasing of geocontainers from a split-hull barge during the Kandia Dam project. The Kandia Dam is situated close to Arnhem in the Netherlands (Bezuijen et al., 2004). During the tests, 55 geocontainers were released and their displacements relative to the split-hull barge were measured. Four layers of geocontainers had to be placed. The placement of the geocontainers was done in an environment where no currents or waves were present. The first layer,

made up of 13 geocontainers, had a water depth of 21.6 m. The second, third and fourth layers, each consisting of 14 geocontainers were located in water depths of 19.7 m, 17.6 m and 15.5 m respectively (Bezuijen et al., 2004).

DGPS technology was used to determine the position of the barge (and thus the position of the geocontainer) before its release. After it had settled on the bottom, the final position of the geocontainer was determined by a combination of multi-beam sonar and DGPS technology.

Figure 2.13 shows the locations of the first four geocontainers that were dropped, as well as the location of the split-hull barge at the time of release (Bezuijen et al., 2004). As shown, the geocontainers deformed during the fall to the bottom. Therefore, the displacement of the centre of gravities was used to give an indication of accuracy.

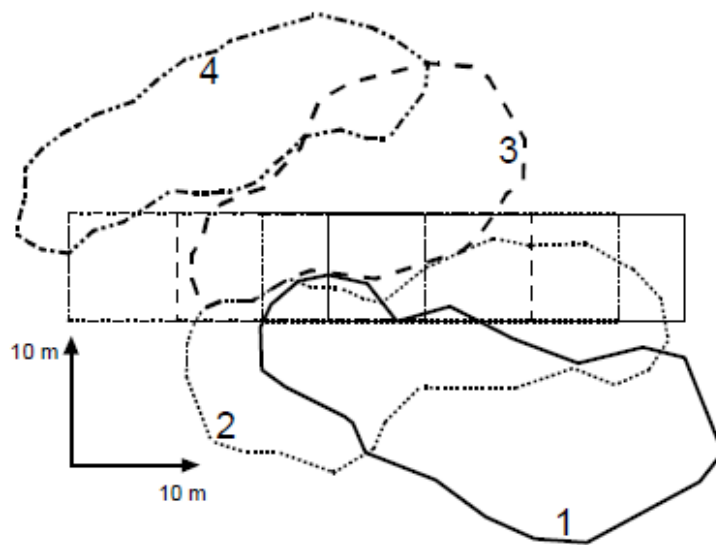


FIGURE 2.13: DISPLACEMENTS OF GEOCONTAINERS RELATIVE TO BARGE (BEZUIJEN ET AL., 2004)

It was found that the manner in which the geocontainers deviated from the barge location after being released was not a clear function of depth, although the standard deviation was. In figure 2.14, the relationship between water depth and standard deviation can be seen (Bezuijen et al., 2004).

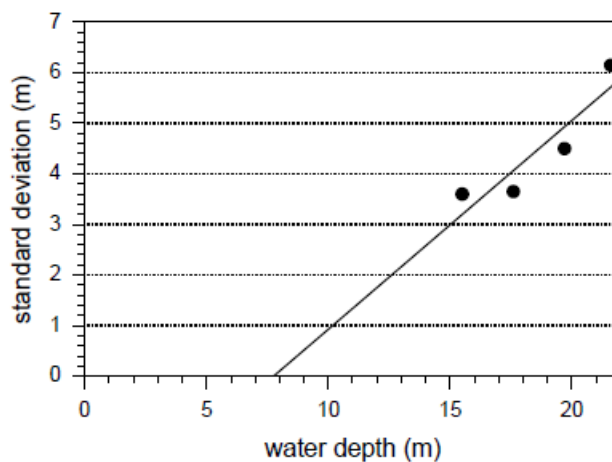


FIGURE 2.14: STANDARD DEVIATION OF RELATIVE DISPLACEMENT OF GEOCONTAINERS (BEZUIJEN ET AL., 2004)

The graph in figure 2.14 shows that geotubes can be placed with sufficient accuracy in water depths of up to approximately 10 m.

Similar tests have been conducted at a small scale, where the effect of currents and waves were taken into account (Bezuijen et al., 2002). When comparing the results of the field tests and the equivalent model tests, where no currents or waves are present, it was found that the standard deviation is higher in the field tests than in the model tests. The model tests that take current and wave action into account indicate a standard deviation of as high as 7 m for geocontainer placement in 16 m water depth (Bezuijen et al., 2002).

Although the geocontainer settles quite a distance from where it is released, the path that it follows is not completely random. If the wave and current conditions are known, it is possible to predict where a geocontainer will end up on the seabed with reasonable accuracy. It will, however, be difficult to stack geocontainers in this fashion, as the rotation of the containers cannot be controlled effectively (Bezuijen, written correspondence, 29 April, 2014).

2.7 CASE STUDIES

A number of case studies are discussed in this section. All the cases except for the last one involve the creation of an artificial reef or detached breakwater using either rock or geotubes. The last case study shows the implementation of a tandem breakwater system. The purpose of this section is to give an indication of projects that have been successfully completed, with some insight of the difficulties encountered during construction.

2.7.1 NARROWNECK REEF

This artificial submerged reef situated on Australia's Gold Coast, forms part of a strategy to protect the world famous Surfers Paradise beaches from erosion during severe storms. Figure 2.15 shows the location of the reef along the East coast of Australia.

The construction took place between 1999 and 2001, and was funded by the Gold Coast City Council. Apart from providing the necessary protection against beach erosion, the reef also creates attractive surfing conditions. These surfing conditions, as well as long stretches of wide sandy beaches are the primary sources of attraction in an area where the economy is driven by tourism (Jackson & Hornsey, 2003). Figure 2.16 shows an aerial view of the submerged reef.

Prior to the construction of Narrowneck reef, a continuous beach nourishment scheme was in place. The effectiveness of the scheme was high, although its long term sustainability was questionable.

During the design of the structure, various construction materials were considered. Amongst others was a combination of rock and concrete materials. In the end, Geosynthetic sand-filled containers were the preferred option, as they proved to be most advantageous in the specific areas that were investigated (Jackson & Hornsey, 2003).

Firstly, choosing to use a geosynthetic structure instead of a rock structure caused the cost of the structure to be halved (Jackson & Hornsey, 2003). The sand-containing structure also reduced the risk of surfers or swimmers being injured, as it does not have the sharp edges found on equivalent rock structures. Emissions into the atmosphere were reduced, as no transportation of rock material was necessary. This meant that the geosynthetic structure would be a more environmentally friendly option in that regard. Finally, the use of geosynthetic sand-filled containers was considered the most flexible option with regards to removal or modification of the structure. Unforeseen difficulties could require

some sort of modification to the structure or even its complete removal. If a rock and concrete structure were to be used, this might not have been possible (Jackson & Hornsey, 2003).

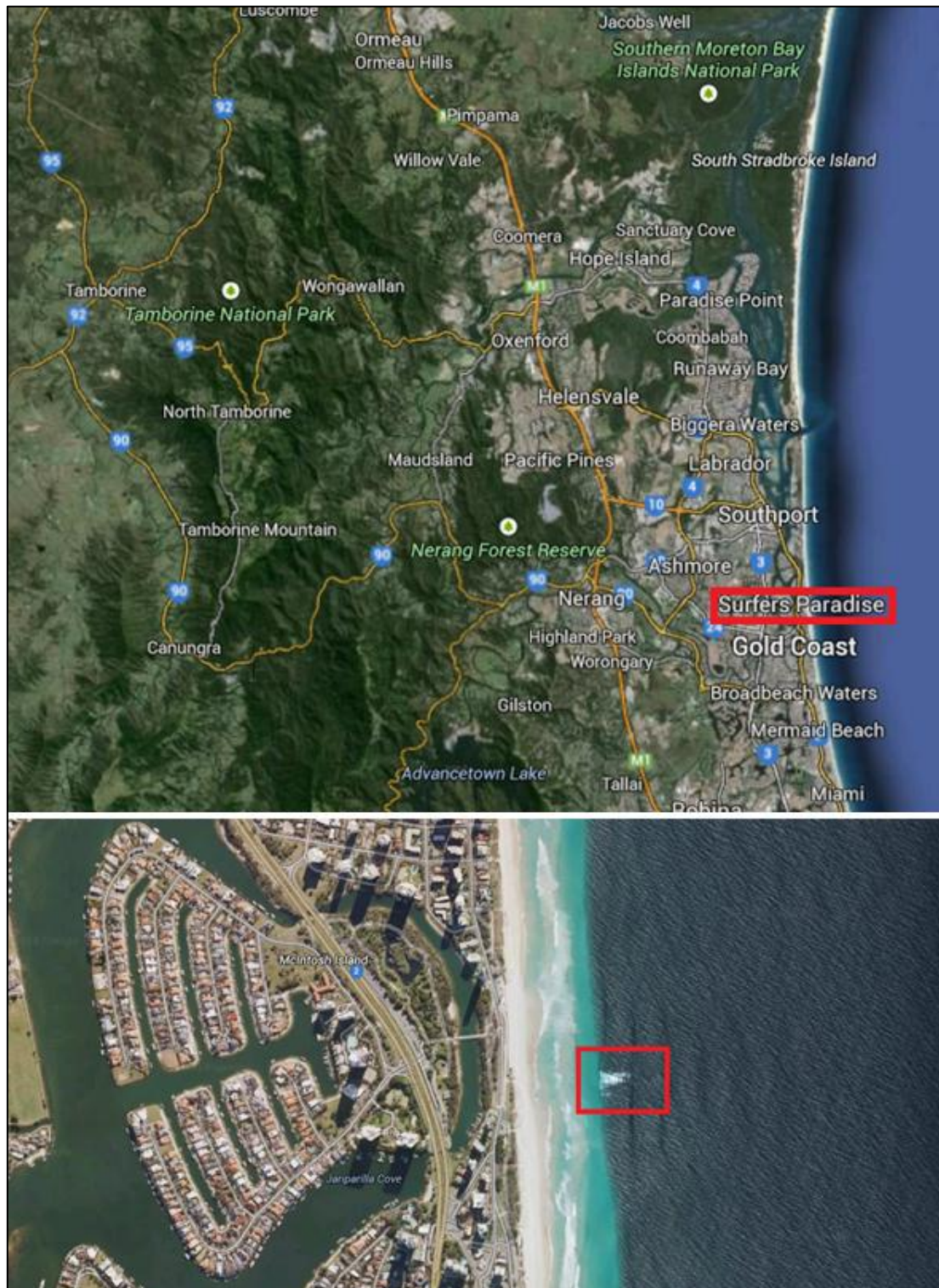


FIGURE 2.15: LOCATION OF NARRONECK REEF (GOOGLE INC., 2014)



FIGURE 2.16: AERIAL VIEW OF NARROWNECK REEF (JACKSON & HORNSEY, 2003)

The artificial reef extends a distance of 200 m offshore, where the water depth is about 11 m. At its closest point to the shore, the water is approximately 2.5 m deep. The maximum tidal range in the area is 2 m.

The placement of the sand-filled containers was done by a split-hulled trailing suction hopper dredger, which was fitted with DGPS technology. The length of all the containers is 20 m, with diameters varying between 3.0 m and 4.6 m (Jackson & Hornsey, 2003).

Hydraulic filling of the containers were done on board the vessel, which was a first. Previously, a barge would be lined with geotextile material and filled with the use of an excavator, after which the ends of the material would be sewn together. In those cases the integrity of the seam was a problem, seeing as it is done on site with swell motions to account for. Hydraulic filling of the containers requires the geotextile containers to be manufactured beforehand, which ensures better quality control. While manufacturing, the only parts of the container that is not sewn shut are a few inlet valves and exhaust vents. These are closed on site after filling. Thus, only a small portion of the containers have to be closed in an uncontrolled environment, and in these cases a double seam is used (Jackson & Hornsey, 2003).

To ensure the accurate filling and consistency of the geotextile containers, a calibrated flow density meter was used. All containers were filled to 80% of their maximum theoretical volume.

A general accuracy of 0.5 m was achieved during the placing of the sand-filled containers. Figure 2.17 shows an area where two containers were placed 150 mm apart (Jackson & Hornsey, 2003).



FIGURE 2.17: PLACEMENT ACCURACY OF 150 MM (JACKSON & HORNSEY, 2003)

2.7.2 BOSCOMBE REEF

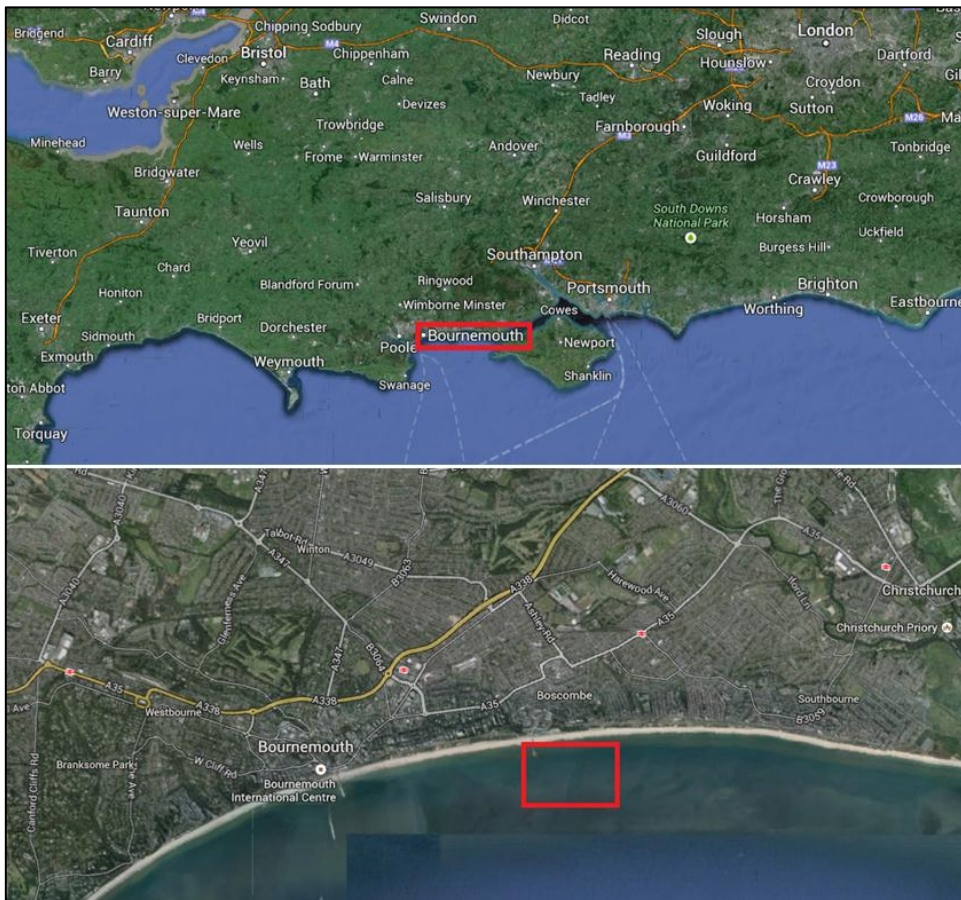


FIGURE 2.18: LOCATION OF BOSCOMBE ARTIFICIAL REEF (GOOGLE INC., 2014)

In 2009 the first artificial surfing reef in the Northern Hemisphere was completed in Boscombe, near Bournemouth. The project had a construction period of 18 months (Rendle & Davidson, 2012). In figure 2.18 the location of the reef along the South coast of England is shown.

The design process of the Boscombe reef, involved a detailed numerical model study, in which an optimum layout for the structure was determined. The aim of the structure was to improve the surfing conditions in the area. In figure 2.19 an aerial view of the artificial surfing reef is shown.



FIGURE 2.19: AERIAL VIEW OF BOSCOMBE REEF (RENDLE & DAVIDSON, 2012)

The final design was a two-layer structure, consisting of 32 sand-filled geotextile containers. These were hydraulically filled on site with sand material from the area. For the most accurate placing of the geocontainers it was decided to use SCUBA divers to position and hold them in place during the filling process. The water depths, which varied between 2.5 and 5.5 m, made it feasible to use divers to help install the geocontainers (Rendle & Davidson, 2012).

Two years after construction, the annual survey indicated damage to two of the structure's major geotextile containers. Since then, concerns regarding the safety of the users have caused the reef to be closed, and it remains closed to date. Mixed opinions have been expressed in the past regarding the success of the structure, but the fact that it remains closed means that it did not accomplish its intended purpose (Rendle & Davidson, 2012). However, for the purposes of this report, certain aspects of the structure can be seen as successful. The geocontainers had high placement accuracy, and if it was constructed as a temporary structure during a rehabilitation period, the structure would have had a sufficient effective protection period.

2.7.3 CABLE STATION REEF

In 1999 the first reef constructed specifically for the purpose of creating an improved surfing environment was constructed at Cable Station. It is located close to Perth, just south of Cottesloe, as indicated in figure 2.20.

The artificial reef was constructed from 1.5 ton granite rocks that were placed on top of an existing limestone reef. Along the perimeter of the structure, stones as large as 3 ton were used (Bancroft, 1999). A plan view of the design of the reef can be seen in figure 2.21.

The project is considered a success, as monitoring of the reef showed a significant improvement in the surfing conditions of the area. The reef provides surfable waves for more than 150 days a year (Bancroft, 1999).

The fact that the reef still remains stable and intact makes it a successful case of implementation with regards to this project as well.

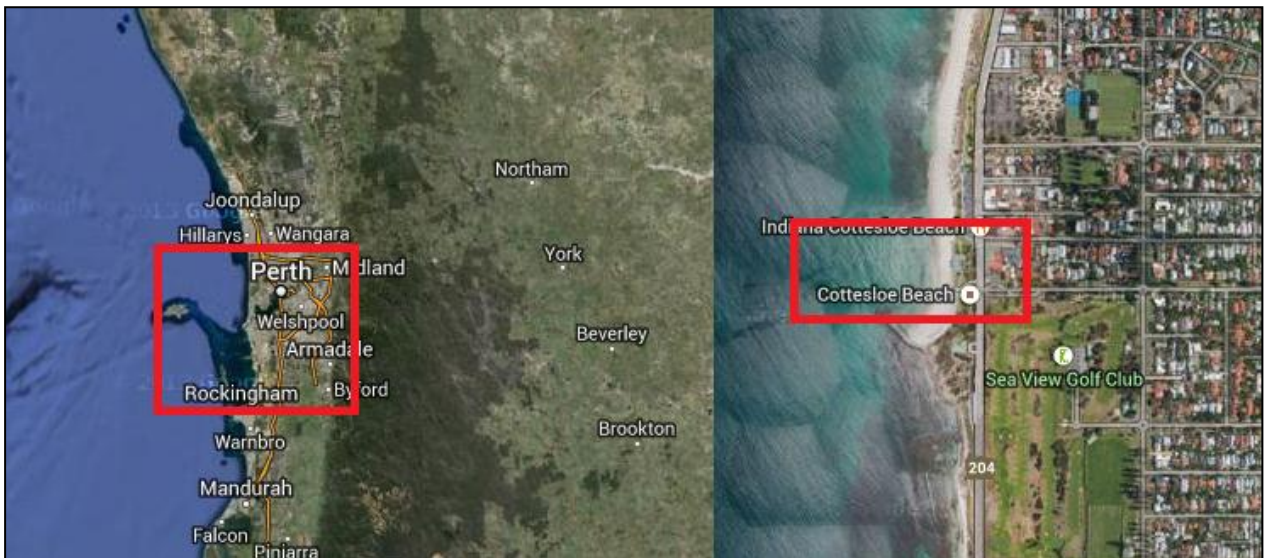


FIGURE 2.20: LOCATION OF CABLE STATION ARTIFICIAL REEF (GOOGLE INC., 2014)

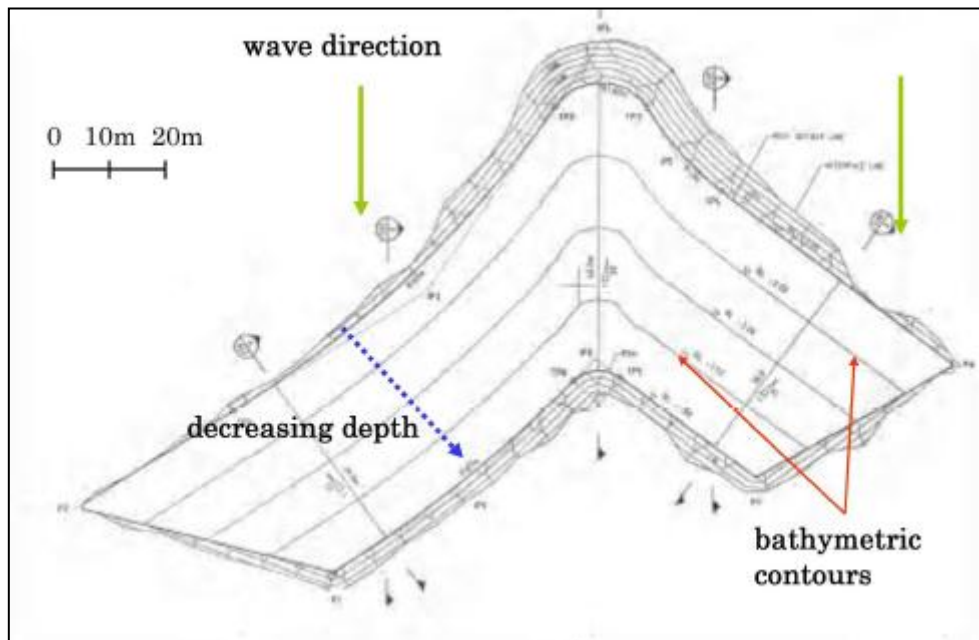


FIGURE 2.21: PLAN VIEW OF CABLE STATION REEF (JOHNSON, 2009)

2.7.4 HAMMOND TANDEM BREAKWATER

In 1989, a two year construction period commenced for the creation of a tandem breakwater system that was developed for the protection of a marina situated in Hammond, Indiana, at the southern end of Lake Michigan (Ryan & Prehn, 2001). The location is shown in figure 2.22.

Lake Michigan has an exposed fetch of hundreds of kilometres over deep water. Consequently, the wind-generated waves that reach the breakwater structure at Hammond are fully developed (Cox & Clark, 1992).

The tandem breakwater is constructed in approximately 4.5 m of water. The design wave for the structure is taken as the 1 in 20 year wave, which has a significant wave height of around 6 m (Cox & Clark, 1992).

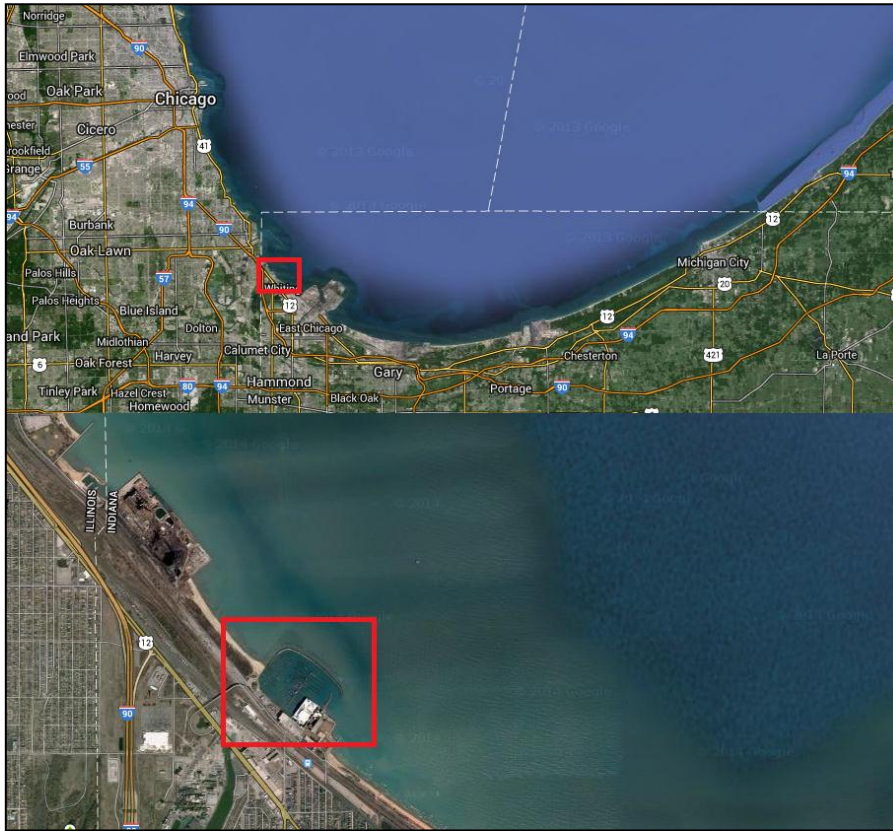


FIGURE 2.22: LOCATION OF HAMMOND TANDEM BREAKWATER (GOOGLE INC., 2014)

During the design stages of the breakwater, several options were considered, the first of which was a conventional rubble mound breakwater. Such a design required armour stone of 8 tons. This design was deemed to be unsatisfactory, because of its high cost and the lack of availability of sufficient material. Further design options included a berm breakwater, a parallel sheet pile wall and a caisson structure, but these were found to be even more expensive than the conventional breakwater design (Cox, 1992).

Following the abovementioned unsuccessful designs, a tandem breakwater system was developed such as described in section 2.3. It was estimated that the implementation of the tandem breakwater system would result in a total cost of \$1 million less than for the conventional rubble mound structure (Cox & Clark, 1992). Figure 2.23 shows the tandem breakwater design. In the figure, the equivalent conventional rubble mound breakwater is also shown. An aerial view of the tandem breakwater is shown in figure 2.24.

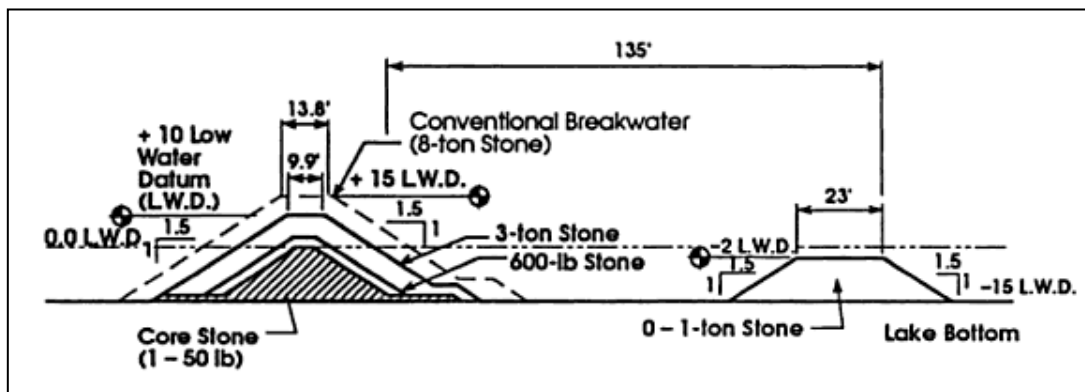


FIGURE 2.23: TANDEM BREAKWATER AT HAMMOND MARINA (COX & CLARK, 1992)

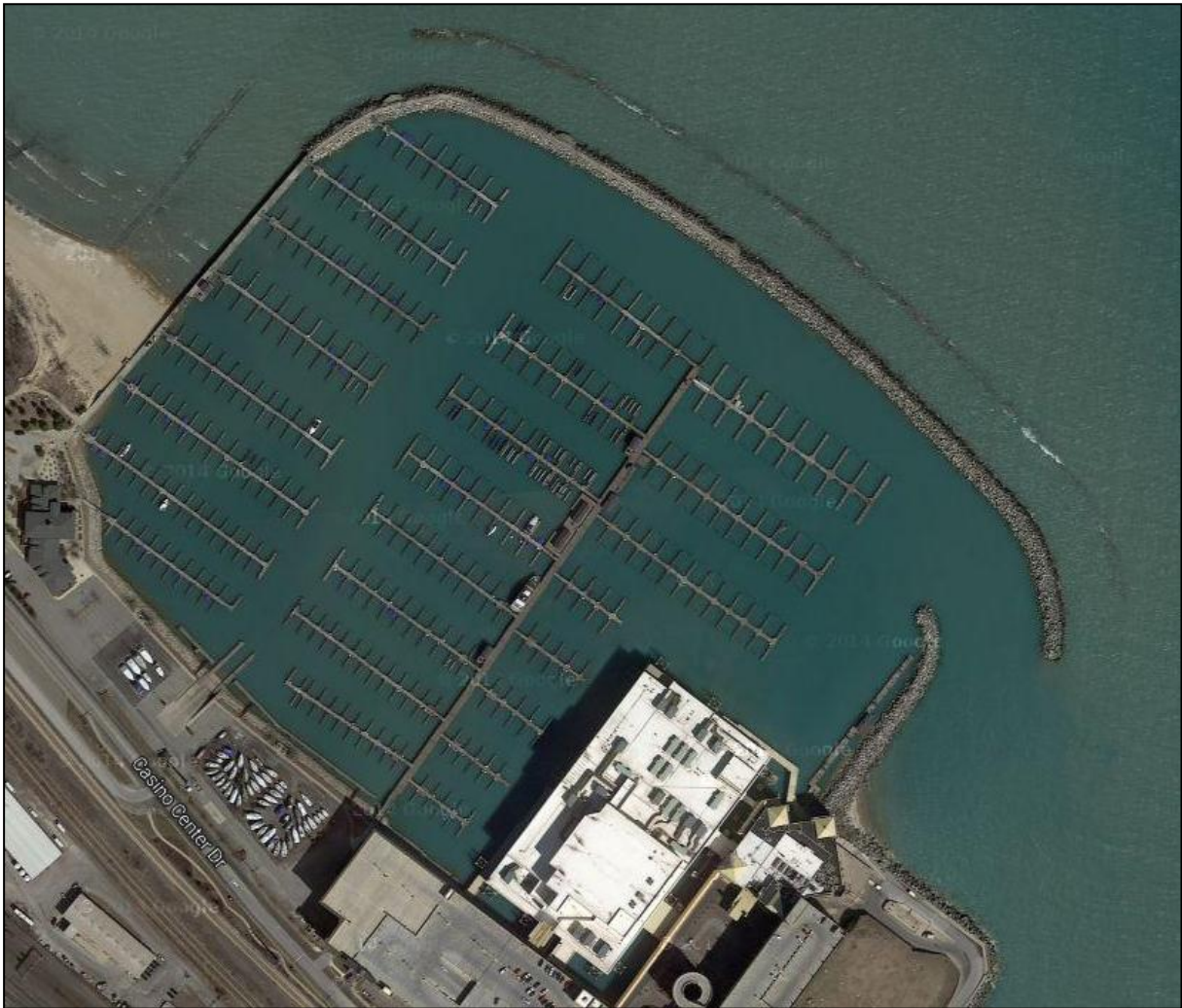


FIGURE 2.24: AERIAL VIEW OF HAMMOND'S TANDEM BREAKWATER (GOOGLE INC., 2014)

Although the application works well in this situation, it should be noted that because the structure is located inside a lake, it is exposed to shorter and smaller waves than it would be if it were located in the open ocean. This also means that tide does not play a significant role.

CHAPTER 3: METHODOLOGY

3.1 GENERAL

This section describes the methodological approach that was followed during the investigation of a tandem breakwater system. The rationale behind the selection of the model types that were used is also discussed. Finally, a case study, which forms the basis of the site conditions of the study, is presented.

3.2 STUDY APPROACH

For this study, the behaviour of a tandem breakwater system under various operational conditions was of interest. Specific areas of interest were: how the damage level of the main rubble mound breakwater is affected by the crest elevation of the submerged reef, as well as how the reef crest elevation affects wave attenuation.

Based on the findings of a review of current literature on the subject of tandem breakwater systems, it was decided that the most efficient way of investigating the behaviour of such a system would be to approximate it with a physical model.

Although numerical models exist that can be used to simulate transmission over submerged reefs, it was decided that they would not be able to provide the accuracy of simulating the various hydraulic processes that a physical model would. The big advantage of using a physical model is that it is not necessary to be able to mathematically describe all the processes that are at work. So long as the scaling of the model is done correctly, the processes that govern the behaviour of the structure will be accurately simulated.

In order to test the influence that a submerged reef has on the wave attenuation and damage level at the main structure, it was first necessary to determine the dimensions of the structure to be tested in the physical model. Instead of designing a breakwater from scratch, it was decided to base the model on an existing structure that might be suitable for the implementation of a tandem breakwater system. Therefore, the investigation becomes a case study for the effects of a tandem breakwater at a specific location.

A South African site that may be suitable for such a structure has been identified in Mossel Bay, although it is subject to further investigation. The identification of the potential location of application was based primarily on the water depths surrounding the breakwater and the steepness of the foreshore slope. Section 3.3 provides information regarding the site.

Tandem breakwater systems are predicted to be the most beneficial when used in relatively shallow water. This is because the probability of a tandem breakwater system providing a cost benefit over a conventional single rubble mound breakwater is higher when it is applied at a site that is located in relatively shallow water and has a gradual sloping foreshore. When the outer reef of a tandem breakwater reduces the significant wave height that reaches the main rubble mound structure, that structure can be designed with smaller armour units. This results in the armour layer being less expensive. However, the additional cost of constructing the reef structure also has to be taken into account. A tandem breakwater system will not provide a cost reduction if the cost of the reef structure outweighs the reduction in armour layer cost it provides. The cost of constructing the reef structure in a tandem breakwater system is strongly related to the water depth at the toe of the main breakwater, the distance between breakwaters and the foreshore slope. The further away the reef is constructed from the main breakwater, the deeper the water is in which its construction takes place, and the more material is needed to construct the structure to the required crest elevation. As always, exceptions do

exist. In certain situations a tandem breakwater could be effective in deeper water. One example of such an exception would be where a natural reef is located at a suitable distance in front of a potential rubble mound breakwater construction site. The tandem breakwater's artificial reef could be constructed on top of the natural reef, which would reduce the amount of material needed for construction, although in such a situation an environmental impact assessment should be conducted beforehand.

Once the location of the application of the tandem breakwater system was identified, the wave conditions found in the surrounding area had to be investigated. This allows for the selection of the test conditions of the various physical model runs. It was decided that two peak periods and two significant wave heights were to be tested. The selection of the conditions was based on literature, as well as numerical wave modelling.

The majority of submerged reefs are designed to be constructed with homogenous size rock, which has proved to be successful in past projects. However, the recent success of using geotextile material in coastal applications has given rise to the possible use of geotubes for the reef structure of a tandem breakwater.

Geotubes provide a few benefits when used as opposed to rock. One is that geotubes are more environmentally friendly with regards to transport emissions. They also provide a cost benefit over the use of rock. Another benefit is that geotubes will most probably provide more efficient wave height reduction than rocks, as the geotube structure will be less permeable and reflect more wave energy. These benefits led to the decision to include the testing of a geotube reef in the physical model, and compare the results to that of a rock reef.

3.3 PORT OF MOSSEL BAY

A site for the possible implementation of a tandem breakwater system has been identified in Mossel Bay. The characteristics of the area seem to be suitable for such an application and therefore a case study involving Mossel Bay is of interest in this investigation.

The port of Mossel Bay is located approximately halfway between Cape Town and Port Elizabeth. It is the smallest commercial port along the coast of South Africa, and concerns itself primarily with the fishing industry, although its facilities to cater for oil industry are expanding.

On Monday, the 2nd of July 2014, the author met up with the harbour engineer of Mossel Bay for a tour of the port. The site visit served a number of purposes, including the visual assessment of the condition of the breakwater and the surrounding waters, as well as the acquiring of certain drawings related to the port.

Among the drawings that were provided by the Transnet National Ports Authority (TNPA) were the layout of the port, the cross-sections at various points along the breakwater and also the water depths around the port, expressed in relation to chart datum (CD).

The location of the port of Mossel Bay along the South African coast is shown in figure 3.1. Figure 3.2 shows the current port layout. The breakwater at Mossel Bay consists of two portions: the old and the new. The old portion refers to the portion of the breakwater that still retains the original armour units with which the breakwater was built approximately 40 years ago (Tulsi & Phelp, 2009). The new portion refers to the portion that has been repaired recently. During the restoration of that portion, the original 6 ton dolos units have been supplemented with 7.5 ton dolos units. The total length of the breakwater, including both old and new portions, is approximately 500 m. The portion of the

breakwater that is considered as a basis for this study is indicated in figure 3.2 as section A-A. For detailed cross-section of section A-A, refer to figure 5.11 in section 5.3.6 of this report.



FIGURE 3.1: LOCATION OF PORT OF MOSSEL BAY (GOOGLE INC., 2014)

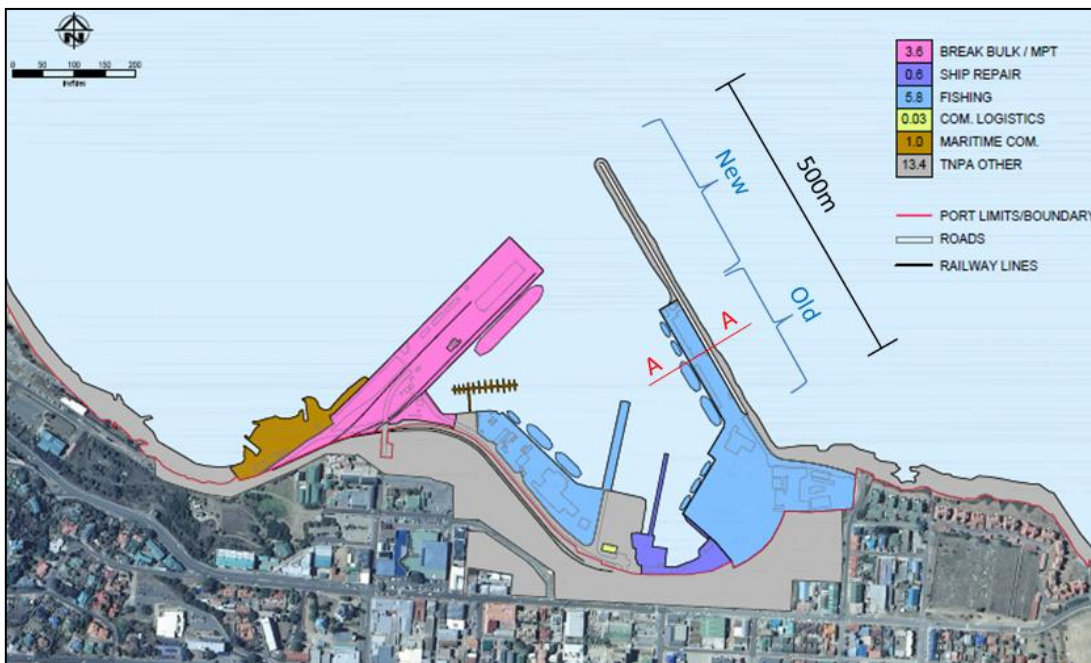


FIGURE 3.2: LAYOUT OF THE PORT OF MOSSEL BAY – ADAPTED FROM TNPA (2014A)

The waters surrounding the Mossel Bay breakwater are relatively shallow. Such conditions are favourable for the implementation of a tandem breakwater system. Water depths at the toe of the structure vary between 3 m and 5 m, depending on the location along the breakwater. Figure 3.3 shows the relative depths around the breakwater.

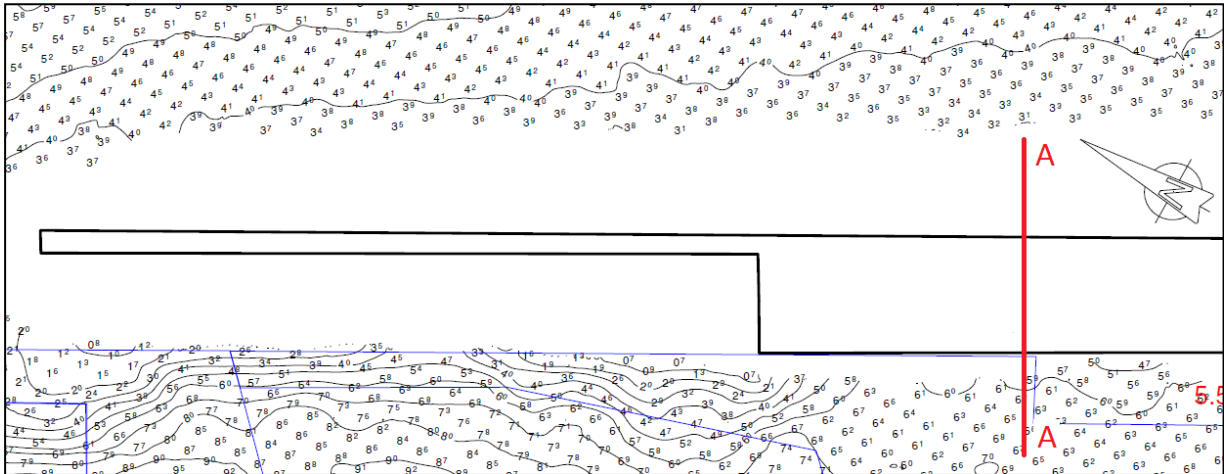


FIGURE 3.3: WATER DEPTHS AROUND MOSSEL BAY BREAKWATER RELATIVE TO CD - ADAPTED FROM TNPA (2014B)

While walking along the Mossel Bay breakwater, evidence of breakwater damage could be seen. At places, broken pieces of dolos units were scattered and at certain points the overtopping wall was damaged. Figure 3.4 shows the view along the breakwater, while figure 3.5 shows damaged sections of the overtopping wall.

From studying the water depths given in figure 3.3 and visually inspecting the breakwater surroundings, it was concluded that Mossel Bay is a good representation of what the typical environment would be for the application of a tandem breakwater system.



FIGURE 3.4: VIEW ALONG MOSSEL BAY BREAKWATER (LOOKING SOUTH-EAST)



FIGURE 3.5: DAMAGED PORTIONS OF THE OVERTOPPING WALL AT VARIOUS POINTS ALONG THE BREAKWATER

CHAPTER 4: NUMERICAL WAVE MODELLING

4.1 GENERAL

This chapter describes the numerical wave modelling performed during the investigation of the wave conditions of the waters surrounding the port of Mossel Bay. The propagation of waves approaching the breakwater structure, from deep water into shallow water, was of particular interest. The most important parameter was the suspected depth-limited significant wave height that reaches the Mossel Bay breakwater. This parameter is eventually used to aid the selection of test conditions used in the physical model study.

The chapter starts off by providing a description of the chosen model, which includes the types of processes that can be modelled, as well as the parameters that can be extracted at specified locations. Thereafter, a description of the set-up of the model is given. This includes the bathymetric data that was used, initial conditions within the model, and the required output parameters. Lastly, the results of the various model runs are given and discussed.

4.2 MODEL SELECTION

Two numerical models were considered to be used for this study, namely SWAN (Simulating Waves Nearshore) and Mike 21 SW (Spectral Waves). In the end, Mike 21 SW was chosen as the model to be used, based primarily on the greater familiarity of the author with the model and its availability.

Mike 21 SW is a third generation spectral wind-wave model developed by the Danish Hydraulics Institute (DHI), capable of simulating the growth, decay and transformation of wind-generated waves and swells in coastal and offshore waters (DHI, 2004).

Mike 21 SW can be run with one of two formulations. The first is the ‘fully spectral formulation’, which is based on the following wave action conservation equation (DHI, 2004):

$$\frac{\partial N}{\partial t} + \nabla(\bar{v}N) = \frac{S}{\sigma} \quad 4-1$$

where

$N(\bar{x}, \sigma, \theta, t)$	=	action density
\bar{x}	=	(x, y) in cartesian coordinates
σ	=	relative angular frequency ($2\pi f$)
θ	=	direction of wave propagation
t	=	time
∇	=	4D differential operator
\bar{v}	=	propagation velocity of wave group in 4D space ($c_x, c_y, c_\sigma, c_\theta$)
S	=	source term for energy balance equation

The source term is given by the following equation (DHI, 2004):

$$S = S_{in} + S_{nl} + S_{ds} + S_{bot} + S_{surf} \quad 4-2$$

where

S_{in}	=	momentum transfer of wind energy to wave generation
S_{nl}	=	energy transfer due to non-linear wave-wave interaction
S_{ds}	=	dissipation of wave energy due to white-capping
S_{bot}	=	dissipation due to bottom friction
S_{surf}	=	dissipation due to depth-induced breaking

The second type of formulation that can be used in the model is the ‘directional decoupled parametric formulation’ that is based on the parameterisation of the aforementioned wave action conservation equation. The parameterisation is made in the frequency domain by introducing the zeroth and first moment of the wave action spectrum as dependent variables (DHI, 2004).

The following physical processes are included in the fully spectral model (DHI, 2004):

- wave growth by action of wind
- non-linear wave-wave interaction
- dissipation due to white-capping
- dissipation due to bottom friction
- dissipation due to depth-induced wave breaking
- refraction and shoaling due to depth variations
- wave-current interaction
- effect of time-varying water depth
- effect of ice coverage on the wave field

A cell-centred finite volume method is used to apply the abovementioned equation in geographical and spectral space. The cells are created by generating an unstructured mesh in the geographical domain (DHI, 2004).

Mike 21 SW software allows the user to extract various types of data at specified points. The following types of data can be requested as an output by the user (DHI, 2004):

- significant wave height
- maximum wave height
- peak wave period
- mean wave period
- peak wave direction
- mean wave direction
- directional standard deviation
- wave velocity components
- radiation stresses
- particle velocities
- wave power

4.3 MODEL SET-UP

This section gives a description of how the Mike 21 SW model was set up for the Mossel Bay case study. The inputs and outputs that were specified in the model are described, before concluding with a discussion of the model runs and the accompanying results.

4.3.1 BATHYMETRY

The numerical wave model was used to find a relationship between the deep water conditions and the corresponding significant wave heights that are encountered inside Mossel Bay, with specific emphasis on the significant wave height at the toe of the breakwater.

As mentioned in section 4.2, a Mike 21 SW model was chosen as the numerical model to be used. The first step in the setting-up of the numerical model was to import the bathymetric data. Such a data set of Mossel Bay was acquired in digital form from the CSIR in Stellenbosch (CSIR, 2014). The map projection of the co-ordinates is WGS_1984_UTM_Zone_35S. Figure 4.1 shows the data points after being imported into the model. Mossel Bay is indicated inside the red rectangle.

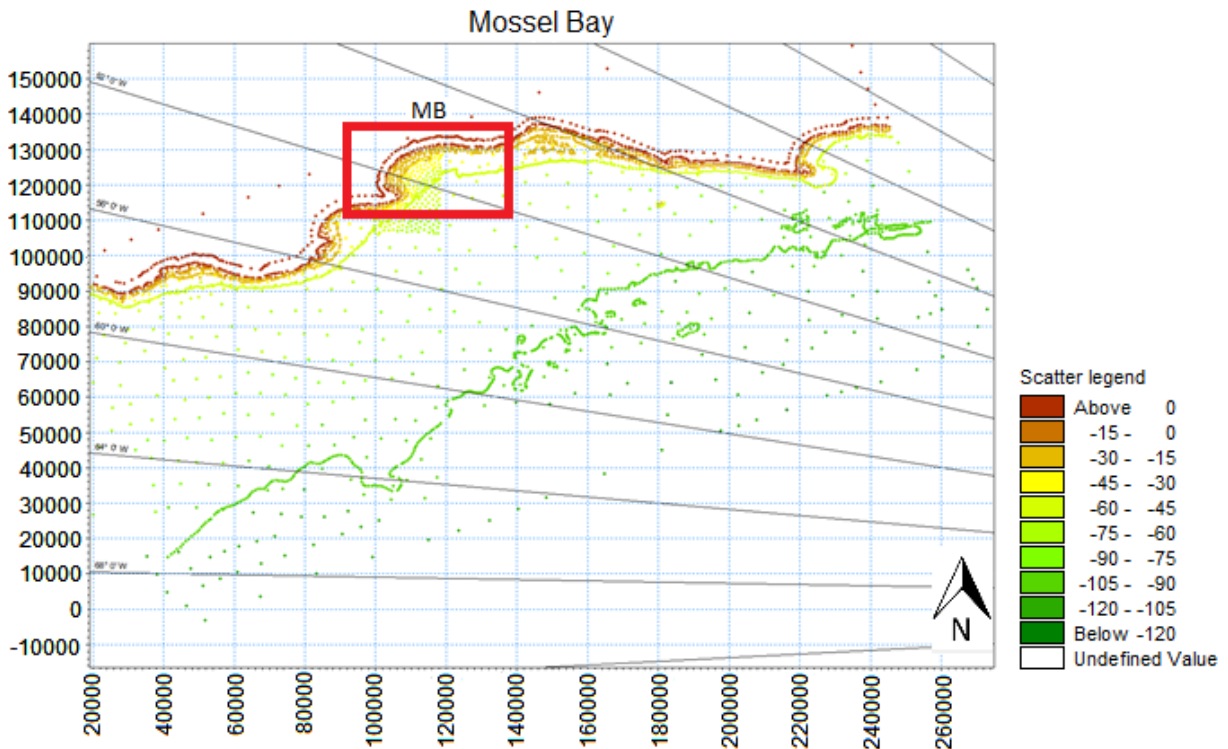


FIGURE 4.1: SCATTER DATA PLOT OF MOSSEL BAY

The next step was to create a mesh from the scatter data. In an attempt to be economical with regards to computational time, different cell sizes were defined for various areas within the model. The cells start off very large in deep water and reduce in size as they approach the shore. The cells in the bay itself, where the point of interest is located, form a fine grid.

The boundary for the model was taken as wide as the available data allows. Inside these boundaries eleven polygons were defined. These polygons contained different amounts of cells depending on where they are located. Figure 4.2 shows the mesh that was generated for the model.

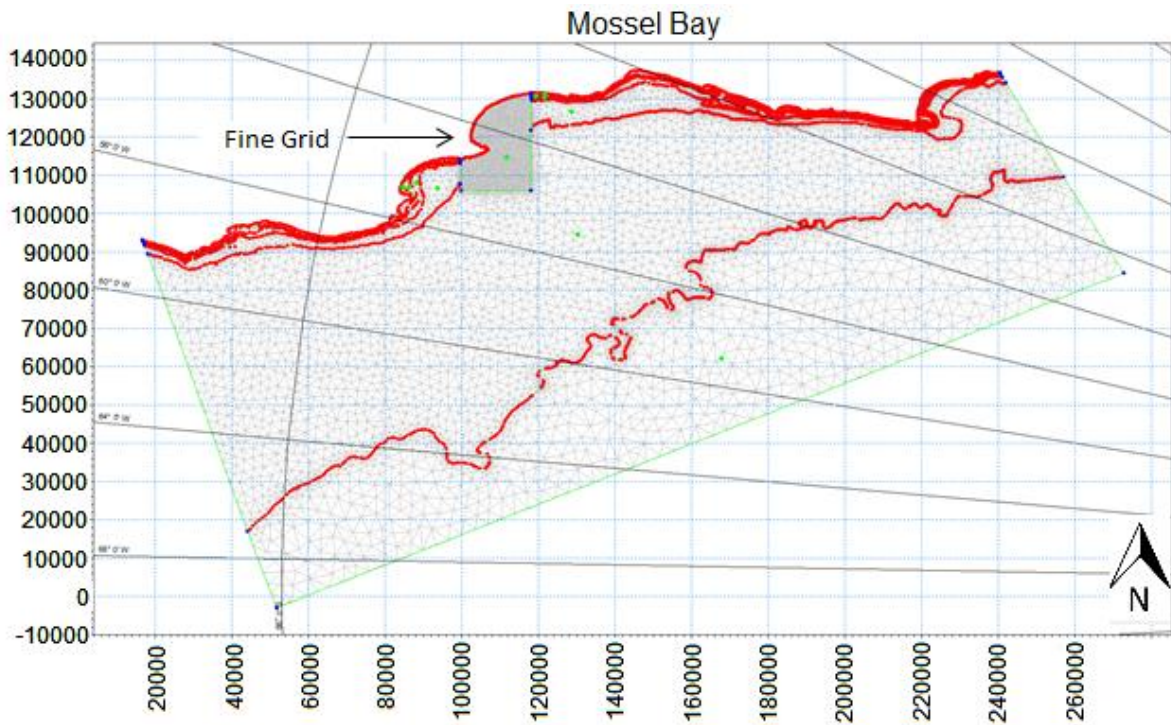


FIGURE 4.2: MOSSEL BAY MESH

In the bathymetric data, a big portion of the area inside the bay has a high resolution. This improves the accuracy of the model. To further increase the accuracy, the entire high resolution portion was covered by a fine mesh.

An unstructured triangular mesh was generated from the different cell sizes defined over the model area. By interpolating between the known depth values, it was possible to simulate the entire area within the boundary. Figure 4.3 shows the resulting bathymetry that was used as the model domain.

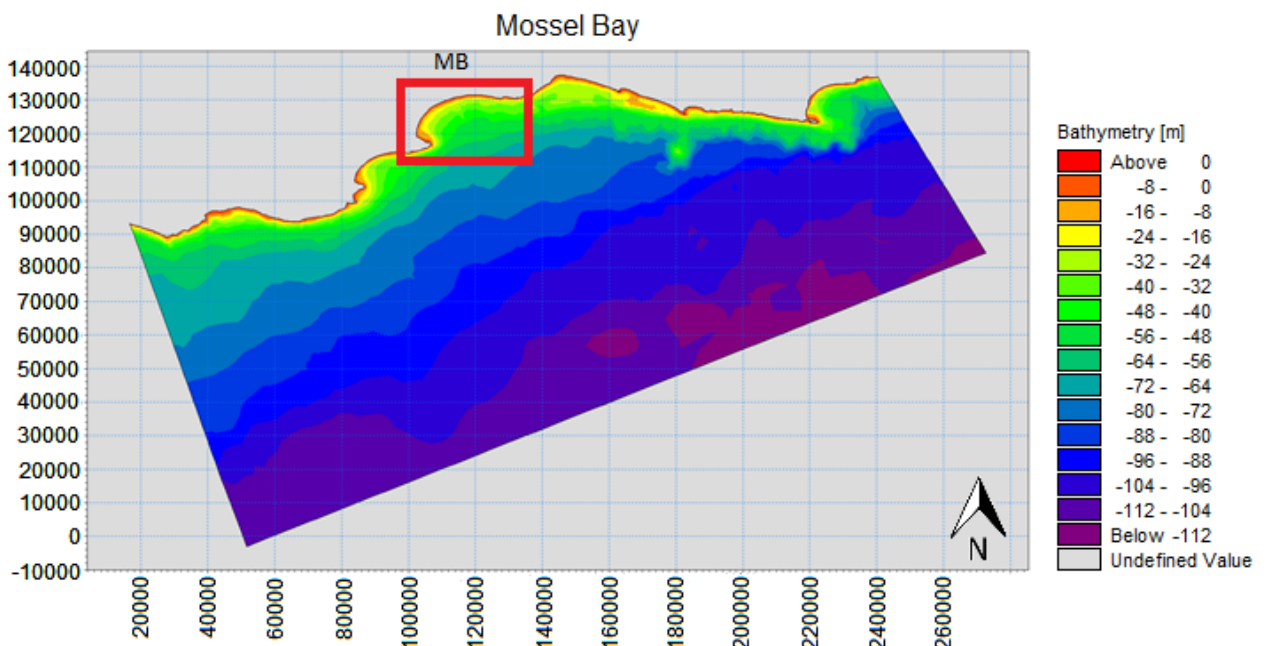


FIGURE 4.3: NUMERICAL MODEL BATHYMETRY

4.3.2 MODEL INPUTS

This section is dedicated to the description of the input values used during the set-up of the Mike 21 SW model.

The generated bathymetry, as described in the previous section, was used as the domain for the Mike 21 SW model.

Four boundaries were defined in the domain. Two of these were lateral boundaries, while the other two were a land boundary and a generation line respectively. The land boundary is self-explanatory. The lateral boundaries allow energy to pass through them laterally. The generation line is where the initial wave conditions are defined. Here it is possible to change the significant wave height, peak period and mean wave direction. The four boundaries are shown in figure 4.4.

The number of time steps was set to zero, as this is a spectral averaging model, which means that the wave spectrum is regarded as a whole instead of several individual waves.

The ‘directionally decoupled parametric formulation’, as described in section 4.2 was used as the basic spectral formulation of the model, while the ‘quasi stationary formulation’ was used for the time formulation. For this type of time formulation, the time is removed as an independent variable and a steady state solution is calculated for each step (DHI, 2004).

For the directional discretisation, a 360 degree rose was used, that was divided up into 36 directions. Thus, each direction was defined by 10 degrees.

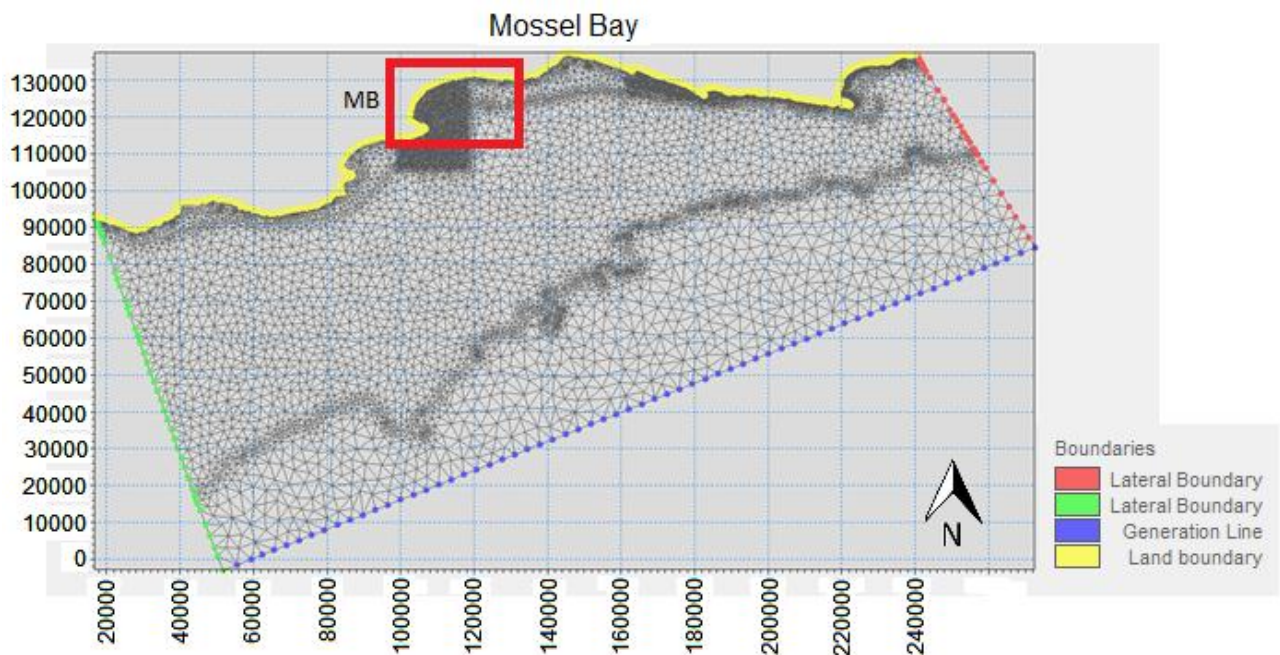


FIGURE 4.4: NUMERICAL MODEL BOUNDARY LAYERS

The water level in the model did not vary with time. It was set to be constant at mean level (ML), i.e. 1.17 m above CD. The average water level in the area was chosen due to the fact that the study of the tandem breakwater system is intended to be applied more generally as well. The same water level was later used in the physical model, as described in chapter 5.

The model did not take into consideration the effects of currents on the significant wave heights. Waves generated by winds were also not simulated in the model.

Effects that were included in the model are:

- non-linear wave-wave interaction
- dissipation due to white-capping, bottom friction and depth-induced breaking
- refraction and shoaling due to water depth variation

4.3.3 MODEL OUTPUTS

Two model output locations were defined for this model. The first was an area series that covers the entire area within the boundaries of the model. This gives an indication of how the wave condition changes as it approaches the bay. The second output was a single point of interest inside the model. The output location was at the toe of the Mossel Bay breakwater. Figure 4.5 shows the relative position of the breakwater output point within the model.

As was mentioned in section 3.3, this investigation considered a typical cross-section of the old portion of the Mossel Bay breakwater. Therefore, the breakwater output point that was defined in the numerical model had to be located in front of the section under consideration. Figure 4.6 shows the location of the breakwater output point relative to the breakwater.

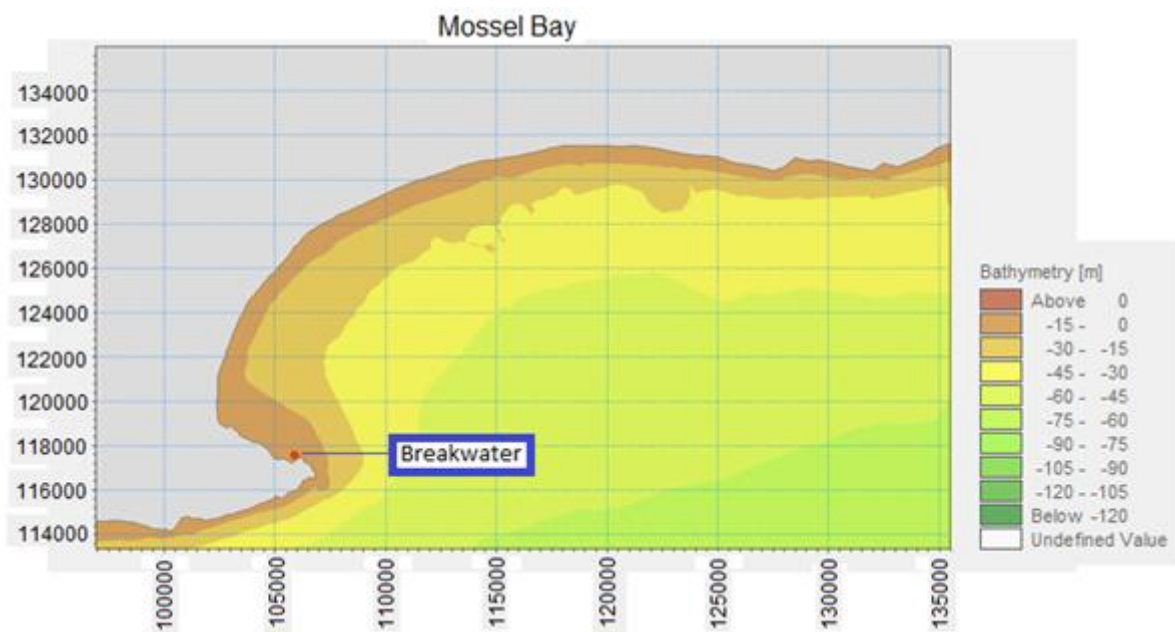


FIGURE 4.5: POSITION OF BREAKWATER OUTPUT POINT IN NUMERICAL MODEL

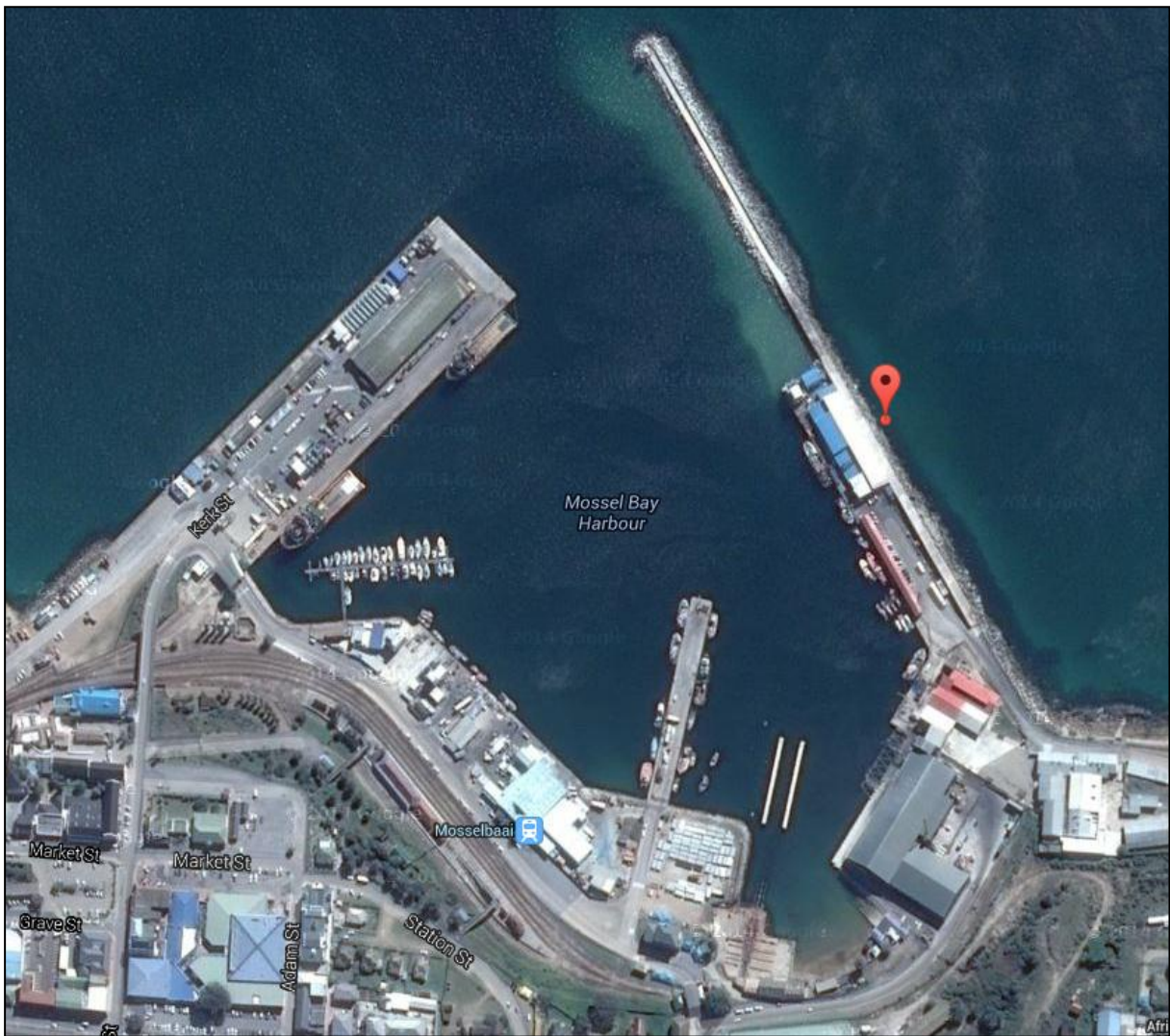


FIGURE 4.6: POSITION OF BREAKWATER OUTPUT POINT RELATIVE TO BREAKWATER (GOOGLE INC., 2014)

4.3.4 MODEL RUNS

A series of different model runs was performed in an attempt to find a relationship between the deep water conditions and the conditions at the point of interest inside the bay, i.e. at the toe of the breakwater.

A CSIR waverider is located inside the bay, which records data regarding various parameters related to the wave conditions. Unfortunately, the wave data does not provide information regarding the mean wave direction. This causes difficulty for specifying the conditions in the model.

The most severe wave conditions around South Africa are encountered along the south and south-west coasts. This severity decreases when moving towards the west and east coasts. Little variance is seen in the wave periods along the coast. The predominant wave direction found along the coast is somewhere between the south-west and south-south-west directions (Rossouw & Theron, 2009). An overview of the wave height and period distribution around the South African coast is given in figure 4.7.

From figure 4.7 it can be seen that the peak period for the waves approaching Mossel Bay lies between 6 s and 14 s. In this range, two symmetrically spaced peak periods were selected to be investigated, namely 8 s and 12 s. The $H_{m0}^{50\%}$ and $H_{m0}^{1\%}$, also indicated in figure 4.7, are defined as the significant wave height that is exceeded 50% and 1% of the time respectively. These values correspond to hindcast predictions made in a water depth of 150 m, as produced by a NCEP model of the water around South Africa (Rossouw & Theron, 2009).

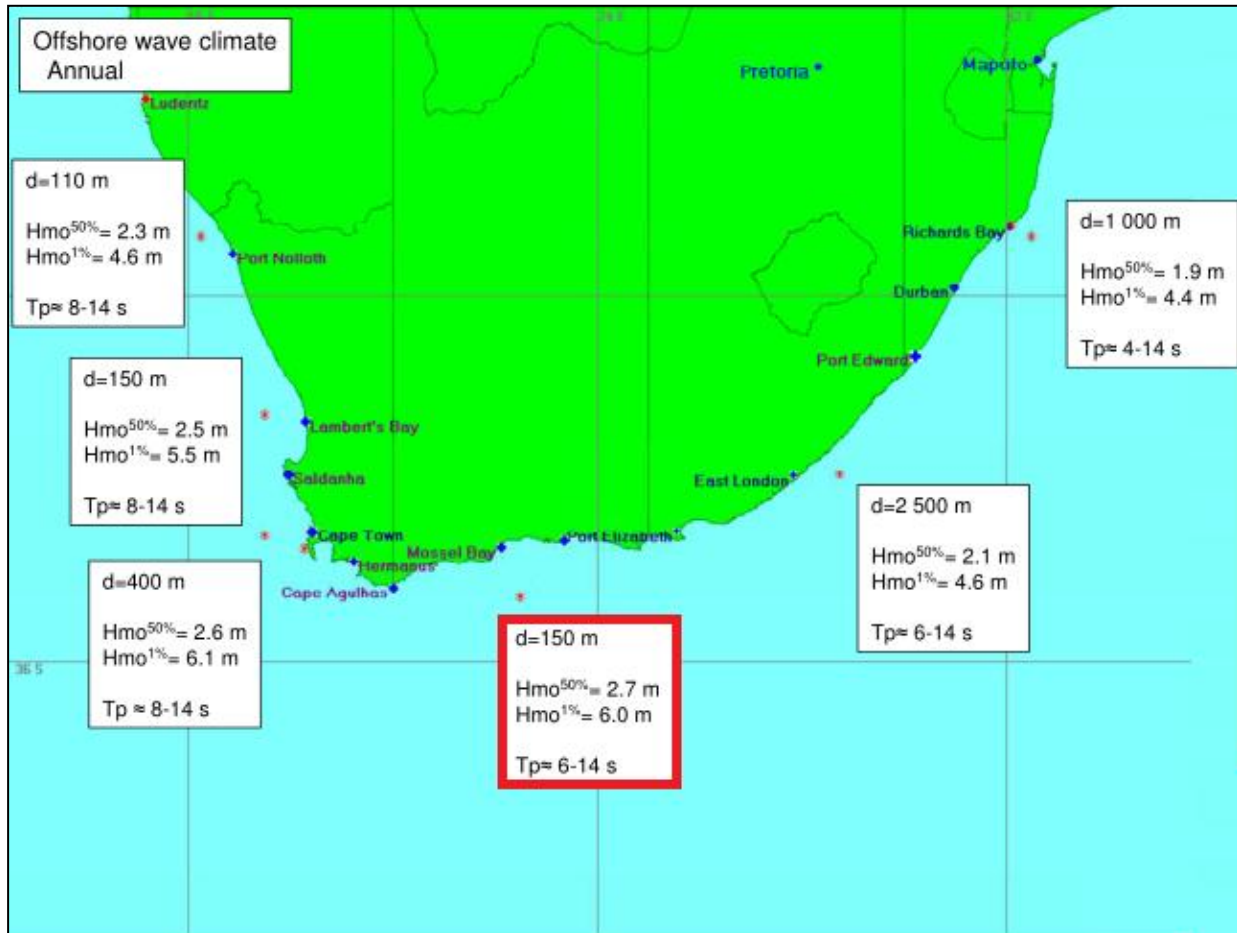


FIGURE 4.7: OVERVIEW OF WAVE HEIGHT AND PERIOD DISTRIBUTION AROUND SOUTH AFRICAN COAST AS PREDICTED WITH NCEP MODEL (ROSSOUW & THERON, 2009)

Two mean wave directions were considered during the modelling, namely south-south-west and east. The first of the two directions represent the predominant wave direction along the coast, while the second direction is representative of a case where waves propagate into Mossel Bay from a direction in which the headland does not provide much sheltering.

Table 4.1 shows the various wave runs that were performed. Information is shown regarding the deep water conditions, which include significant wave height, peak period and mean wave direction, as well as the corresponding significant wave heights encountered at the breakwater. For all the wave runs, the water level was set to ML, as mentioned previously.

TABLE 4.1: NUMERICAL MODEL WAVE RUNS

Test Name	Sig. Wave Height (Deep Water) Hm0 (Deep Water) [m]	Peak Period Tp [s]	Mean Wave Direction MWD [-]	Sig. Wave Height (BW) Hm0 (BW) [m]
WR01	4	8	SSW	0.8
WR02	4	12	SSW	1.2
WR03	6	8	SSW	0.9
WR04	6	12	SSW	1.6
WR05	8	8	SSW	0.9
WR06	8	12	SSW	1.8
WR07	4	8	E	1.7
WR08	4	12	E	1.9
WR09	6	8	E	1.8
WR10	6	12	E	2.2
WR11	8	8	E	1.8
WR12	8	12	E	2.3

The results in table 4.1 indicate that the wave heights encountered at the breakwater are significantly lower when waves propagate into the bay from a south-south-westerly direction than from an easterly direction. The waves are between 20% and 54% lower at the breakwater, depending on deep water conditions (wave height and period).

The maximum significant wave height expected to be encountered at the breakwater from the easterly direction is 2.3 m and is as a result of the 8 m 12 s deep water wave condition. The 6 m 12 s condition produces a fairly similar result of 2.2 m. According to Rossouw & Theron (2009), the expected deep water significant wave height that is exceeded 1% of the time in the waters surrounding Mossel Bay, is 6 m. The occurrence of a wave with a significant wave height of more than 6 m is therefore unlikely. It is safe to say that the waves that reach the breakwater when the water level corresponds to ML are depth-limited to around 2.3 m.

When dealing with depth-limited breaking, the water depth is of course extremely important. In the case under consideration, water depth fluctuations due to the tidal effect, for example, will result in a larger depth-limited significant wave height occurring at the toe of the breakwater. Therefore, when discussing depth-limited waves, it is important to link the values to the sea water level. In this case, the depth-limited significant wave height of 2.3 m is associated with a sea water level located at ML.

The abovementioned depth-limited significant wave height should not be confused with the design wave height. A design wave is typically a significant wave height that occurs at an intended structure's construction site, in extreme storm conditions. How 'extreme' this storm condition is, is a matter of risk and cost. If it is decided that the design condition for a proposed structure should be that of a 1 in 100 year storm, the risk of the design condition being exceeded in the lifetime of the structure would be lower, but the associated cost higher, than if the structure was designed for a 1 in 25 year storm, for example.

When deciding upon a design wave, especially when investigating a site which has depth-limited wave breaking, the design water level would include factors such as tide, storm surge, and in recent times, sea level rise.

The figures that follow show the outputs of the depth-limited significant wave height at the Mossel Bay breakwater, associated with the various deep water wave conditions that were modelled. All model runs were conducted for a general representation of the water conditions surrounding Mossel Bay, in which an average tide level was considered, and no storm surge or sea level rise effects.

Deep Water Conditions for WR01:

Significant Wave Height = 4 m
 Peak Period = 8 s
 Mean Wave Direction = SSW

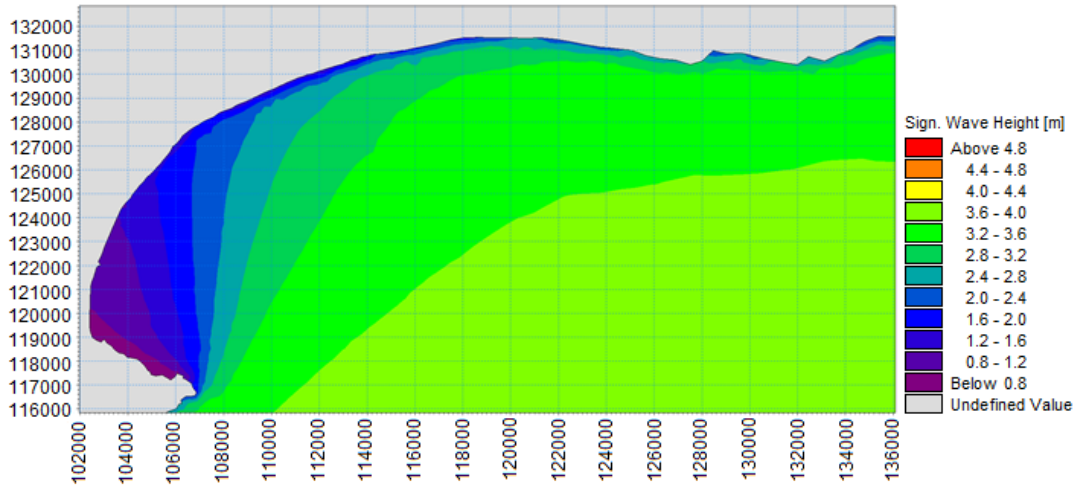


FIGURE 4.8: SIGNIFICANT WAVE HEIGHTS AROUND MOSSEL BAY (4M 8S SSW)

Deep Water Conditions for WR02:

Significant Wave Height = 4 m
 Peak Period = 12 s
 Mean Wave Direction = SSW

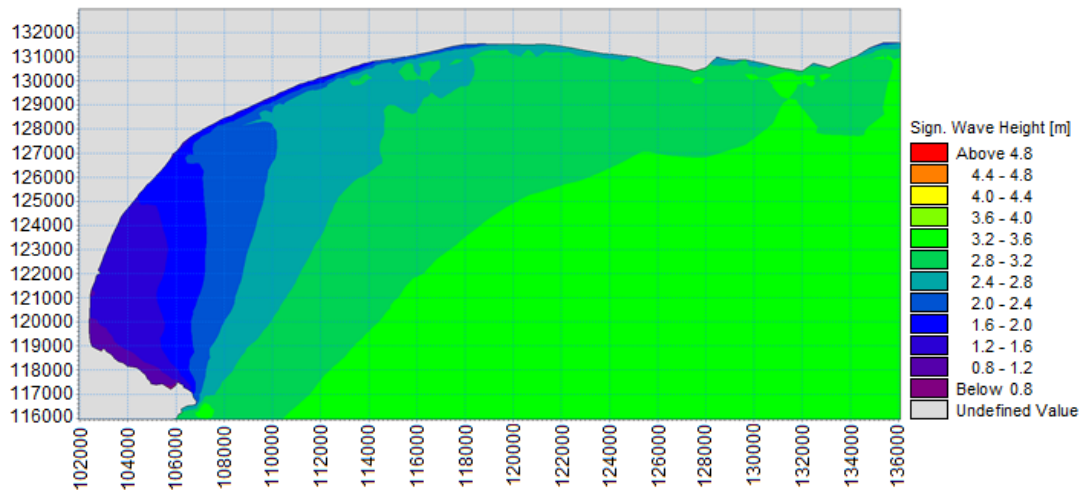


FIGURE 4.9: SIGNIFICANT WAVE HEIGHTS INSIDE MOSSEL BAY (4M 12S SSW)

Deep Water Conditions for WR03:

Significant Wave Height = 6 m

Peak Period = 8 s

Mean Wave Direction = SSW

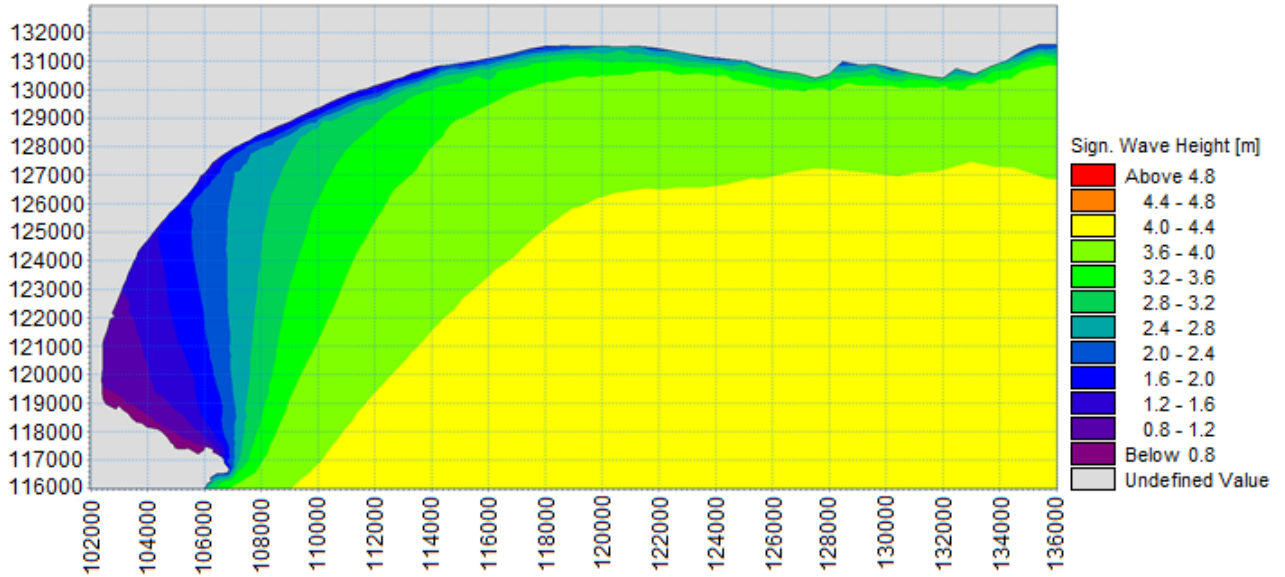


FIGURE 4.10: SIGNIFICANT WAVE HEIGHTS AROUND MOSSEL BAY (6M 8S SSW)

Deep Water Conditions for WR04:

Significant Wave Height = 6 m

Peak Period = 12 s

Mean Wave Direction = SSW

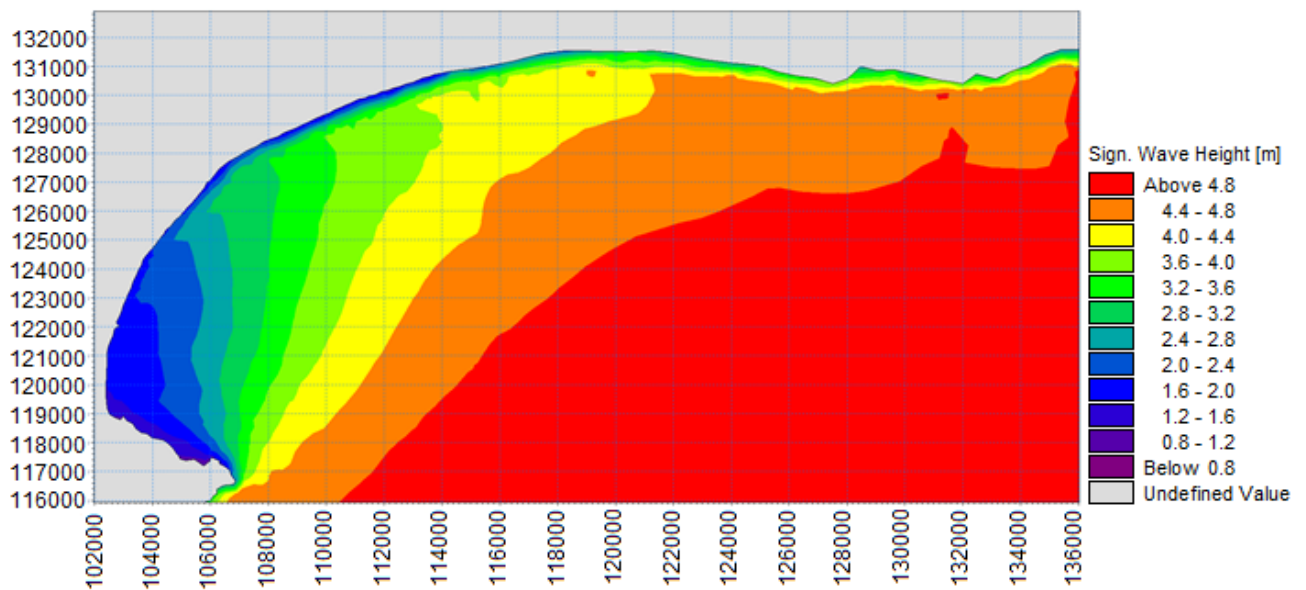


FIGURE 4.11: SIGNIFICANT WAVE HEIGHTS INSIDE MOSSEL BAY (6M 12S SSW)

Deep Water Conditions for WR05:

Significant Wave Height = 8 m

Peak Period = 8 s

Mean Wave Direction = SSW

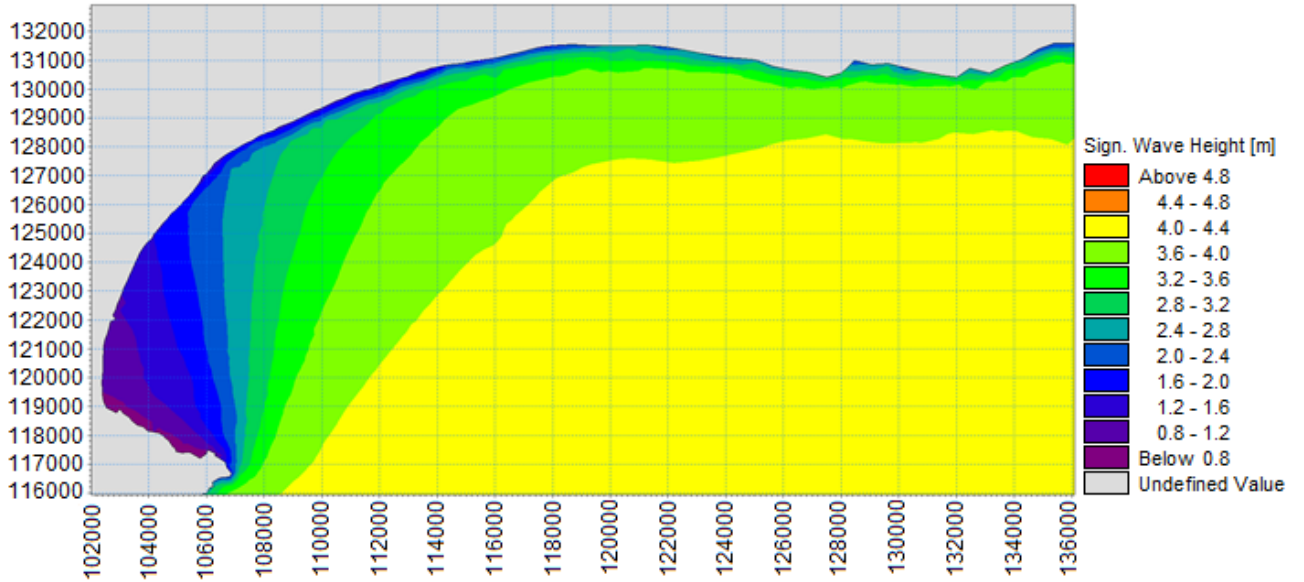


FIGURE 4.12: SIGNIFICANT WAVE HEIGHTS AROUND MOSSEL BAY (8M 8S SSW)

Deep Water Conditions for WR06:

Significant Wave Height = 8 m

Peak Period = 12 s

Mean Wave Direction = SSW

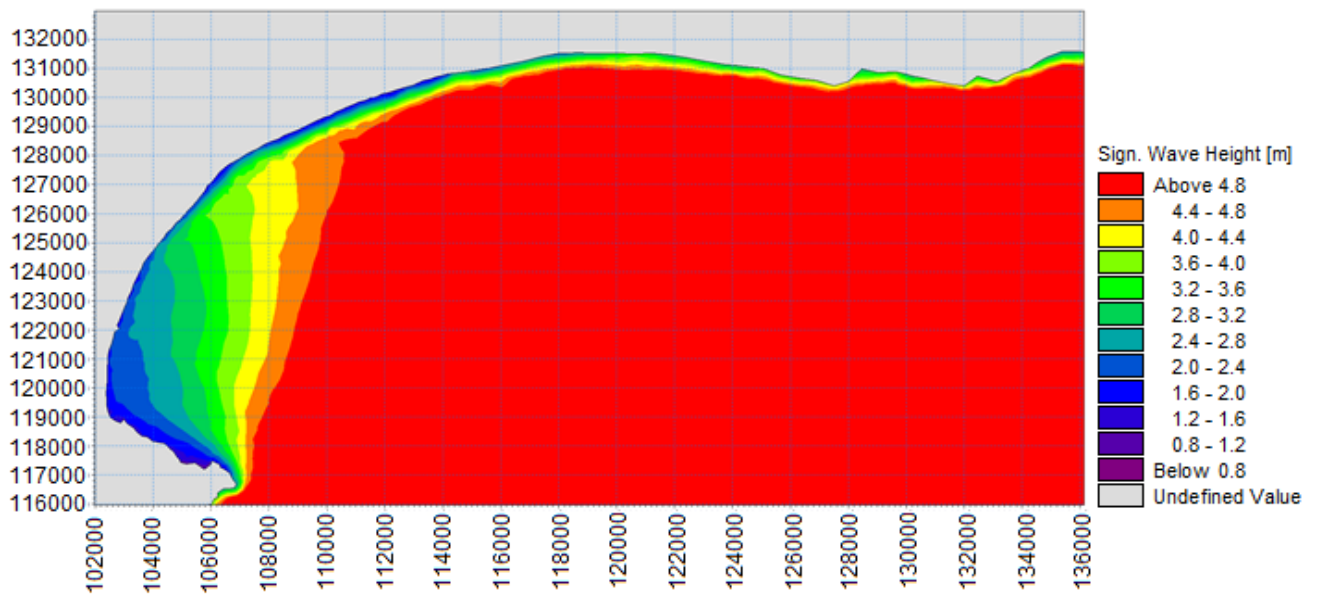


FIGURE 4.13: SIGNIFICANT WAVE HEIGHTS INSIDE MOSSEL BAY (8M 12S SSW)

Deep Water Conditions for WR07:

Significant Wave Height = 4 m

Peak Period = 8 s

Mean Wave Direction = E

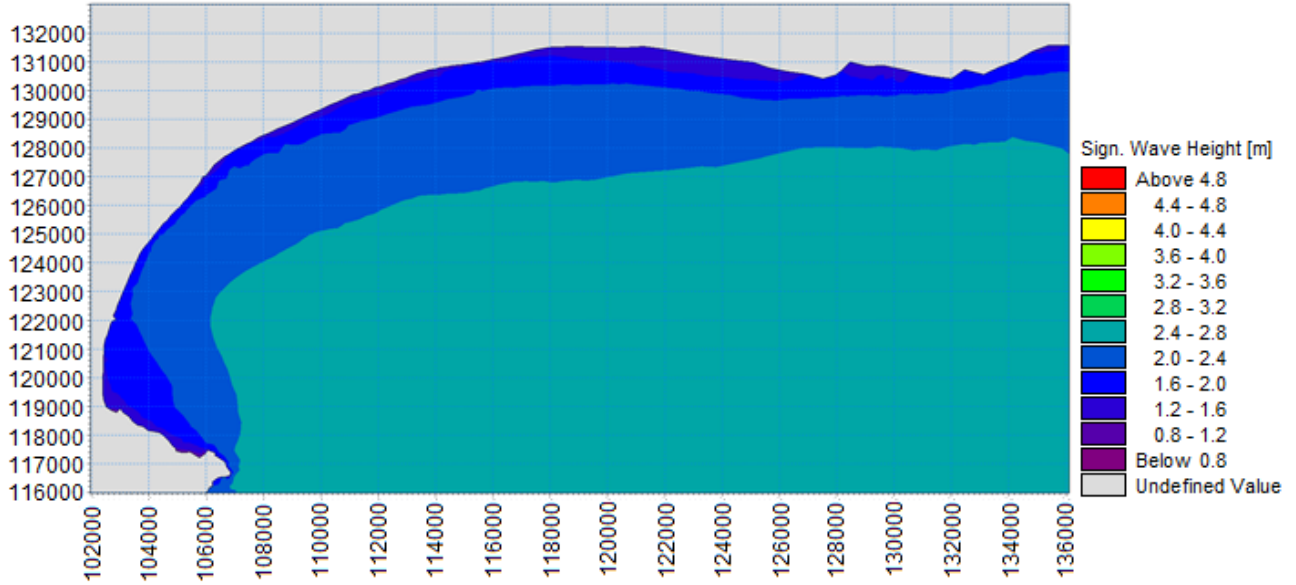


FIGURE 4.14: SIGNIFICANT WAVE HEIGHTS AROUND MOSSEL BAY (4M 8S E)

Deep Water Conditions for WR08:

Significant Wave Height = 4 m

Peak Period = 12 s

Mean Wave Direction = E

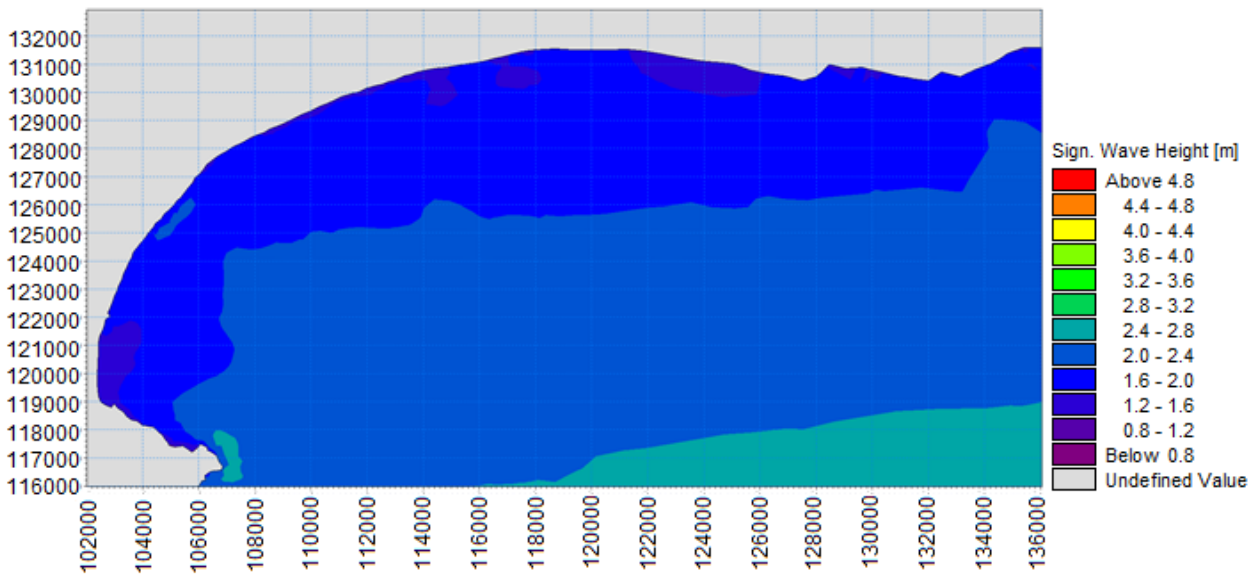


FIGURE 4.15: SIGNIFICANT WAVE HEIGHTS INSIDE MOSSEL BAY (4M 12S E)

Deep Water Conditions for WR09:

Significant Wave Height = 6 m

Peak Period = 8 s

Mean Wave Direction = E

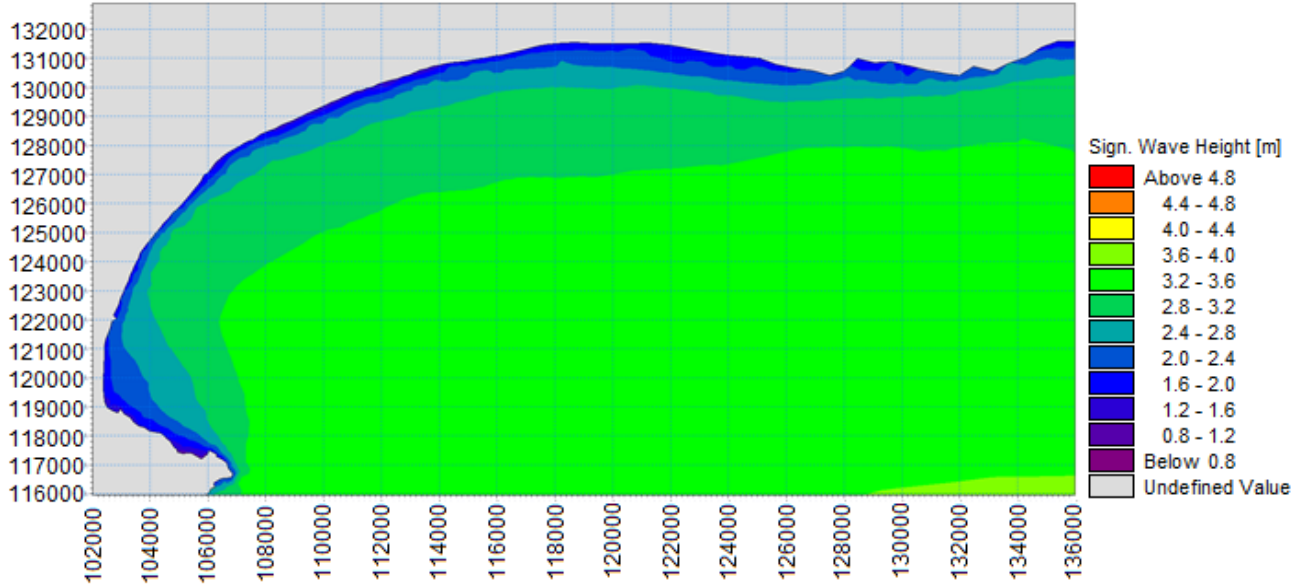


FIGURE 4.16: SIGNIFICANT WAVE HEIGHTS AROUND MOSSEL BAY (6M 8S E)

Deep Water Conditions for WR10:

Significant Wave Height = 6 m

Peak Period = 12 s

Mean Wave Direction = E

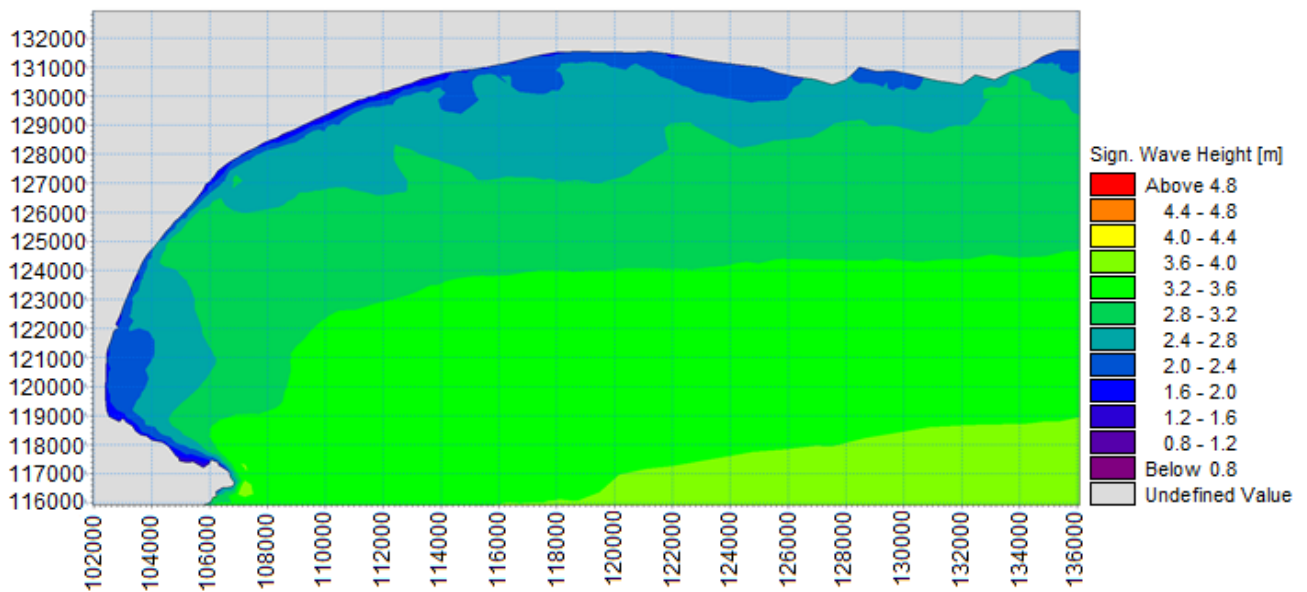


FIGURE 4.17: SIGNIFICANT WAVE HEIGHTS INSIDE MOSSEL BAY (6M 12S E)

Deep Water Conditions for WR11:

Significant Wave Height = 8 m

Peak Period = 8 s

Mean Wave Direction = E

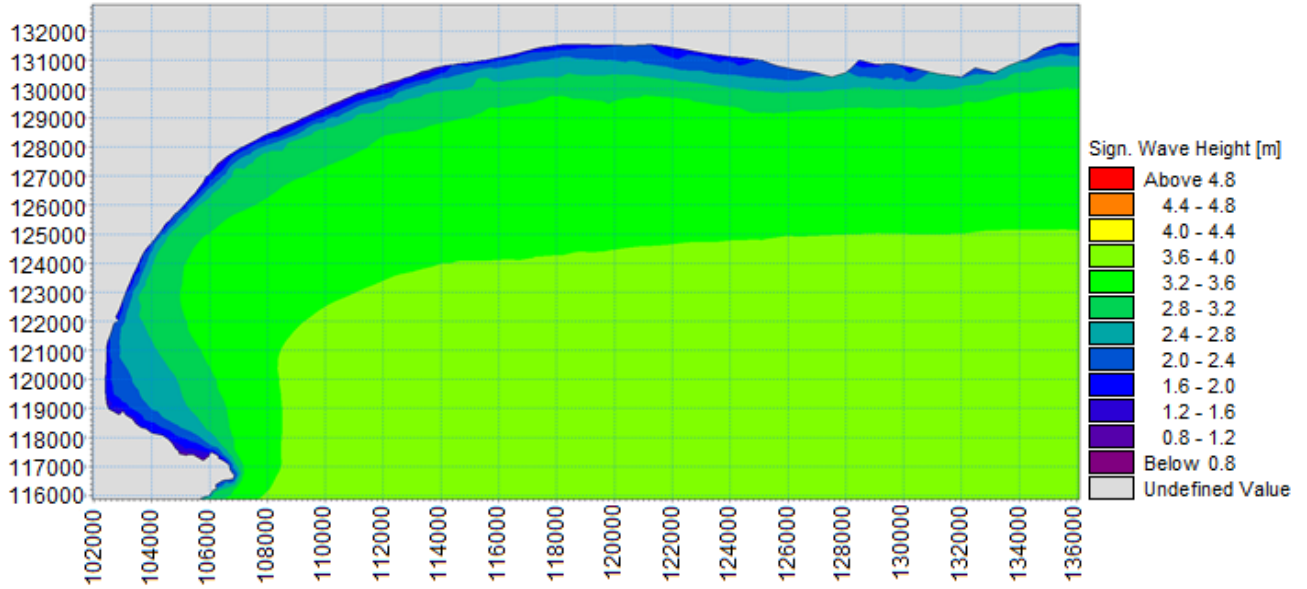


FIGURE 4.18: SIGNIFICANT WAVE HEIGHTS AROUND MOSSEL BAY (8M 8S E)

Deep Water Conditions for WR12:

Significant Wave Height = 8 m

Peak Period = 12 s

Mean Wave Direction = E

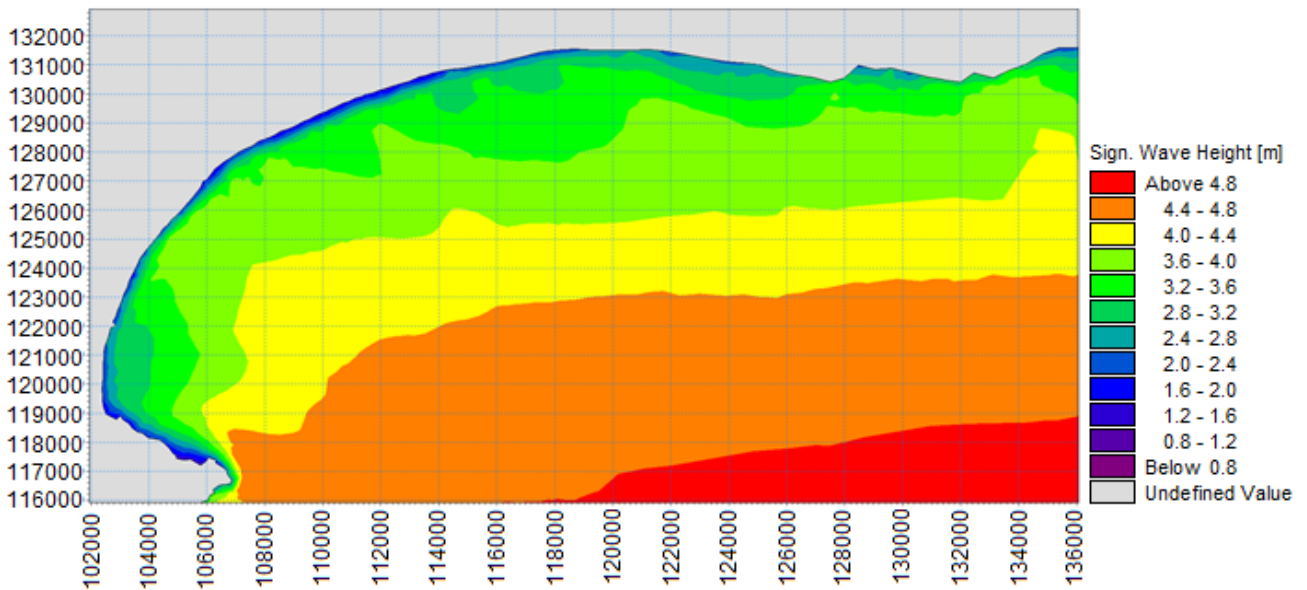


FIGURE 4.19: SIGNIFICANT WAVE HEIGHTS INSIDE MOSSEL BAY (8M 12S E)

The next two figures give a graphical representation of how the two mean wave directions, south-south-west and east, compare with regards to the significant wave heights that reach the breakwater.

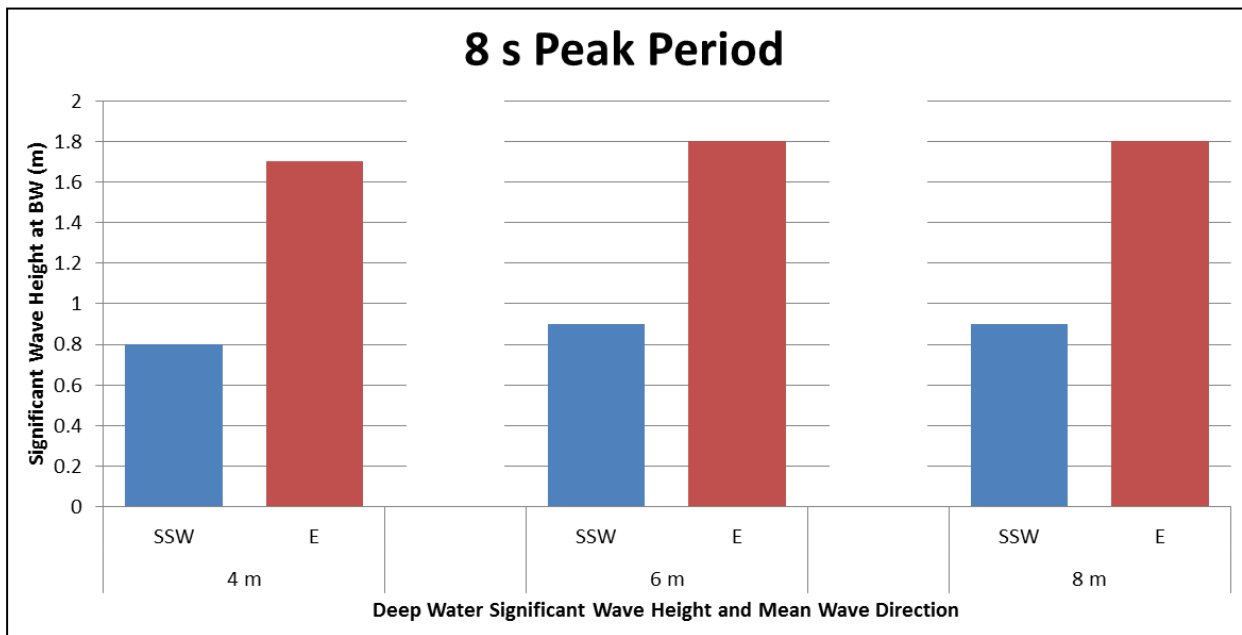


FIGURE 4.20: COMPARISON OF SIGNIFICANT WAVE HEIGHTS OF 8S WAVE

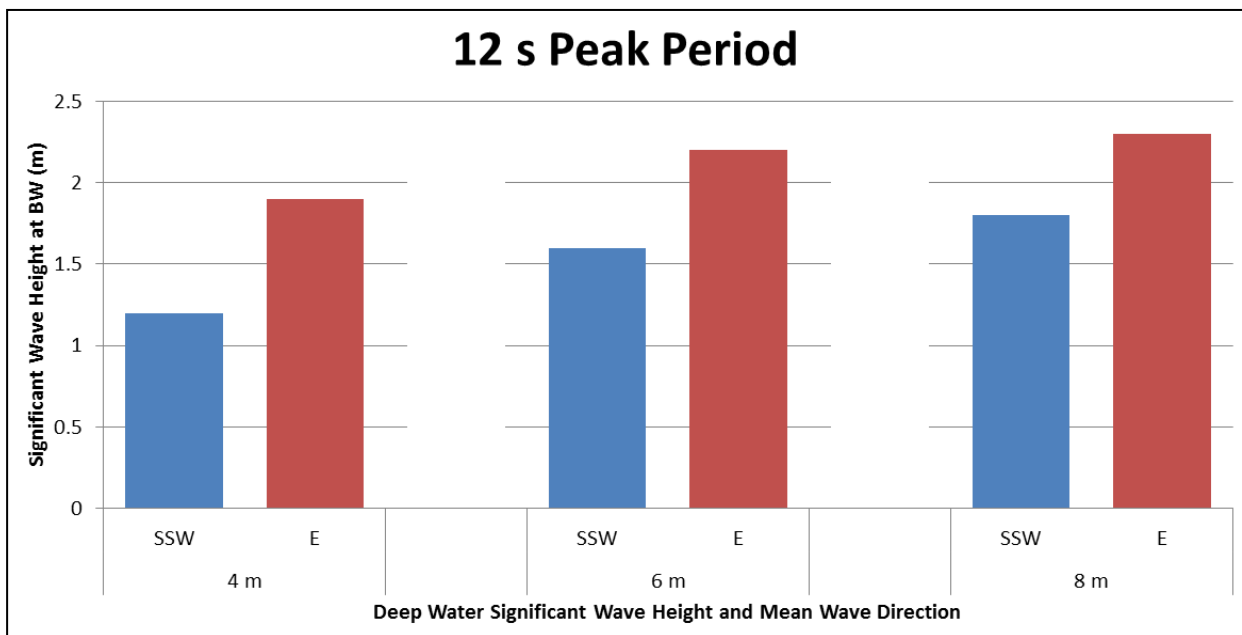


FIGURE 4.21: COMPARISON OF SIGNIFICANT WAVE HEIGHTS OF 12S WAVE

The information given in this chapter provides insight into the typical wave conditions in and around Mossel Bay, and is used to aid in the selection of the test conditions used in the physical model study, as described in chapter 5. It was found that the depth-limited significant wave height at the toe of the breakwater is 2.3 m for a water level associated with an average tide condition. Furthermore, the mean wave direction of the deep water waves plays an important role in the significant wave height that reaches the breakwater. The breakwater is fairly well protected from waves propagating from a south-south-westerly direction by the headland located just to its south. However, in the event that waves propagate from an easterly direction, the protection provided by the headland is significantly less.

4.4 SUMMARY

The propagation of various deep water wave conditions into Mossel Bay was simulated with the aid of a Mike 21 SW model. Three deep water significant wave heights (4 m, 6 m, and 8 m) were tested with two peak periods (8 s and 12 s) and two mean wave directions (SSW and E) at one water level (ML). From the model's output, the depth-limited significant wave height at the structure's toe could be determined. It was found that waves propagating into the bay area from the E result in significantly higher wave heights at the structure. This is as expected, as the headland provides sheltering against waves propagating from the SSW. The results in this chapter is used to aid in the selection of the test conditions used in the physical model study of a tandem breakwater system located in Mossel Bay, as described in chapter 5.

CHAPTER 5: PHYSICAL MODELLING

5.1 GENERAL

In this chapter a detailed description of the set-up of the physical model is given. First the design and construction of the main rubble mound structure is discussed, which includes detail about the bathymetry, design wave height, type of armour units, model scale, grading of rock material and breakwater dimensions. Thereafter, the modelling of both types of reef structures are discussed; rock and geotube.

5.2 MODEL FACILITY AND EQUIPMENT

The physical model study was conducted in the Coastal and Hydraulics Laboratory of the Council for Scientific and Industrial Research (CSIR) in Stellenbosch. The equipment used during the physical modelling process is discussed in the following sub-sections.

5.2.1 2D CONCRETE FLUME

The breakwater system under consideration was constructed in the laboratory's 2D concrete flume, which has dimensions of 0.75 m wide x 1.0 m deep x 30 m long. Figure 5.1 shows an image of the concrete flume in which the tests were performed.



FIGURE 5.1: 2D CONCRETE FLUME

5.2.2 WAVEMAKER

A single-paddle wavemaker, which spans the width of the flume, is responsible for producing either regular or irregular (random) waves. In the case where random waves are selected, the wavemaker receives a signal from its control computer that communicates either a standard spectral shape, such as JONSWAP or Pierson-Moskowitz, or a user-defined spectrum. In the latter, a series of spectral densities and their associated frequencies are manually input into a file by the user before it is sent to the wavemaker. The wavemaker is also equipped with dynamic wave absorption (DWA) technology. This enables it to adjust each consecutive paddle stroke to compensate for any wave energy that might have been reflected by the model under consideration. This technology was developed so as to overcome the problem of waves being re-reflected off the paddle, which could cause the wave spectra to contain unwanted reflections (HR Wallingford, 2014). In figure 5.2, the top of the single-paddle wavemaker is shown, as well as the control room containing the wavemaker computer.

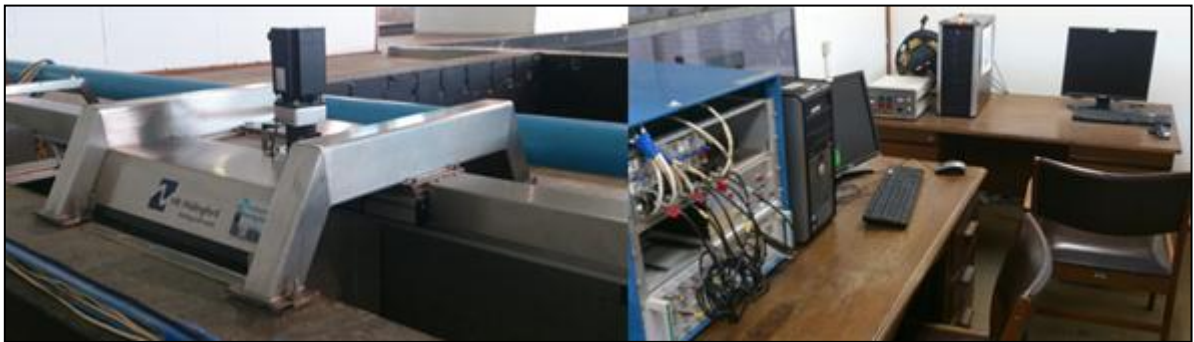


FIGURE 5.2: SINGLE-PADDLE WAVEMAKER (LEFT) AND CONTROL ROOM (RIGHT)

5.2.3 WAVE MEASUREMENT SYSTEM

During the tests it was necessary to make use of a wave probe system to measure the change in water surface elevation with time. This system comprises of HR DAQ data acquisition software, as well as a number of probes. Capacitance probes, rather than resistance probes, were used to monitor the waves in the flume. The main advantage of using this type of probe is that it is less influenced by fluctuations in temperature. The capacitance probes have an accuracy of 0.5 mm model scale (CSIR, 2008). Figure 5.3 shows the capacitance probes located inside the flume.

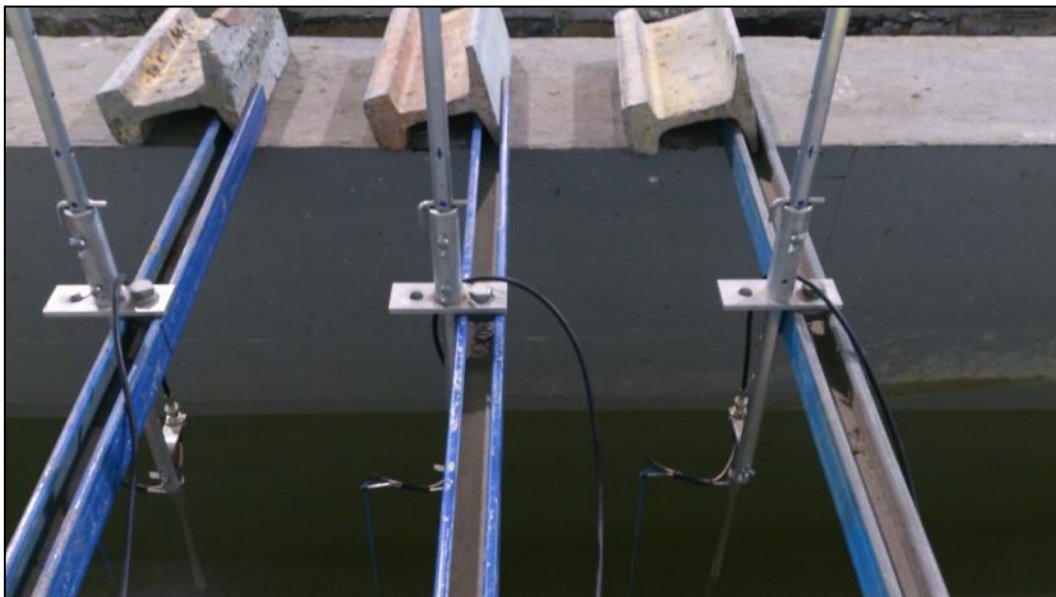


FIGURE 5.3: CAPACITANCE PROBE ARRAY

After each test, the GEDAP software package was used to analyse the recorded wave data. GEDAP is derived from “General experiment control, data acquisition, data analysis and plotting package” (Miles, 1989). Parameters of interest, such as significant spectral wave height (H_{m0}), maximum wave height (H_{max}), and peak period (T_p), were calculated from the data for each test.

5.2.4 CAMERA

To measure the damage caused to the breakwater by the various wave conditions, before and after photographs of the breakwater slope were compared. These photographs were taken with a GoPro® camera that was fixed in position in front of the main rubble mound breakwater. It was tilted so that it sat perpendicular to the armoured slope of the breakwater. The camera’s Wi-Fi capabilities enabled photographs to be taken before and after tests without having to press any buttons on the camera itself. Instead, another Wi-Fi device, with the appropriate software installed on it, was used to control the GoPro® camera. This ensured that photographs were taken from the same position before and after tests, and reduced the effort required to overlap the photographs during the damage analysis process. The waterproof casing in which the camera was placed during tests is shown in figure 5.4.



FIGURE 5.4: WATERPROOF GOPRO® CAMERA CASING

5.3 RUBBLE MOUND BREAKWATER

The design and construction processes of the rubble mound breakwater are discussed in this section. Firstly, the model bathymetry is discussed, then the calculations involving the design wave height. Next, the selection of the type and size of armour units are discussed, followed by the determination of the model scale. The grading of the rock material is discussed, as well as the dimensions of the breakwater, before ending the section with a brief description of the construction process.

5.3.1 BATHYMETRY

Although the biggest part of the physical model was set up to resemble the Mossel Bay breakwater and its surroundings, the actual bathymetry of the slope in front of the breakwater could not be well represented in the physical model. The reason being that the existing slope, from a previous project performed in the flume, was used so as to save time and expenses in this study. Within the scope of this study, it was considered to be acceptable for the existing slope to be used. The existing flume slope measurements are shown in figure 5.5. For a more detailed bathymetric slope, including the model breakwater, refer to section 5.3.7.

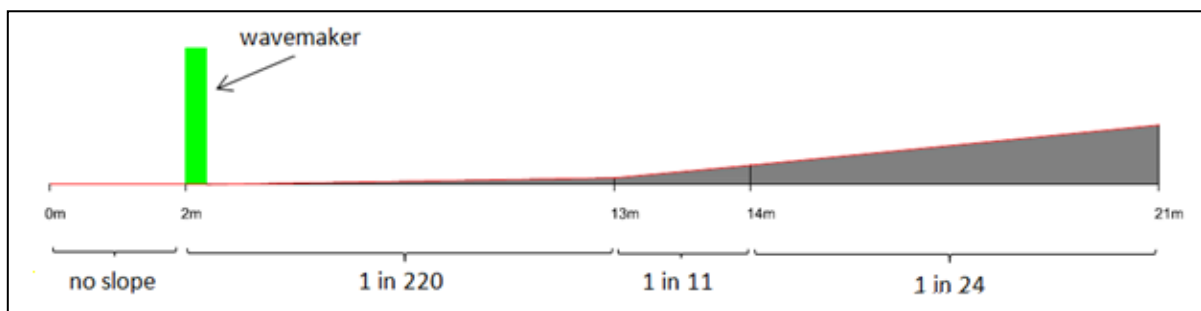


FIGURE 5.5: EXISTING SLOPE IN CONCRETE FLUME (DRAWING NOT TO SCALE, MODEL DIMENSIONS GIVEN)

The wavemaker is located at 2 m from the start of the flume. It is installed on a level portion of the flume. Thus, there exists no slope from the start of the flume to just in front of the wavemaker. The average slope between 2 m and 13 m along the flume is 1 in 220, while the average slope between 14 m and 21 m along the flume is 1 in 24. Between the 13 m and 14 m marks there is a jump in the bathymetry, which results in a slope of 1 in 11 for that portion.

Contained within the concrete flume bottom are plastic drainage pipes. They connect the front part and the back part of the flume, and their purpose is to ensure that the water level in front of the model remains the same as behind it. Without these pipes installed, the water that overtops the structure will accumulate as the test goes on and cause a pressure gradient to form through the breakwater.

A fixed bed model was chosen for this study. This means that the seabed in reality is represented by a concrete layer in the physical model, which does not allow for sediment movement. For the purposes of this investigation, such a representation is sufficient.

At the very back end of the flume, a wave absorption structure was built. This consisted of a rock beach that was piled at a gentle slope angle. The absorption beach dissipated energy that might reach the end of the flume due to wave overtopping of the main breakwater, and eliminated most of the unwanted reflections.

5.3.2 DESIGN WAVE HEIGHT

A set of wave data collected by the waverider buoy located inside Mossel Bay was kindly supplied by the CSIR (CSIR, 2014). The data covers a period of seven years, from 2007/05/22 to 2014/05/31. The sampling interval of the waverider is 30 minutes. From the wave data, a time series graph was created. Only a portion of the time series is shown in figure 5.6, as there are too many data points to fit the entire time series on one graph. The portion that is shown ranges from May 2009 to April 2010, and includes the maximum significant wave height of 5.6 m recorded at the waverider. In figure 5.7 the relative position of the waverider inside the bay is shown.

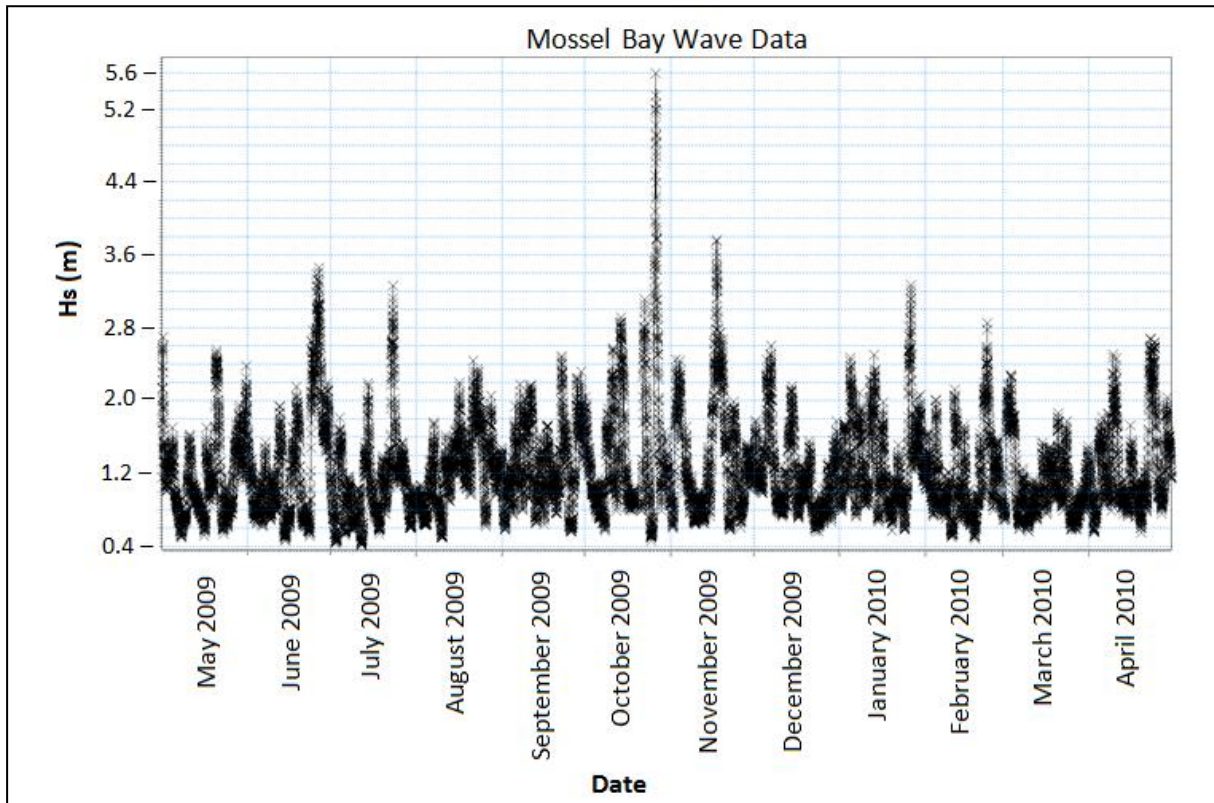


FIGURE 5.6: MOSSEL BAY WAVERIDER DATA (MAY 2009 - APRIL 2010) (CSIR, 2014)

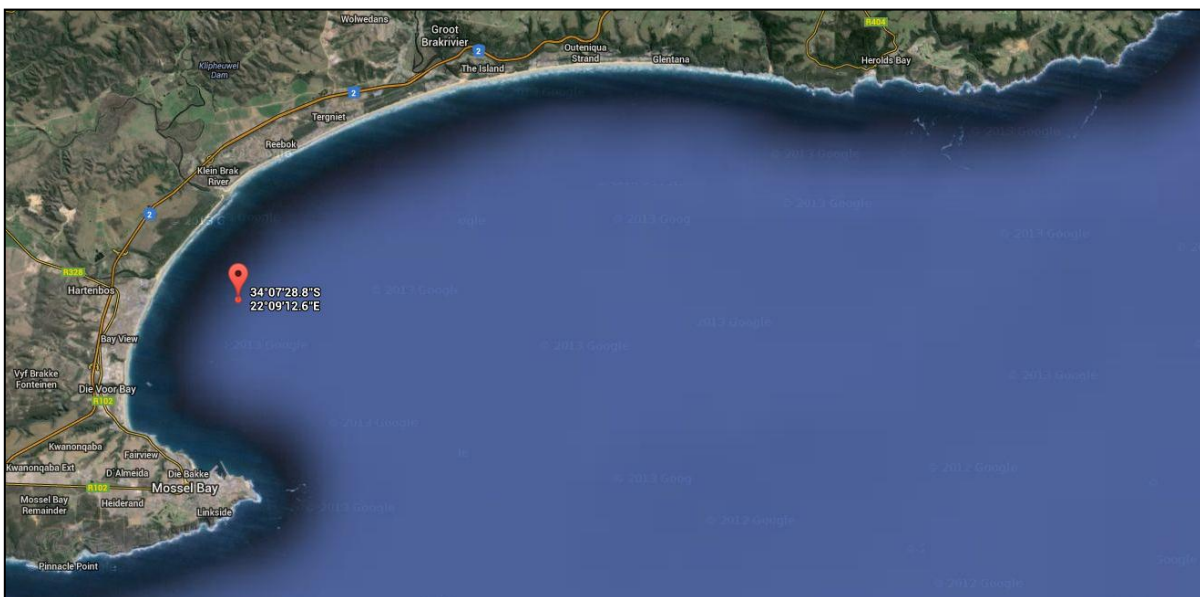


FIGURE 5.7: POSITION OF CSIR WAVERIDER INSIDE MOSSEL BAY (GOOGLE INC., 2014)

Due to the fact that the breakwater is located in relatively shallow water, it was suspected that the waves that reach the structure are depth-limited by the natural bathymetry in front of the breakwater. To determine whether or not this is true, a sensitivity analysis of the significant wave height at the breakwater was done with regards to the deep water significant wave heights and peak periods.

The wave data recorded at the waverider, which is located in a water depth of approximately 24 m, was assumed to give an accurate representation of what the deep water wave conditions are inside the bay.

Nearly all of the waves that are found in the waters surrounding Mossel Bay have a peak period in the range of 6 s to 14 s (Rossouw & Theron, 2009). Thus, it was decided to consider five different peak periods in the sensitivity analysis, all within the abovementioned range. These peak periods were: 6 s, 8 s, 10 s, 12 s and 14 s.

The significant wave heights that were used in the analysis were in the range of 4.5 m to 6 m. For convenience, intervals of 0.5 m were used between wave heights, so that the wave heights of 4.5 m, 5 m, 5.5 m and 6 m were considered. The upper limit of the range was chosen so that it exceeded the maximum significant wave height measured at the waverider (5.6 m) during the seven years of data collection.

CIRIA CUR CETMEF (2007) provides a simplified method to estimate the significant wave height on uniform sloping foreshores under the influence of breaking. The method involves the use of graphs to determine the significant wave height in shallow water if the seabed slope, water depth at the point of interest, deep water significant wave height, and deep water wavelength are all known.

To apply this method to the area surrounding the Mossel Bay breakwater it was necessary to consider the seabed slope that approaches the breakwater as a uniform slope. The average slope of seabed that stretches a distance of 2 km into the sea, measured perpendicular to the breakwater, is approximately 1 in 110, or 0.009 m/m (Liebenberg, 2013).

At the point of interest, the toe of the breakwater is located 3 m below CD. When investigating depth-limited waves, the water depth has a major impact on the maximum significant wave height that can occur at any given site. Shallower water depths result in waves becoming steeper more quickly. If waves become too steep, they will start to break. Therefore, it is important to account for factors that influence the water depth when investigating depth-limited waves, such as tide and storm surge. In this case, an additional 1.5 m was added to the water level to allow for tidal fluctuations (SANHO, 2013), as well as 0.5 m for storm surge (CFOO, 2001). The resulting water depth at the toe of the structure was 5 m. The influence of sea level rise was not considered in this investigation.

The graphs shown in figure 5.8 were used to calculate the depth-limited significant wave height at the toe of the structure (CIRIA CUR CETMEF, 2007). The calculation of the parameters used to enter the graphs is described hereafter.

The deep water wavelength was calculated from the peak period as described in the following equation, with L_0 being the deep water wave length, T_p the peak period and the gravitational acceleration (g) equal to 9.81 m/s^2 :

$$L_0 = gT_p^2 / (2\pi) \quad 5-1$$

Furthermore, the wave steepness (s) is defined as the ratio of significant wave height and the deep water wave length (H_s/L_0), while the local relative water depth is defined as the ratio of the water depth at the point of interest and the deep water wavelength (h/L_0).

For each of the five peak periods, the wave steepness and the local relative water depth was used to enter the graphs shown in figure 5.8. A foreshore slope of 1 in 110, or 0.009 m/m was used, as mentioned earlier.

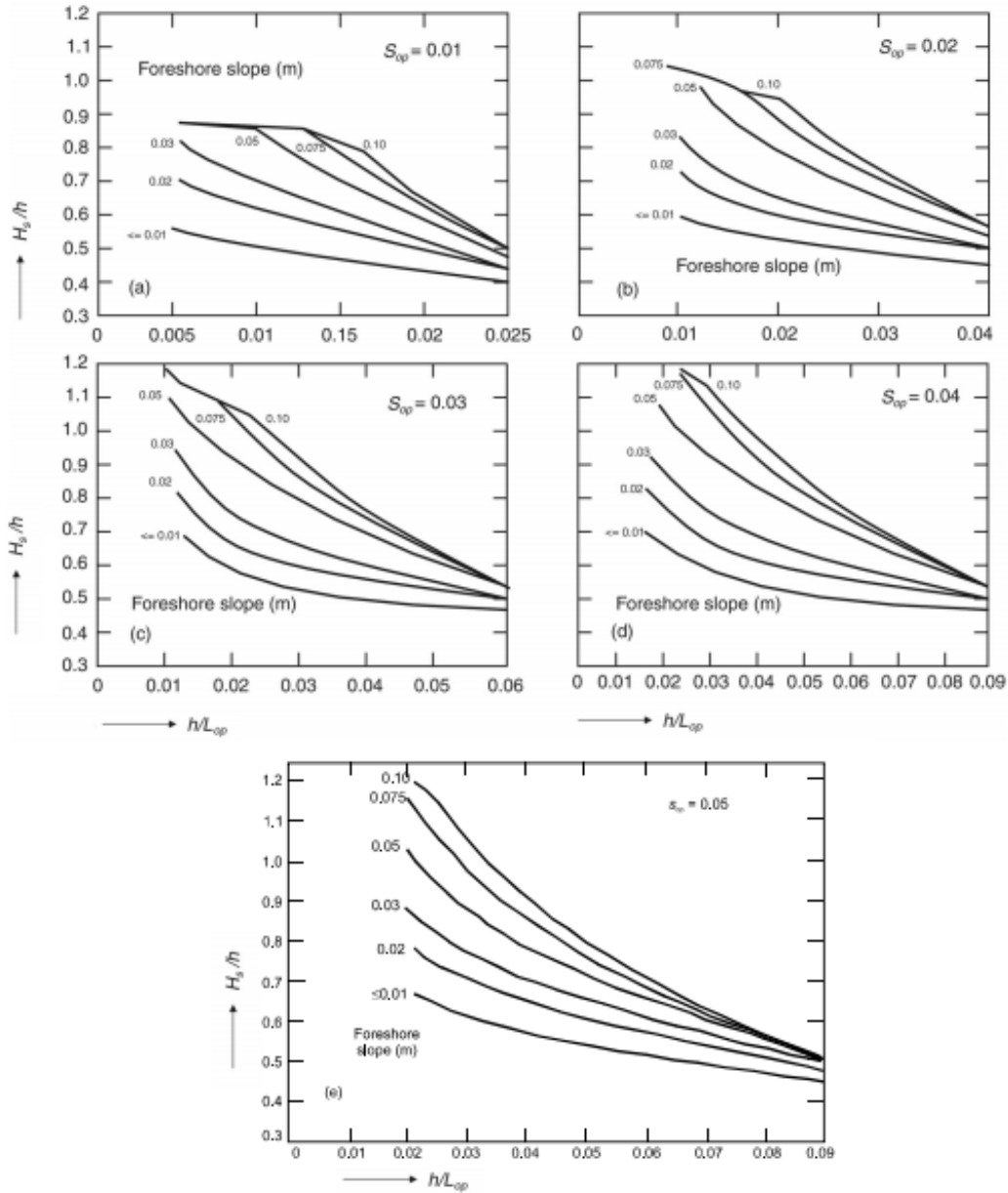


FIGURE 5.8: SHALLOW WATER SIGNIFICANT WAVE HEIGHTS ON UNIFORM SLOPING FORESHORE (CIRIA CUR CETMEF, 2007)

Table 5.1 shows the maximum depth-limited significant wave height that can occur at the toe of the structure as a result of the different combinations of deep water significant wave height and peak periods that were investigated. The majority of the waves did not have a steepness that coincided well with the steepness in the graphs. For example, a wave might have a steepness of 0.0385, which lies between the 0.03 and 0.04 steepness graphs. In these cases, the depth-limited significant wave height was calculated with both the graphs, after which linear interpolation was used to determine the in-between value. From table 5.1 it can be seen that the depth-limited significant wave height varies between 2.5 and 2.8 m, depending on the deep water wave conditions.

TABLE 5.1: MAXIMUM DEPTH-LIMITED SIGNIFICANT WAVE HEIGHT AT TOE OF STRUCTURE

Period T_p [s]	Deep water Sig. Wave Height H_{s0} [m]	Depth-limited Sig. Wave Height H_s [m]
8	4.5	2.5
	5.0	2.7
	5.5	2.7
	6.0	2.7
10	4.5	2.5
	5.0	2.6
	5.5	2.7
	6.0	2.8
12	4.5	2.6
	5.0	2.6
	5.5	2.6
	6.0	2.7
14	4.5	2.5
	5.0	2.7
	5.5	2.7
	6.0	2.8
16	4.5	2.5
	5.0	2.5
	5.5	2.6
	6.0	2.6

Following the above calculations, an extreme value analysis (EVA) was performed on the wave data recorded at the waverider buoy. This was done with the aid of the EVA Editor, which forms part of DHI's Mike Zero package. This toolbox includes features such as the extraction of the extreme value series from a wave record, two types of extreme value models (annual maximum series and partial duration series), various probability distribution functions, as well as two different uncertainty analysis methods (Monte Carlo simulation and Jackknife resampling) (DHI, 2009).

The software provides two methods of extracting the extreme value series from the data, namely the partial duration series (PDS) and the annual maximum series (AMS). The PDS method extracts any data points that exceed a user-defined threshold value. The AMS method, on the other hand, extracts the maximum value for each analysis year (DHI, 2009).

For this investigation, the PDS method was chosen. The reason for this was that in this way all data points that exceeded the lowest predicted depth-limited significant wave height (2.5 m as shown in table 5.1) could be extracted from the data set. If the AMS method was used, the probability of ignoring some important data points would exist. For example, if the data contains two values that exceed 2.5 m in any given year, only the highest of the two values would be extracted, and therefore ignoring the other.

Figure 5.9 shows the resulting EVA graph. On it, the significant wave height, return period and probability of non-exceedance is shown. The return periods of each of the four deep water significant wave heights that were used in the sensitivity analysis mentioned earlier, can be seen on the graph.

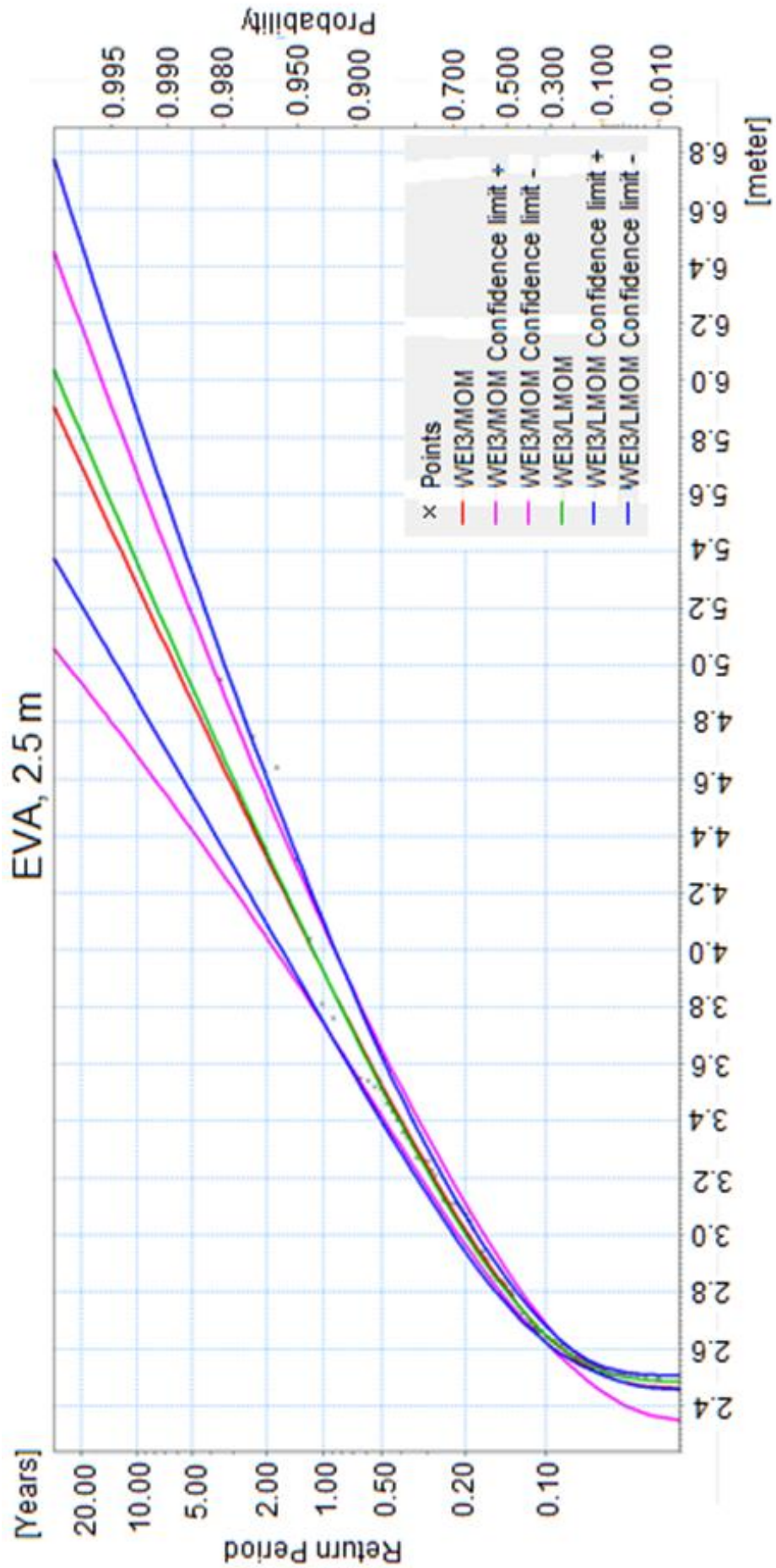


FIGURE 5.9: EXTREME VALUE ANALYSIS

The abovementioned return periods are approximately 1 in 3 years for the 4.5 m wave, 1 in 6 years for the 5 m wave, 1 in 13 years for the 5.5 m wave and 1 in 25 years for the 6 m wave.

It was decided at this point that the 1 in 25 year deep water wave condition is an adequate choice for the design wave condition. Therefore, the design wave height is that of the corresponding depth-limited significant wave height at the toe of the structure. The design wave height is as follows: 2.6 m for a 16 s wave, 2.7 m for an 8 s and 12 s wave, and 2.8 m for a 10 s and 14 s wave.

5.3.3 ARMOUR UNIT SELECTION AND SIZE

The selection of an armour unit type was straightforward in this study, as the model was based on an existing structure. The Mossel Bay breakwater has a double layer of dolos armour units to absorb the wave energy, and therefore the model breakwater also made use of dolos units.

The main rubble mound breakwater was designed for a significant wave height of 2.8 m according to the formula developed by Burcharth & Liu (1992) for dolos armour units on non-overtopped slopes, as shown in equation 5-2. The formula is based on experimental test results acquired by Brorsen et al. (1974), Burcharth & Brejnegaard-Nielsen (1986), Holtzhausen & Zwamborn (1990), and Burcharth & Liu (1992). The formula was developed specifically for an armour layer slope of 1:1.5, which is the same as the slope found in Mossel Bay, and is as follows:

$$\frac{H_s}{\Delta D_n} = (47 - 72r)\varphi_{n=2} D_n^{1/3} N_z^{-0.1} \quad 5-2$$

where

H_s	=	significant wave height
ρ_a	=	mass density of armour unit
ρ_w	=	mass density of water
Δ	=	$(\rho_a/\rho_w) - 1$
D_n	=	nominal diameter of armour unit
r	=	dolos waist ratio
$\varphi_{n=2}$	=	packing density of double armour layer
D	=	damage number
N_z	=	number of waves

The design of the armour layer was done primarily with input parameter values that are representative of the situation at Mossel Bay. However, in cases where specific information was not available, these parameters were approximated with typical values.

From information gathered by Zwamborn et al. (1980) it is known that the dolos armour units used on the section of the Mossel Bay breakwater under consideration in this study, have a waist ratio of 0.33. The waist ratio of a dolos is defined as the ratio of its centre diameter to its height. Zwamborn et al. (1980) also mentions that the Mossel Bay breakwater was originally designed to withstand a design significant wave height of 3 m, which is close to the 2.8 m wave used in this case.

Information regarding the packing density of the dolos armour units on the Mossel Bay breakwater could not be obtained. Burcharth & Liu (1992) specifies that the design formula is applicable to

packing densities in the range of 0.61 to 1 for double layer dolos armour. Within this range, the stability number is linearly proportional to the packing density (Burcharth & Liu, 1992). To be conservative, the lower end of the range was chosen, so that the packing density was 0.61.

For the design of double layer dolos armour, damage in the range of 1% to 2% is deemed as acceptable (U.S. Army Corps of Engineers, 2002). It was decided to design the armour layer for an acceptable damage level of 1.5%, the average of the recommended range. This means that the design allows for up to 1.5% ($D = 0.015$) of the total amount of dolos units to be damaged in the structure's lifetime.

Burcharth & Liu (1992) recommends that the dolos armour layer be designed for 3000 waves, as experimental tests showed that dolos armour layers reach equilibrium after approximately 3000 waves.

By inserting the abovementioned parameter values into equation 5-2, the required nominal diameter of the individual armour units (D_n) can be found. Then the mass of each armour unit can be found by using the following equation:

$$M = D_n^3 \rho_a \quad 5-3$$

where

M	=	armour unit mass
D_n	=	nominal diameter of armour unit
ρ_a	=	mass density of armour unit

A summary of the input values as well as the resulting armour unit mass, as calculated with the Burcharth & Liu equation, is shown in table 5.2. The calculated armour unit mass of 5.64 tons was rounded up to the nearest ton. The design armour unit mass then becomes 6 tons. Rounding up the calculated armour unit weight serves two purposes. The first is to provide some sort of a safety factor or buffer, and the second is to keep to the similarity of the Mossel Bay breakwater, which also uses 6 ton dolos units at the section under consideration.

TABLE 5.2: CALCULATED ARMOUR UNIT MASS USING BURCHARTH & LIU EQUATION

Design Wave Hs [m]	Waist Ratio r [-]	Packing Density $\phi_{n=2}$ [-]	Damage Number D [%]	Number of Waves Nz [-]	Nominal Diameter Dn [m]	Mass M [t]
2.8	0.33	0.61	1.5	3000	1.3	5.64

5.3.4 MODEL SCALING

An undistorted geometric scale was used for the physical model under investigation. Furthermore, the size of the model was chosen to be as large as the facility would accommodate. The fact that a relatively shallow water breakwater was tested meant that there was more than sufficient room in the flume to accommodate the model. Rather, it was limited by the size of the available dolos armour units at the testing facility.

In the model the forces of inertia and gravity were expected to be dominant. The influence of viscous and surface-tension forces was assumed to be negligible. This meant that the Froude criterion for scaling should be applied.

For Froude similarity the Froude number should be the same in prototype and in the physical model. The Froude number describes the relative influence of the forces of inertia and gravity, and is shown in the following equation (Hughes, 1995):

$$\sqrt{\frac{\text{inertial force}}{\text{gravity force}}} = \sqrt{\frac{\rho L^2 V^2}{\rho L^3 g}} = \frac{V}{\sqrt{gL}} \quad 5-4$$

where

ρ	=	mass or fluid density
L	=	length
V	=	velocity
g	=	gravitational acceleration

A mathematical representation for the requirement that the Froude number be the same in prototype (denoted by the subscript p) and in the model (denoted by the subscript m) is given in the next equation (Hughes, 1995):

$$\left(\frac{V}{\sqrt{gL}}\right)_p = \left(\frac{V}{\sqrt{gL}}\right)_m \quad 5-5$$

Each of the parameters in the above equation can also be expressed in its scale ratio, i.e. the ratio of a certain parameter in prototype and in model. The general form of a scale ratio is shown below (Hughes, 1995):

$$N_x = \frac{X_p}{X_m} = \frac{\text{Value of } X \text{ in Prototype}}{\text{Value of } X \text{ in Model}} \quad 5-6$$

The scale ratios for each of the parameters in equation 5-5 can be used to further extend into ratios regarding all three areas of similitude. These areas are geometric similitude, kinematic similitude and dynamic similitude. Table 5.3 shows the different scale ratios as they apply to the Froude criterion.

At the CSIR, model dolos units were available at various masses ranging from 8.85 g to 543.95 g. As mentioned before, the model scale was not limited by the flume capacity, but instead by the size of the available armour units. Although the 543.95 g dolos units would result in the largest scale, not enough of these units were available. The biggest units with adequate numbers available had a mass of 197.65 g and a height of 75 mm. Figure 5.10 shows one of the model armour units.

TABLE 5.3: SIMILITUDE RATIOS FOR FROUDE SIMILARITY (HUGHES, 1995)

Characteristic	Dimension	Froude
Geometric		
Length	$[L]$	N_L
Area	$[L^2]$	N_L^2
Volume	$[L^3]$	N_L^3
Kinematic		
Time	$[T]$	$N_L^{1/2} N_\rho^{1/2} N_\gamma^{-1/2}$
Velocity	$[LT^{-1}]$	$N_L^{1/2} N_\rho^{-1/2} N_\gamma^{1/2}$
Acceleration	$[LT^{-2}]$	$N_\gamma N_\rho^{-1}$
Discharge	$[L^3T^{-1}]$	$N_L^{5/2} N_\rho^{-1/2} N_\gamma^{1/2}$
Kinematic Viscosity	$[L^2T^{-1}]$	$N_L^{3/2} N_\rho^{-1/2} N_\gamma^{1/2}$
Dynamic		
Mass	$[M]$	$N_L^3 N_\rho$
Force	$[MLT^{-2}]$	$N_L^3 N_\gamma$
Mass Density	$[ML^{-3}]$	N_ρ
Specific Weight	$[ML^{-2}T^{-2}]$	N_γ
Dynamic Viscosity	$[ML^{-1}T^{-1}]$	$N_L^{3/2} N_\rho^{1/2} N_\gamma^{1/2}$
Surface Tension	$[MT^{-2}]$	$N_L^2 N_\gamma$
Volume Elasticity	$[ML^{-1}T^{-2}]$	$N_L N_\gamma$
Pressure and Stress	$[ML^{-1}T^{-2}]$	$N_L N_\gamma$
Momentum, Impulse	$[MLT^{-1}]$	$N_L^{7/2} N_\rho^{1/2} N_\gamma^{1/2}$
Energy, Work	$[ML^2T^{-2}]$	$N_L^4 N_\gamma$
Power	$[ML^2T^{-3}]$	$N_L^{7/2} N_\rho^{-1/2} N_\gamma^{3/2}$



FIGURE 5.10: DOLOS UNIT USED IN THE MODEL

The density of the model units was determined to be 2422 kg/m³, which corresponds to that of common concrete. Refer to Appendix A for the procedure followed to determine its mass density.

As found in section 5.3.3, the model armour unit had to represent an armour unit of mass 6 tons. To represent this size of armour unit in the physical model with the available dolos units according to the Froude scale law, a scale of 1:32 was required.

5.3.5 MATERIAL SELECTION AND GRADING

The model breakwater was made up of three different sizes of rocks, as well as an armour layer. The different layers are the core layer, under layer and toe layer respectively. The mass of each of these layers is described in terms of its relation to the armour unit mass. The chosen ratios are based on a combination of the guidelines provided by U.S. Army Corps of Engineers (2002) and similarity of the Mossel Bay breakwater.

In table 5.4 each layer's ratio of the armour unit mass, its median mass (M_{50}), its nominal lower limit (NLL) and its nominal upper limit (NUL) are given. In this case the NLL is defined as 15%, while the NUL is 85%.

TABLE 5.4: M_{50} , NLL AND NUL FOR EACH BREAKWATER LAYER

Layer	Ratio	Median Mass [kg]	Nominal Lower Limit [kg]	Nominal Upper Limit [kg]
Armour	1/1	6000	6000	6000
Toe	1/6	1000	500	1500
Under	1/10	600	200	1000
Core	1/100	60	20	100

From the values given in table 5.4 it was possible to construct the theoretical grading curve in accordance with the Rosin-Rammler (Ros-Ram) equation (CIRIA CUR CETMEF, 2007). Once the theoretical curves were constructed for all three layers of rock required to build the model, these values could be scaled down and equivalent curves were produced for the model rock. A trial-and-error approach was then followed, in which various rock samples were made up until these theoretical curves were satisfactorily reproduced by mixing different rock sizes. The rock grading curves can be found in Appendix B.

5.3.6 BREAKWATER DIMENSIONS

The selection of dimensions for the main breakwater in the model was based on correlation with the Mossel Bay breakwater, as well as convenience. Convenience in the sense that dimensions would be rounded up to the nearest 0.5 m, resulting in a somewhat ideal cross section for the breakwater.

During a site visit to the port of Mossel Bay on the 2nd of June 2014, the original breakwater construction drawings from 1967 were acquired with permission of the TNPA (TNPA, 1967). One of these drawings is shown in figure 5.11, which shows a typical cross section of the breakwater at the area of interest. Note that all dimensions are given in feet and inches, as was the custom in that era.

Another custom of the British era in South Africa that is present on the drawing is the use of low water of ordinary spring tide (LWOST) as a tidal datum. This is assumed to be the equivalent of mean low water springs (MLWS), which is customary nowadays. In order to find the lowest astronomical tide (LAT), which is used as chart datum (CD), it is necessary to refer to the South African Navy

Hydrographic Office (SANHO) tide table for Mossel Bay to find the MLWS height relative to CD. The tide information for Mossel Bay is given in table 5.5.

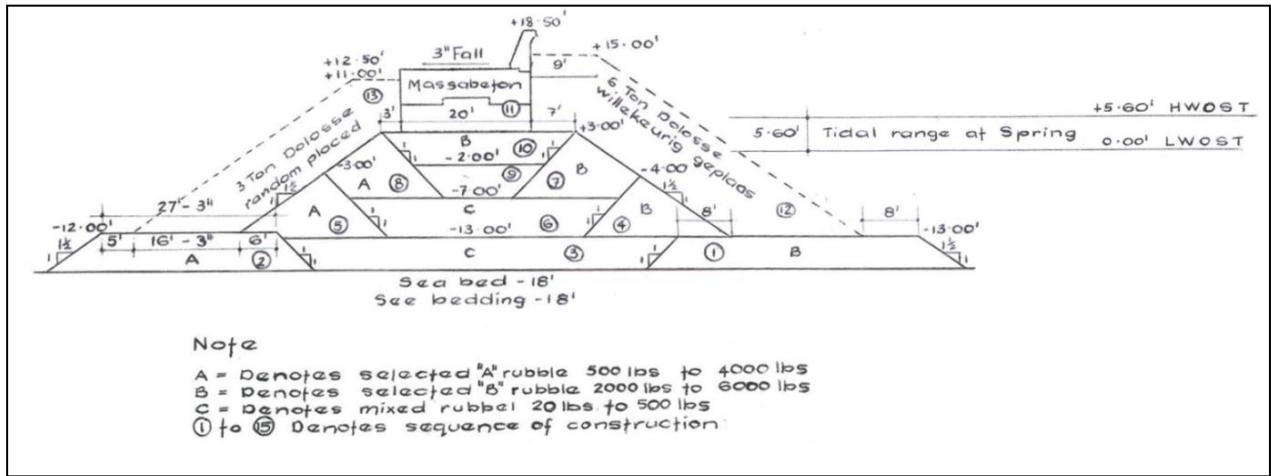


FIGURE 5.11: MOSSEL BAY BREAKWATER SECTION FROM 1967 (TNPA, 1967)

TABLE 5.5: MOSSEL BAY TIDAL INFORMATION (IN METRES) (SANHO, 2013)

LAT	MLWS	MLWN	ML	MHWN	MHWS	HAT
0	0.26	0.88	1.17	1.46	2.10	2.44

The acronyms in the above table are as follows:

- HAT - Highest Astronomical Tide
- MHWS - Mean High Water Springs
- MHWN - Mean High Water Neaps
- ML - Mean Level
- MLWN - Mean Low Water Neaps
- MLWS - Mean Low Water Springs
- LAT - Lowest Astronomical Tide

The information in the SANHO tide table (SANHO, 2013), along with the original Mossel Bay breakwater drawing (TNPA, 1967), was sufficient for dimensioning the model breakwater. Figure 5.12 shows the dimensions of the model breakwater. All dimensions are given in prototype values (metres). Elevations are given in relation to chart datum (metres). Chart datum is located at LAT.

In this study only the stability of the seaward slope of the breakwater was of interest. Therefore, only the seaward slope was constructed in the physical model. The portion to the left of the red line in figure 5.12 was constructed. For the complete model layout, including water levels and bathymetry refer to section 5.3.7.

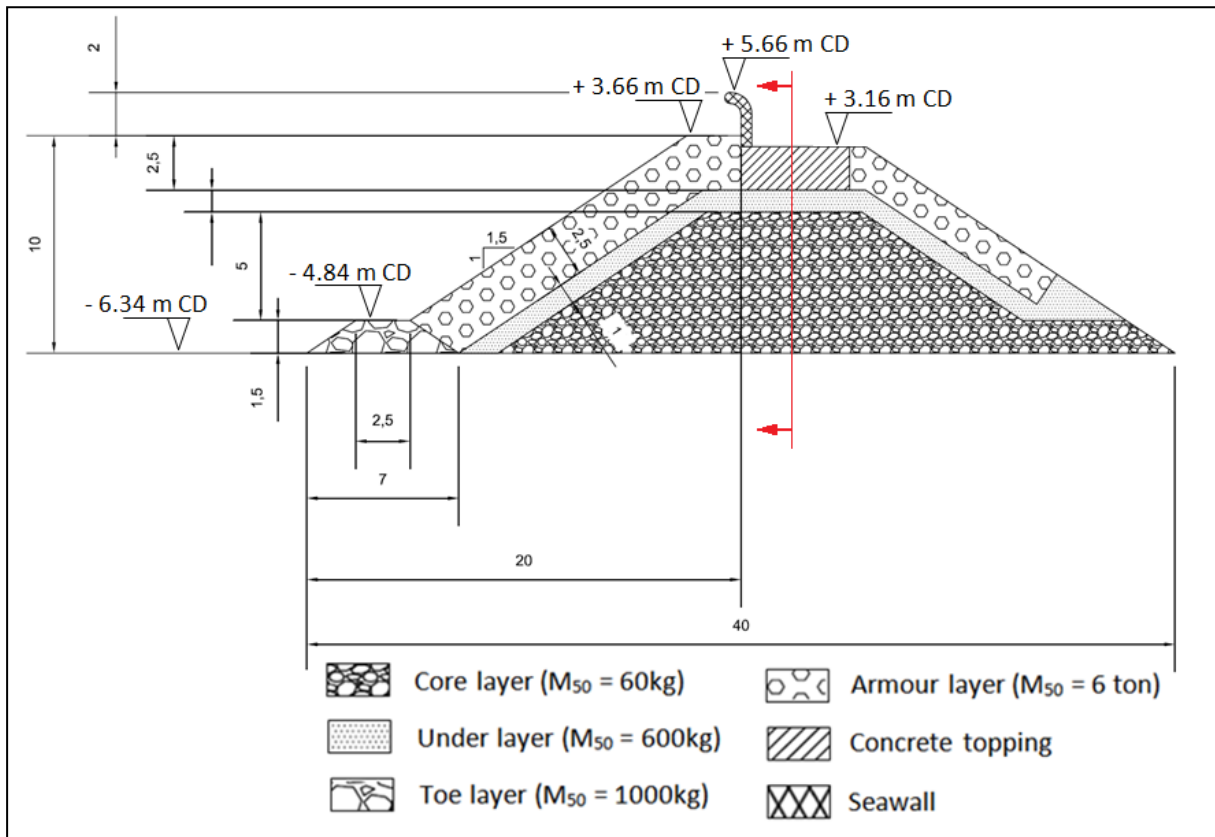


FIGURE 5.12: CROSS-SECTION OF MODEL RUBBLE MOUND BREAKWATER (DIMENSIONS IN METRES PROTOTYPE)

5.3.7 CONSTRUCTION

This section provides a short description of the construction process of the main rubble mound breakwater. For a more detailed description of the process, refer to Appendix C.

The front of the structure's toe layer is located at 20.5 m (model) along the flume, which is 18.5 m (model) from the wavemaker. In prototype, this corresponds to approximately 600 m. The crest height of the structure, excluding the overtopping wall is 312.5 mm (model). The overtopping wall extends another 62.5 mm (model) on top of that. In prototype this equates to 10 m and 2 m respectively. A long section through the flume, with the model rubble mound breakwater installed, is shown in figure 5.13. This shows the main breakwater position, support structure behind the breakwater, probe positions, wavemaker position, as well as ML, which was the water level in all the tests. The markings along the flume are in model scale.

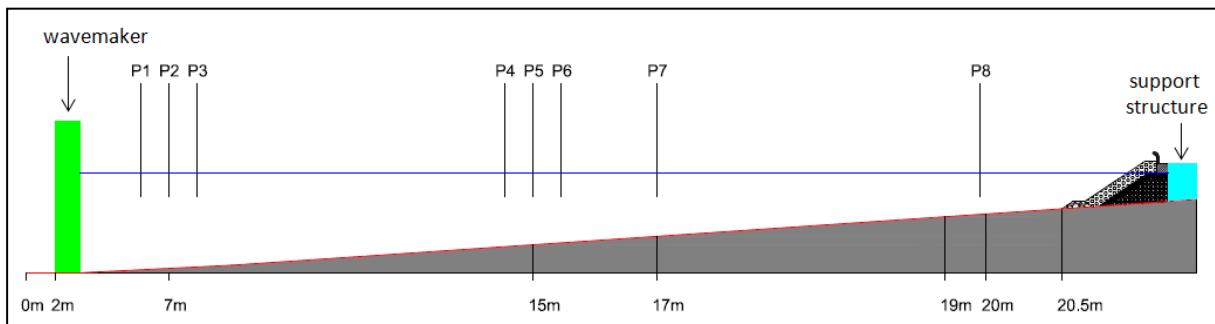


FIGURE 5.13: LONG SECTION THROUGH CONCRETE FLUME - NO REEF STRUCTURE (DRAWING NOT TO SCALE, MODEL DIMENSIONS GIVEN)

Because only the front slope of the breakwater was considered in this study, not the whole breakwater was constructed in the model. Rather, only the front part, slightly bigger than half the breakwater, was constructed. Figure 5.14 shows the model breakwater as constructed in the concrete flume.



FIGURE 5.14: COMPLETED MAIN RUBBLE MOUND BREAKWATER IN FLUME

5.4 REEF BREAKWATER

This section covers the design and construction processes of the reef breakwater structure in the model. Both the rock and geotube reef structures are discussed in the two subsequent sections.

5.4.1 ROCK REEF STRUCTURE

Two types of reef structures were tested, namely a rock reef structure and a geotube reef structure. Each of these reefs was tested at three different crest elevations. These elevations are located at ML, LAT and below-LAT. ML and LAT are self-explanatory, but below-LAT not so much. Below-LAT is simply located the same distance below LAT as ML is located above LAT. The prototype distance between LAT and both ML and below-LAT is 1.17 m.

Because reef breakwaters are generally designed to be dynamically stable structures consisting of a homogenous pile of rocks, the structure's slope angle is normally more gradual than would be encountered for a rubble mound structure consisting of multiple layers. Therefore, it was decided that the rock reef breakwater should have a slope angle of 1V:2H.

The reef structure is built 1.5625 m (model) away from the main structure, which is 50 m in prototype. This is one wavelength away for the 8 s wave and approximately half of a wave length away for the 12 s wave.

In figure 5.15 the three structures are overlaid to show the different crest elevations used during the testing. For the sake of efficiency, the smallest structure was tested first, then the middle one and finally the largest one. This made it possible to simply add additional rock until the next crest height was achieved, while keeping the previous structure as starting point for the construction.

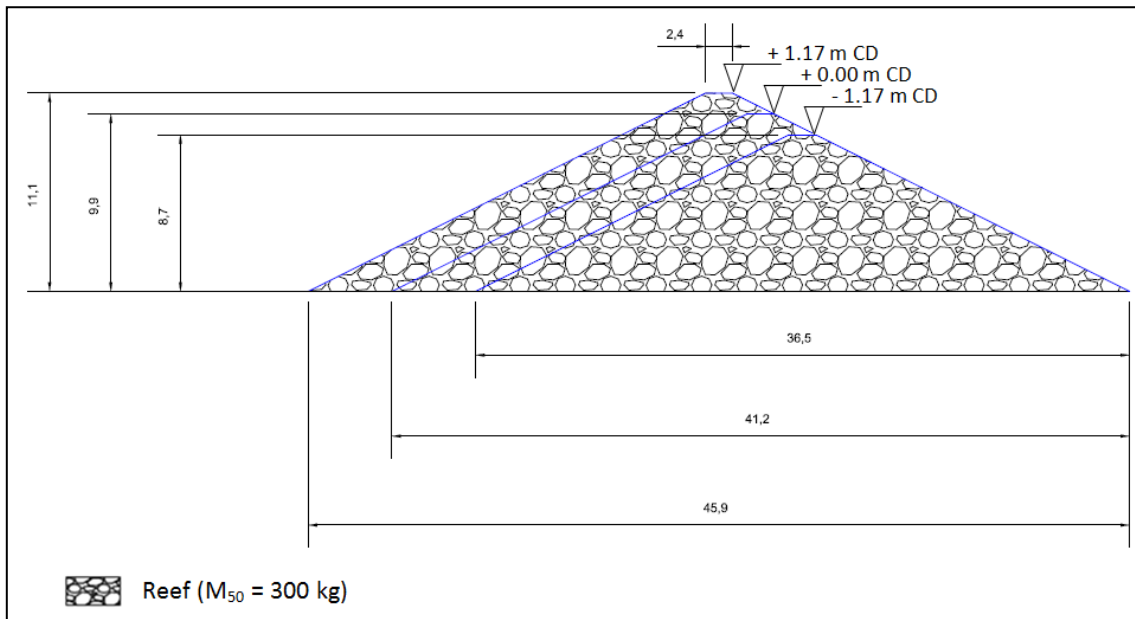


FIGURE 5.15: CROSS-SECTION OF MODEL ROCK REEF BREAKWATER (DIMENSIONS IN METRES PROTOTYPE)

The width of the crest is taken to be as wide as 5 rocks. This equates to a crest width of 2.4 m. Guidelines in U.S. Army Corps of Engineers (1993) stipulate a minimum crest width for dynamically stable low-crested reef structures to be 3 armour rocks.

The rock size used for the construction of the reef structure was chosen randomly, within certain limits. The reef was designed to be dynamically stable, and therefore the rock was chosen to be light enough that a drop in the crest level would be observed during testing. This of course means that different rock sizes would yield different results. Unfortunately, only one rock size could be tested due to time limitations. The prototype rock had a median mass of 300 kg, a NLL of 100 kg and a NUL of 500 kg. The rock grading curve of the reef can be seen in Appendix B.

It is recognised that a dynamically stable structure complicates the interpretation of results somewhat, due to the fact that the amount of protection provided by the structure varies over time. Even though that is the case, the dynamically stable reef provides a better representation of reality.

During testing the shape of the reef structure was altered by the wave energy. Rocks from the crest were displaced onto the slopes until an equilibrium shape was reached. This equilibrium profile was dependent on the severity of the wave condition that passed over it. The change in the structure's shape during testing required that the reef structure be rebuilt between tests. Luckily, this rebuilding only consisted of reshaping the rock until the desired profile was again achieved.

In figure 5.16, a long section through the flume is shown. This shows the submerged reef, the main rubble mound structure, the support structure behind the breakwater, probe positions, wavemaker position, as well as ML. The markings along the flume are in model scale.

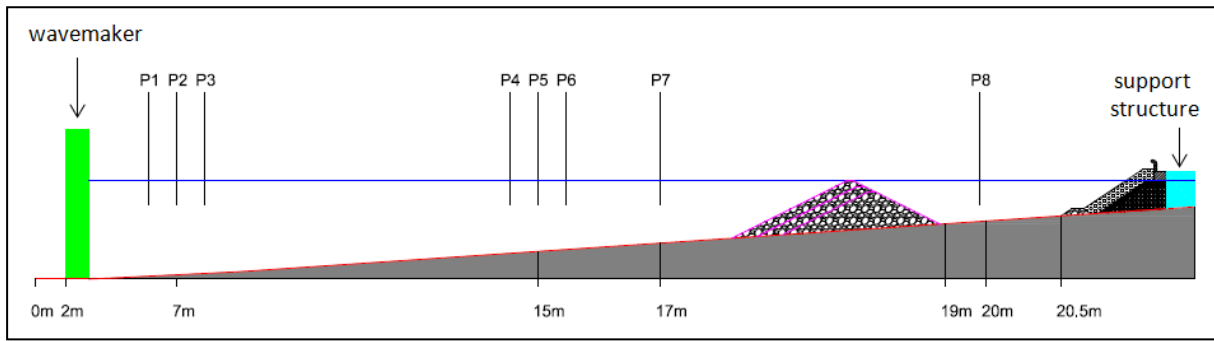


FIGURE 5.16: LONG-SECTION THROUGH CONCRETE FLUME - ROCK REEF STRUCTURE (DRAWING NOT TO SCALE, MODEL DIMENSIONS GIVEN)

5.4.2 GEOTUBE REEF STRUCTURE

The second of the two types of submerged structures tested in the flume was a geotube structure. This structure consisted of a number of long sand-filled geotube containers that were stacked on top of one another in a pyramid-like fashion.

Like the reef structure constructed from rock, the geotube structure was also constructed up to three different crest levels: below-LAT, LAT, and ML.

This investigation only focussed on the stability of the main rubble mound breakwater. The stability of the reef structure itself did not fall within the scope of this study. Therefore, for the construction of the geotube reef, it was not required to scale down the friction forces acting between adjacent geotubes.

Each geotube container was filled to a prototype height of 1.6 m. This process involved the placing of the empty tube between two wooden planks that were spaced 50 mm apart, and then filling it with sand. After adding a few scoops of sand, the material was compacted. This process was repeated until the geotube container reached its capacity. The form used to aid in the filling of the geotubes is shown in figure 5.17.

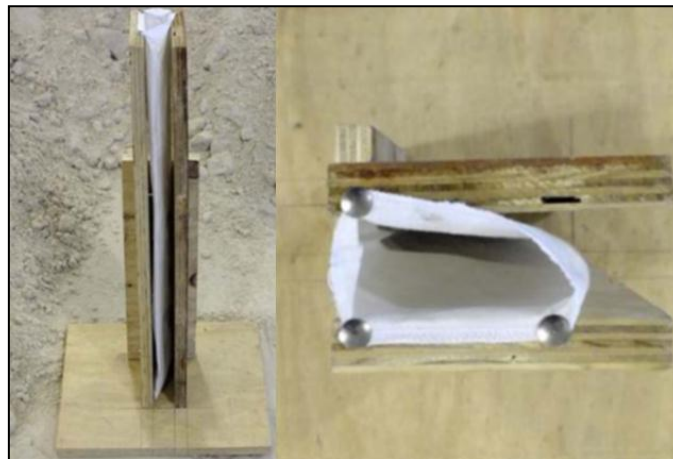


FIGURE 5.17: FORMWORK USED WHILE FILLING MODEL GEOTUBES

During construction, the different layers of the geotube structure were fixed together with wire to form a single, solid structure. Again, this was due to the fact that the stability of the submerged reef structure lies outside the scope of this study.

Similar to the testing of the rock reef structure, the test series involving a geotube structure also started with the lowest crest elevation first and incrementing to the highest crest elevation. The reason for this sequence was also the same: efficiency.

The geotube reef was constructed at the same position within the flume as the rock reef. The sand-filled containers were stacked on each other in such a way that they conformed to the slope of the templates drawn on the sides of the flume. A cross section through the geotube reef is shown in figure 5.18. The dimensions are the same as for the rock reef.

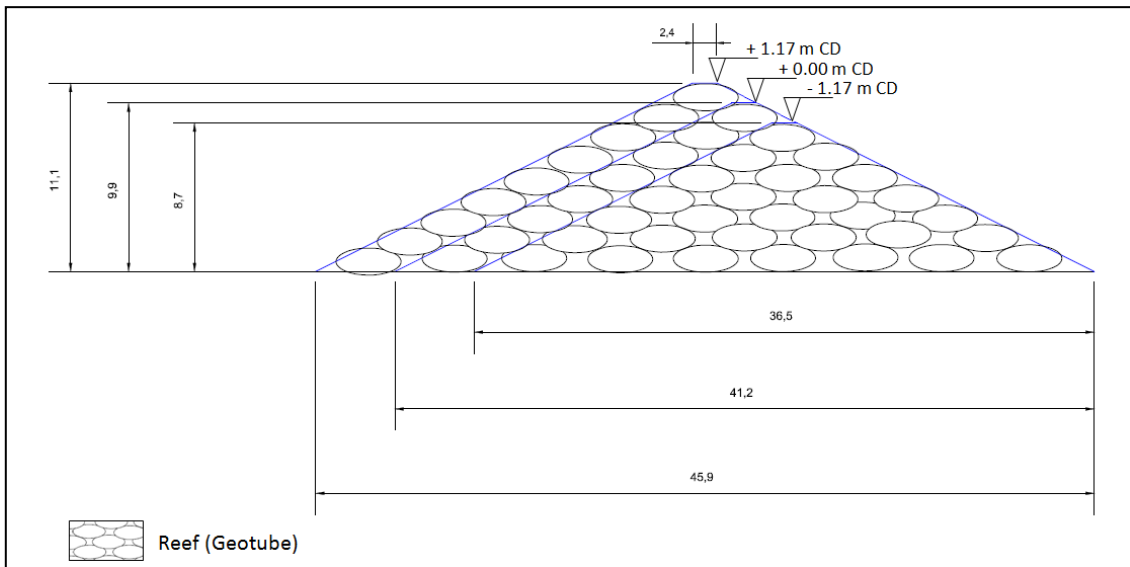


FIGURE 5.18: CROSS-SECTION OF MODEL GEOTUBE REEF BREAKWATER (DIMENSIONS IN METRES PROTOTYPE)

Figure 5.19 shows the geotube reef as constructed in the flume and figure 5.20 shows a long-section through the flume with the relative positions of the main breakwater, the breakwater support structure, the geotube reef, the probes, the wavemaker and the water level (ML). The markings along the flume are in model scale.



FIGURE 5.19: CONSTRUCTION OF GEOTUBE REEF BREAKWATER

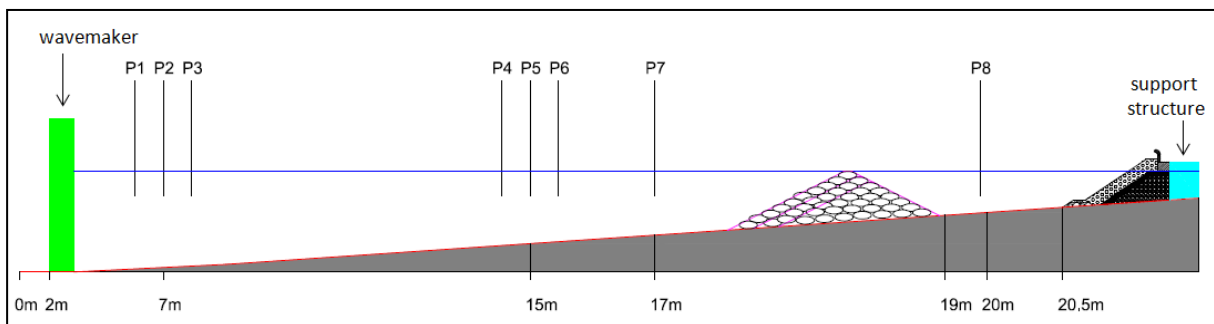


FIGURE 5.20: LONG-SECTION THROUGH CONCRETE FLUME - GEOTUBE REEF STRUCTURE (DRAWING NOT TO SCALE, MODEL DIMENSIONS GIVEN)

5.5 TEST SERIES

This section is dedicated to the test schedule and test results. The results include the measured damage at the main rubble mound structure, as well as the measured significant wave heights at a location in front of the rubble mound structure that corresponding to 20 m in prototype. These measurements are used to determine the effect that the presence of a reef structure has on the performance of the rubble mound breakwater.

5.5.1 TEST SCHEDULE

The test series comprised of 22 unique test conditions, of which 3 were tested for repeatability. The tests featured various combinations of significant wave heights, peak periods and reef structure type and crest elevations.

The tests were conducted with the purpose of determining the influence that a submerged reef breakwater has on the wave heights that reach the main rubble mound breakwater as well as the severity of the damage to the main breakwater.

The main breakwater was first tested without any reef structure present, so as to acquire baseline values to which the subsequent tests could be compared. Thereafter, two types of reef structures were installed as described in section 5.4. Table 5.6 shows the schedule of the main test series that was conducted. All tests were done with a still water level at ML, i.e. +1.17 m CD.

TABLE 5.6: TEST SCHEDULE

Test Name [-]	Peak Period [s]	Significant Wave Height [m]	Submerged Structure [-]	Crest Elevation [m above CD]
TS01_1	8	2.5	No Structure	-
TS01_2	12	2.5	No Structure	-
TS02_1	8	3.0	No Structure	-
TS02_2	12	3.0	No Structure	-
TS03_1	8	2.5	Rock Structure	-1.17
TS03_2	12	2.5	Rock Structure	-1.17
TS04_1	8	3.0	Rock Structure	-1.17
TS04_2	12	3.0	Rock Structure	-1.17
TS05_1	8	2.5	Rock Structure	0
TS05_2	12	2.5	Rock Structure	0
TS06_1	8	3.0	Rock Structure	0
TS06_2	12	3.0	Rock Structure	0
TS07_1	8	2.5	Rock Structure	1.17
TS07_2	12	2.5	Rock Structure	1.17
TS08_1	8	3.0	Rock Structure	1.17
TS08_2	12	3.0	Rock Structure	1.17
TS09_1	8	3.0	Geotube Structure	-1.17
TS09_2	12	3.0	Geotube Structure	-1.17
TS10_1	8	3.0	Geotube Structure	0
TS10_2	12	3.0	Geotube Structure	0
TS11_1	8	3.0	Geotube Structure	1.17
TS11_2	12	3.0	Geotube Structure	1.17

5.5.2 WAVE CALIBRATION

Prior to the actual test series, a wave calibration process had to be undertaken. The process involved the alteration of the gain setting of the wavemaker until the desired incident significant wave height was measured at the shallow water probe array (P4, P5 and P6), as determined by a reflection analysis.

During calibration, only the main breakwater was inside the flume. Four test conditions had to be calibrated. These were the different combinations of the two peak periods, 8 s and 12 s, and the two significant wave heights, 2.5 m and 3 m. In table 5.7, the incident significant wave heights that were achieved in the calibration tests, are shown. The largest deviation of the achieved incident H_{m0} from the target incident H_{m0} , for any of these final calibration tests, was less than 5%. This was considered to be acceptable.

All tests were done with the dynamic wave absorption turned on as explained in section 5.2.2. The absorption gain was set to 332, according to a previous calibration procedure that was done for the concrete flume (CSIR, 2013). The wavemaker setting which allows for the compensation of long period set-down phenomena was switched on throughout the test series.

TABLE 5.7: INCIDENT SIGNIFICANT WAVE HEIGHTS OF CALIBRATED WAVES

Test Name [-]	Peak Period [s]	Target Incident H_{m0} [m]	Achieved Incident H_{m0} [m]
C01_1B	8	2.5	2.6
C01_2C	12	2.5	2.4
C02_1A	8	3.0	3.1
C02_2A	12	3.0	2.9

5.5.3 ROCK REEF CREST REDUCTION

The rock reef structure used in the physical model was designed to be dynamically stable, which means that the structure is allowed to be shaped into an equilibrium profile by the waves that pass over it. This natural response to hydrodynamic loads allows dynamically stable structures to be designed with smaller rock sizes, which gives it an economical attractiveness superior to its statically stable counterparts (van Gent, 1996).

For the purposes of the study at hand, the reduction in crest elevation is the most important aspect to consider. The amount of protection that the reef structure provides to the main rubble mound structure is strongly related to the crest elevation of the reef.

When using a dynamically stable reef structure, the interpretation of the results becomes a bit more complicated. However, this type of structure gives a better representation of reality. In this way, the waves break over a reef structure that has a stable equilibrium shape, as would be the case in reality, instead of a uniform slope. The influence of such a slope on the wave dynamics is difficult to reproduce mathematically (although numerical models have been developed, such as van Gent (1996), for example). Thus, a physical model was considered to be the most efficient way to obtain the most accurate results with the available resources.

To take the reshaping of the reef into account when interpreting the results, certain measurements with regards to the dimensions of the reef were taken after each test. These measurements were the change in crest elevation and the change in crest width. Furthermore, the shape of the equilibrium profile of

the reef was inspected visually after tests. Table 5.8 shows the reduction in crest elevation observed after the various test runs.

TABLE 5.8: ROCK REEF CREST REDUCTION AND EFFECTIVE CREST ELEVATION

Test Name [-]	Peak Period [s]	Significant Wave Height [m]	Crest Elevation (as built) [m above CD]	Crest Reduction [m]	Effective Crest Elevation [m above CD]
TS03_1	8	2.5	-1.17	0.93	-2.10
TS03_2	12	2.5	-1.17	0.96	-2.13
TS04_1	8	3	-1.17	1.02	-2.19
TS04_2	12	3	-1.17	1.02	-2.19
TS05_1	8	2.5	0	0.96	-0.96
TS05_2	12	2.5	0	1.02	-1.02
TS06_1	8	3	0	0.99	-0.99
TS06_2	12	3	0	1.06	-1.06
TS07_1	8	2.5	1.17	1.09	0.08
TS07_2	12	2.5	1.17	1.09	0.08
TS08_1	8	3	1.17	1.18	-0.01
TS08_2	12	3	1.17	1.25	-0.08

After being reshaped by the action of waves, the equilibrium crest shape was not as horizontal as the initial crest shape. Instead, the crest took on a slightly curved form. However, the curve was observed to be very flat, and therefore it was assumed that its influence would be minimal. Furthermore, the width of the crest after attaining its equilibrium profile was noted to be practically unchanged.

The shape of the slope was visually inspected after tests. All of the tests had the same general equilibrium slope that resembled a flattened S-curve. It was decided to only inspect the slope visually, instead of measuring the profile precisely, due to the fact that the physical modelling incorporates the effect that the slope has on wave dynamics. The most important aspect was considered to be the reduction in crest elevation, which was measured carefully after tests. The general change in reef structure shape that was observed during testing is shown in figure 5.21.

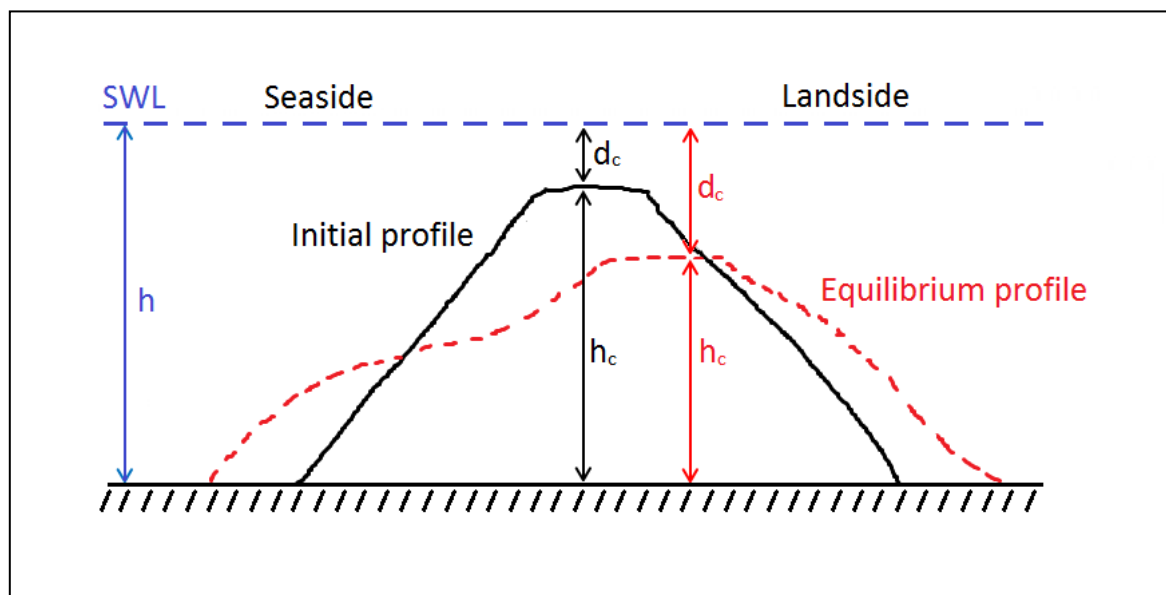


FIGURE 5.21: INITIAL AND EQUILIBRIUM PROFILE OF ROCK REEF

Another important aspect that was noted during tests was that the time it took for the reef to reach an equilibrium profile was very short, with the reshaping of the reef starting after about the first 5 to 15 waves. The reduction in the crest level occurred quickly, followed by the slope being shaped into its natural form. From observing the time required for the reef to reach an equilibrium profile, it was assumed that varied protection provided by the reef over time would have little effect on the results. The final crest elevation was reached within the first 5% of the test duration, which means that more than 95% of the waves travelled over a structure with an equilibrium profile.

5.5.4 BREAKWATER DAMAGE RESULTS

A damage analysis was performed for each of the tests in the series. The tests that were done with a reef structure installed were compared to the tests done with no submerged structure. In this way, the influence of the tandem breakwater on the damage level of the main breakwater could be observed.

In order to analyse the damage done to the main breakwater for each test, before and after photos of the structure were compared once the test was done. By using an image flicker technique, it was possible to easily determine where armour unit movement had occurred. This technique simply involves jumping back and forth between the two photos that were taken from the same orientation with the aid of a Wi-Fi enabled, mounted camera.

In this study, damage is defined as:

The movement of an armour unit over a distance that is equal to, or larger than, half of the height of the armour unit.

Some of the units that are defined as ‘damaged units’ by the above definition, may also be considered to be ‘extracted units’. The definition of an extracted unit in this study is as follows:

The movement of an armour unit that causes it to change its position in relation to its surrounding units.

What this means is that for a unit to be defined as an ‘extracted unit’, it has to be removed from its original spot and placed somewhere else on the breakwater where it is not surrounded by all of the same units that initially surrounded it.

In figure 5.22 an example of a test where two units were extracted is shown. The extraction was caused by a wave with a 12 s peak period and a 3 m significant wave height. Also, a submerged reef made from rock material and constructed to a crest level of -1.17 m CD (below-LAT), was present. During the test, the crest level reshaped to an elevation of -2.19 m CD.



FIGURE 5.22: BEFORE (LEFT) AND AFTER (RIGHT) IMAGES OF ARMOUR LAYER SHOWING EXTRACTED UNITS

The total number of units present on the model breakwater was 158. The damage that was encountered in each test is expressed as a percentage of the total number of units. The damage percentage for each of the tests is shown in table 5.9.

The highest percentage damage encountered in the test series was 7.6%, and is caused by the 8 s 3 m wave, with no submerged structure. However, none of the damaged units were extracted from its position. The damage for this test, TS02_1, is shown in figure 5.23. Refer to Appendix D for the entire set of damage analysis images.



FIGURE 5.23: BEFORE (LEFT) AND AFTER (RIGHT) IMAGES USED IN THE DAMAGE ANALYSIS

From the results in table 5.9 it can be seen that extractions only occurred in tests with 12 s waves. This is due to the fact that the 12 s wave has a greater wave length, which causes the waves to run higher up the armoured slope and come back down with a greater suction force.

In table 5.9 the effective crest elevations are given, which corresponds to the crest elevation measured after tests. In the cases where a rock reef structure was installed, the initial crest elevation is shown between brackets.

The reduction in damage on the main breakwater caused by the installation of the two types of reef structures can also be seen from the results. For a submerged reef constructed up to a crest elevation of -1.17 m CD (below-LAT), the maximum reduction of damage due to a rock and a geotube reef are 4.4% and 5.7% respectively. The crest elevations of + 0 m CD (LAT) and + 1.17 m CD (ML), for both types of structures, result in no damage occurring on the main breakwater.

Of course no damage is desirable, however, the cost of such a tandem breakwater has to be analysed for the specific area of intended implementation. This might not always be the most economical option. It depends on several factors, including the availability of material and expertise in the region, water depth at the structure, as well as the natural slope of the bathymetry.

Three of the tests listed in table 5.9 were tested for repeatability. These tests are TS02_2, TS03_2 and TS10_1. Apart from the test done in the main series, two additional tests were done for each of the abovementioned tests to investigate whether the results are reproducible. Table 5.10 shows the results of the repeatability of the damage tests. For the cases where a reduction in reef crest elevation was observed, the initial crest level is given between brackets.

TABLE 5.9: DAMAGE ENCOUNTERED IN TEST SERIES (AS BUILT CREST ELEVATION FOR ROCK REEFS SHOWN BETWEEN BRACKETS)

Test Name [-]	Tp [s]	Hm0 [m]	Submerged Structure [-]	Crest Elevation [m above CD]	# Displaced Units [-]	of which Extracted [-]	Damage [%]
TS01_1	8	2.5	No Structure	-	9	0	5.7
TS01_2	12	2.5	No Structure	-	7	0	4.4
TS02_1	8	3	No Structure	-	12	0	7.6
TS02_2	12	3	No Structure	-	9	1	5.7
TS03_1	8	2.5	Rock Structure	-2.10 (-1.17)	4	0	2.5
TS03_2	12	2.5	Rock Structure	-2.13 (-1.17)	2	0	1.3
TS04_1	8	3	Rock Structure	-2.19 (-1.17)	5	2	3.2
TS04_2	12	3	Rock Structure	-2.19 (-1.17)	5	0	3.2
TS05_1	8	2.5	Rock Structure	-0.96 (0)	0	0	0
TS05_2	12	2.5	Rock Structure	-1.02 (0)	0	0	0
TS06_1	8	3	Rock Structure	-0.99 (0)	0	0	0
TS06_2	12	3	Rock Structure	-1.06 (0)	0	0	0
TS07_1	8	2.5	Rock Structure	0.08 (1.17)	0	0	0
TS07_2	12	2.5	Rock Structure	0.08 (1.17)	0	0	0
TS08_1	8	3	Rock Structure	-0.01 (1.17)	0	0	0
TS08_2	12	3	Rock Structure	-0.08 (1.17)	0	0	0
TS09_1	8	3	Geotube Structure	-1.17	3	0	1.9
TS09_2	12	3	Geotube Structure	-1.17	1	0	0.6
TS10_1	8	3	Geotube Structure	0	0	0	0
TS10_2	12	3	Geotube Structure	0	0	0	0
TS11_1	8	3	Geotube Structure	1.17	0	0	0
TS11_2	12	3	Geotube Structure	1.17	0	0	0

TABLE 5.10: REPEATABILITY OF DAMAGE TESTS

Test Name [-]	Tp [s]	Hm0 [m]	Submerged Structure [-]	Crest Elevation [m above CD]	# Displaced Units [-]	of which Extracted [-]	Damage [%]
TS02_2A	12	3	No Structure	-	9	1	5.7
TS02_2B	12	3	No Structure	-	9	0	5.7
TS02_2C	12	3	No Structure	-	8	1	5.1
TS03_2A	12	2.5	Rock Structure	-2.13 (-1.17)	2	0	1.3
TS03_2B	12	2.5	Rock Structure	-2.19 (-1.17)	3	0	1.9
TS03_2C	12	2.5	Rock Structure	-2.16 (-1.17)	3	0	1.9
TS10_1A	8	3	Geotube Structure	0	0	0	0
TS10_1B	8	3	Geotube Structure	0	0	0	0
TS10_1C	8	3	Geotube Structure	0	0	0	0

To determine the effect that the reef has on the damage level of the main structure in a generic way, it is necessary to define a term called the relative reef submergence. It is represented by the following equation:

$$RRS = d_c/H_i$$

5-7

where

RRS	=	relative reef submergence
d_c	=	depth of crest submergence
H_i	=	incident significant wave height

The relative reef submergence can then be plotted against the damage reduction at the main structure, as seen in figure 5.24. Once the plots are made, the trends in the data are approximated with an exponential function. The reduction of the crest elevation of the rock reef structure, as described in section 5.5.3, was taken into account in the data plots. The graph represents the behaviour of a rubble mound structure that makes use of dolos units. Other types of armour units might behave differently.

The trends in the data plotted in figure 5.24 give some information regarding the performance of the two types of structures. As is expected, the higher the crest elevation of the reef, the less damage is present on the main structure, regardless of the type of reef that was used. When comparing the trends of the rock and geotube reefs, a slight deviation can be observed. For higher RRS values, a greater deviation between the two structures' performances seems to be present. This might be, in part, due to the fact that the geotube trendline is plotted from less data points than the rock trendline. Nevertheless, some deviation in the two trendlines is expected, and can be ascribed to the different permeabilities of the two types of structures. A structure with a higher permeability allows more wave energy to pass through it. On the other hand, the lower a structure's permeability, the more energy is reflected back into deep water. The effect that the permeability of the structure has on the damage reduction seems to be smaller when the crest elevation is closer to the water level.

The plotted data confirms that the most important factor related to the ability of a reef structure to prevent damage to a main rubble mound structure, is the crest elevation. This parameter has the biggest influence to the reef's performance.

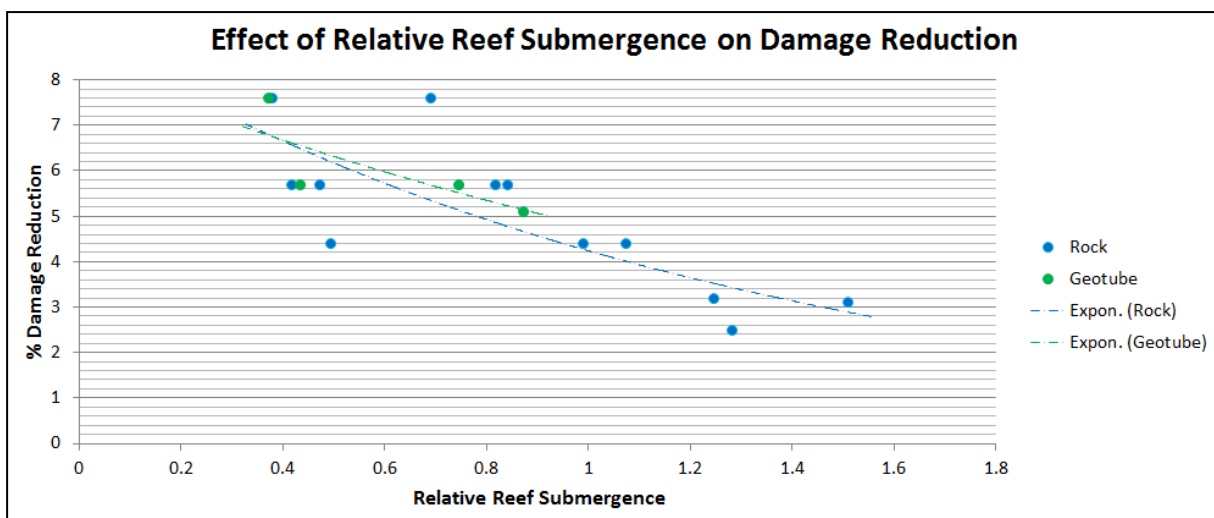


FIGURE 5.24: EFFECT OF RELATIVE REEF SUBMERGENCE ON DAMAGE REDUCTION

5.5.5 WAVE ATTENUATION RESULTS

Another parameter that was measured during testing is the reduction in significant wave height at probe 8 (P8), located between the reef and the main breakwater, caused by the installation of the reef breakwater.

The equation used to calculate the attenuation of the significant wave height at P8 is as follows:

$$\% \text{ Attenuation} = \frac{\text{Wave Height without reef} - \text{Wave Height with reef}}{\text{Wave Height without reef}} \times 100\% \quad 5-8$$

In other words, the significant wave height that was measured during a specific test with the reef structure in place is related to the baseline case where no reef structure was installed. The percentage of the reduction in significant wave height can be calculated from this.

Table 5.11 contains information regarding the attenuation of the significant wave heights caused by the reef structures of various crest elevations. For the cases with a rock reef structure installed, the shown crest elevation refers to the elevation after reduction due to the reshaping of the reef profile. The initial crest elevation as it was built is also given between brackets where it is applicable.

The first thing to notice about the data shown in table 5.11 is that the use of a geotube breakwater results in significantly more wave reduction. Tests TS04_1 and TS10_1 indicate a difference between reduction caused by the rock structure and reduction caused by the geotube structure to be as high as 14% for the 8 s wave and tests TS08_2 and TS11_2 shows wave reductions as high as 15% for the 12 s wave.

TABLE 5.11: WAVE ATTENUATION IN TEST SERIES (AS BUILT CREST ELEVATION FOR ROCK REEFS SHOWN BETWEEN BRACKETS)

Test Name [-]	Tp [s]	Hm0 [m]	Submerged Structure [-]	Crest Elevation [m above CD]	Hm0 at P8 [m]	Attenuation [%]
TS01_1	8	2.5	No Structure	-	2.9	N/A
TS01_2	12	2.5	No Structure	-	3.2	N/A
TS02_1	8	3.0	No Structure	-	3.5	N/A
TS02_2	12	3.0	No Structure	-	3.7	N/A
TS03_1	8	2.5	Rock Structure	-2.10 (-1.17)	2.2	22.0
TS03_2	12	2.5	Rock Structure	-2.13 (-1.17)	2.3	28.9
TS04_1	8	3.0	Rock Structure	-2.19 (-1.17)	2.6	23.8
TS04_2	12	3.0	Rock Structure	-2.19 (-1.17)	2.7	27.6
TS05_1	8	2.5	Rock Structure	-0.96 (0)	1.9	32.4
TS05_2	12	2.5	Rock Structure	-1.02 (0)	2.1	35.6
TS06_1	8	3.0	Rock Structure	-0.99 (0)	2.3	34.0
TS06_2	12	3.0	Rock Structure	-1.06 (0)	2.5	33.7
TS07_1	8	2.5	Rock Structure	0.08 (1.17)	1.7	39.7
TS07_2	12	2.5	Rock Structure	0.08 (1.17)	1.9	41.8
TS08_1	8	3.0	Rock Structure	-0.01 (1.17)	2.0	41.5
TS08_2	12	3.0	Rock Structure	-0.08 (1.17)	2.3	39.2
TS09_1	8	3.0	Geotube Structure	-1.17	2.1	37.9
TS09_2	12	3.0	Geotube Structure	-1.17	2.3	38.6
TS10_1	8	3.0	Geotube Structure	0	2.0	41.9
TS10_2	12	3.0	Geotube Structure	0	2.2	42.5
TS11_1	8	3.0	Geotube Structure	1.17	1.6	53.7
TS11_2	12	3.0	Geotube Structure	1.17	1.7	54.4

The same tests that were investigated for repeatability in terms of damage were used to test repeatability in terms of wave attenuation. The results are shown in table 5.12. For the cases where a rock reef is in place, the initial crest elevation is given between brackets next to the reduced crest elevation.

TABLE 5.12: REPEATABILITY OF WAVE ATTENUATION TESTS

Test Name [-]	T _p [s]	H _{m0} [m]	Submerged Structure [-]	Crest Elevation [m above CD]	H _{m0} at P8 [m]	Attenuation [%]
TS02_2A	12	3	No Structure	-	3.7	N/A
TS02_2B	12	3	No Structure	-	3.7	N/A
TS02_2C	12	3	No Structure	-	3.7	N/A
TS03_2A	12	2.5	Rock Structure	-2.13 (-1.17)	2.3	28.9
TS03_2B	12	2.5	Rock Structure	-2.19 (-1.17)	2.4	26.2
TS03_2C	12	2.5	Rock Structure	-2.16 (-1.17)	2.3	27.7
TS10_1A	8	3	Geotube Structure	0	2.0	41.9
TS10_1B	8	3	Geotube Structure	0	2.0	41.5
TS10_1C	8	3	Geotube Structure	0	2.0	42.0

The concept of relative wave attenuation distance is introduced hereafter. It is based on a non-dimensional parameter that was used by Roa & Shirlal (2003) in a similar study, and is described by the following equation:

$$WAD = \frac{X}{T_p \sqrt{g d_c}} \quad 5-9$$

where

WAD	=	relative wave attenuation distance
X	=	distance between breakwaters
T _p	=	peak period
g	=	gravitational acceleration
d _c	=	depth of crest submergence

The inclusion of the depth of crest submergence in the abovementioned equation shows how the various crest elevations of the reef affect the significant wave heights that reach the rubble mound structure. Throughout this investigation, the distance between breakwaters (X) was kept constant. The prototype distance between the main rubble mound breakwater and the submerged reef breakwater was 50 m. Therefore, equation 5-9 becomes:

$$WAD = \frac{50}{T_p \sqrt{g d_c}} \quad 5-10$$

Even though the distance between breakwaters was kept constant in this study, the dimensionless nature of the relative wave attenuation distance also aims to provide some indication of what influence the distance between breakwaters may have on the wave attenuation.

Take, for example the relative wave attenuation value of 1.845. This value can be achieved by using values of $X = 50$ m, $d_c = 1.17$ m, and $T_p = 8$ s. The value can also be achieved by values of $X = 85$ m, $d_c = 1.50$ m, and $T_p = 12$ s. It is not possible to say that these two cases would provide the same amount of wave attenuation, but an assumption can be made based on the observed trend. It makes sense to assume that there might be a reef structure that is built further away from the main breakwater, at a lower crest elevation, that provides the same amount of wave protection as a structure close to the breakwater, with a higher crest elevation. For the structure built further away, some of the wave energy will be dissipated by the reef (although presumably less than the energy dissipation caused by the higher reef), after which further natural energy dissipation takes place until the waves reach the main breakwater. Because the lower structure is further away than the higher one, there is more time for natural energy dissipation between breakwaters. Battjes & Janssen (1978) noted that the attenuation process of waves breaking over submerged reefs may extend as much as 40 times the significant wave height behind the initial point of breaking. As mentioned before, the influence of the distance between breakwaters cannot be determined with complete certainty in this way, but reasonable assumptions can be made. The topic is subject to further investigation.

In figure 5.25 the relative wave attenuation distance is plotted against the percentage of significant wave height attenuation for both the rock and the geotube structure. The plots take into account the reduction in crest elevation observed during the tests involving rock reefs. It seems as though a linear relationship exists between the two parameters.

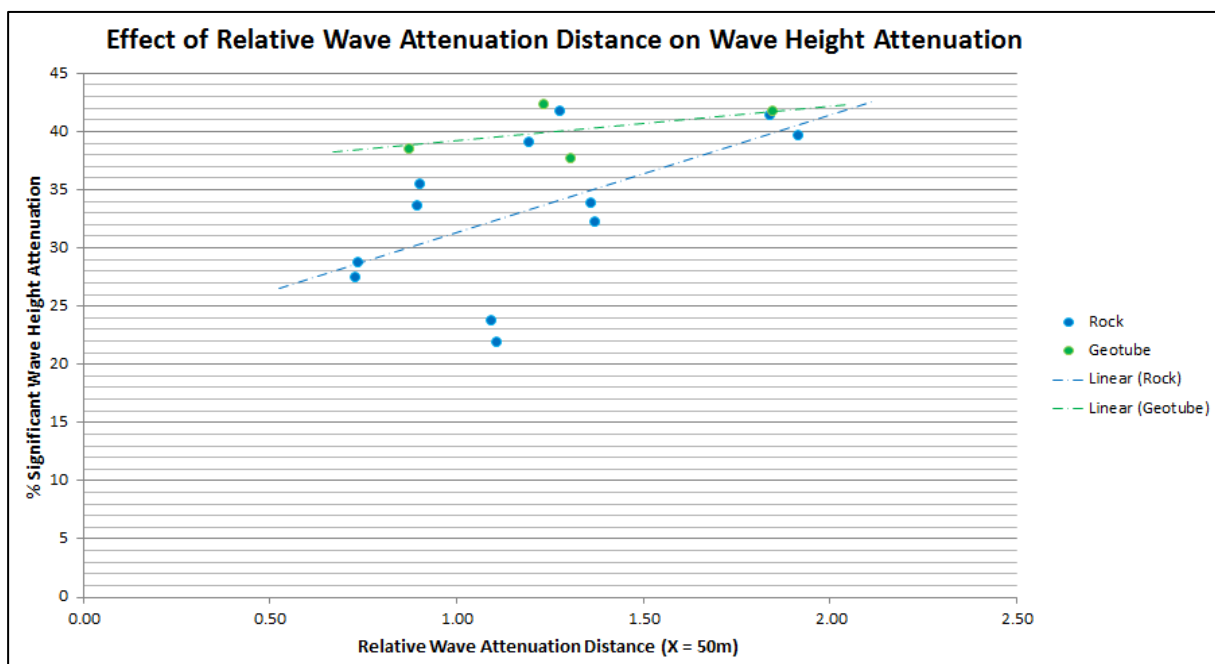


FIGURE 5.25: EFFECT OF RELATIVE WAVE ATTENUATION DISTANCE ON WAVE HEIGHT ATTENUATION

The trend in the above graph shows that for an increase in the depth of crest submergence, the percentage wave height attenuation decreases. In other words, if two reefs with different crest elevations are exposed to the same conditions, the one with the higher crest elevation (lower depth of crest submergence) will result in smaller waves reaching the main breakwater. This is as expected.

The difference in steepness of the two trendlines should be noted. The geotube trendline is much flatter than the rock trendline. This means that the protection provided by the geotube structure does not vary as much with different crest elevations as the protection provided by the rock structure does.

As the relative wave attenuation distance becomes smaller (the depth of crest submergence becomes larger), the deviation between the trends observed for the different structure types become larger. This is similar to what was seen in the plots relating relative reef submergence to damage reduction at the main breakwater. The difference between the trendlines can be ascribed to the difference in permeability for rock and geotube reefs. It seems as though the effectiveness of the two structure types are similar when crest elevations approach SWL. The lower the crest elevation of the reef, the more effective the geotube reef is in relation to the rock reef.

Cox & Clark (1992) as well as Roa & Shirlal (2003) have performed similar tests on tandem breakwater systems. Although, the WAD values that they used are mostly lower than the values used in this investigation, with some overlapping. Figure 5.26 shows the data plots of all three sets of data.

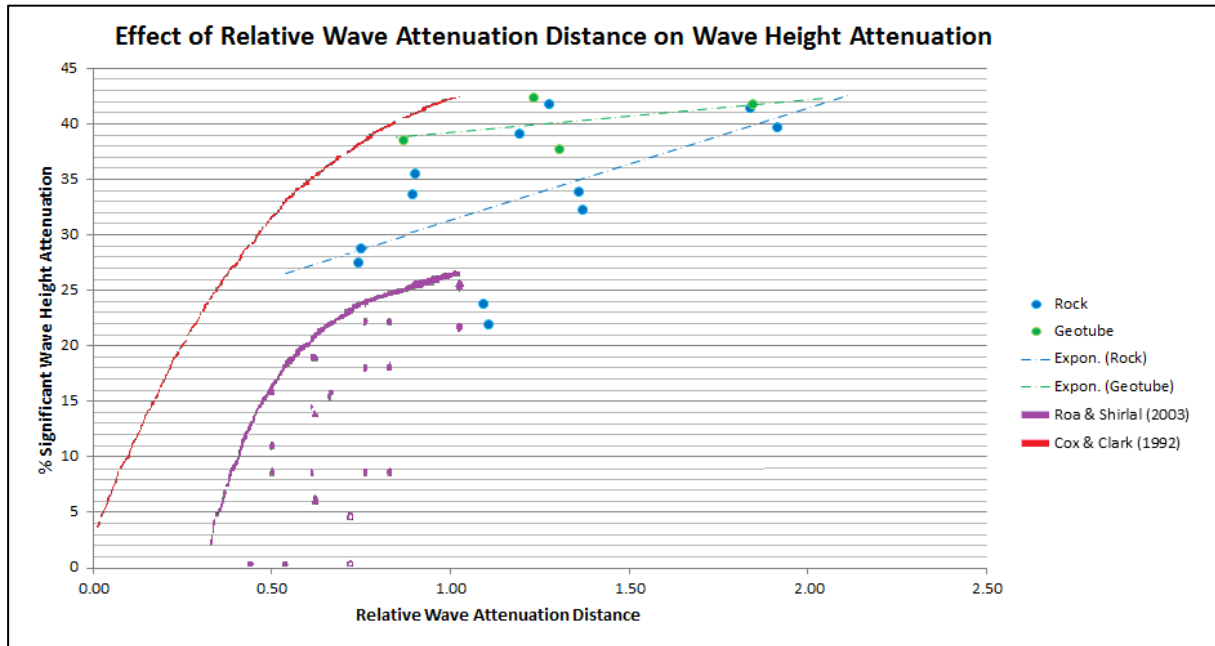


FIGURE 5.26: COMPARISON OF PRESENT AND PREVIOUS STUDIES WITH REGARDS TO WAVE ATTENUATION (COX & CLARK, 1992; ROA & SHIRLAL, 2003)

A comparison of the trends in the data sets indicated that the data collected in the present study conforms well to the data gathered by Cox & Clark (1992) and Roa & Shirlal (2003). When considering the entire data set, it seems as though the trend in the data collected in this study can be approached with an exponential function that flattens out to take on a linear form for the higher values of WAD that were considered in this study.

Another useful comparison to make with the gathered data is that of the measured and predicted transmission coefficients, K_t . The model proposed by Tomasicchio & d'Alessandro (2013), as discussed in section 2.5 of this report, is used to predict the transmission coefficients for the different reef configurations. These values can then be compared to the measured values during the test series. Table 5.13 shows the measured and predicted values of the transmission coefficients for the various tests, while figure 5.27 presents a visual comparison. For the rock reefs, the crest height reduction is taken into account. The effective crest elevation is shown, with the initial crest elevation given between brackets.

TABLE 5.13: MEASURED VS PREDICTED TRANSMISSION COEFFICIENTS (AS BUILT CREST ELEVATION FOR ROCK REEFS SHOWN BETWEEN BRACKETS)

Test Name [-]	Peak Period [s]	H _s [m]	Submerged Structure [-]	Crest Elevation [m above CD]	Measured K _t [-]	Predicted K _t [-]
TS03_1	8	2.5	Rock Structure	-2.10 (-1.17)	0.78	0.74
TS03_2	12	2.5	Rock Structure	-2.13 (-1.17)	0.71	0.86
TS04_1	8	3	Rock Structure	-2.19 (-1.17)	0.76	0.71
TS04_2	12	3	Rock Structure	-2.19 (-1.17)	0.72	0.83
TS05_1	8	2.5	Rock Structure	-0.96 (0)	0.68	0.64
TS05_2	12	2.5	Rock Structure	-1.02 (0)	0.65	0.77
TS06_1	8	3	Rock Structure	-0.99 (0)	0.66	0.61
TS06_2	12	3	Rock Structure	-1.06 (0)	0.66	0.74
TS07_1	8	2.5	Rock Structure	0.08 (1.17)	0.60	0.59
TS07_2	12	2.5	Rock Structure	0.08 (1.17)	0.58	0.71
TS08_1	8	3	Rock Structure	-0.01 (1.17)	0.59	0.58
TS08_2	12	3	Rock Structure	-0.08 (1.17)	0.61	0.71
TS09_1	8	3	Geotube Structure	-1.17	0.62	0.68
TS09_2	12	3	Geotube Structure	-1.17	0.61	0.80
TS10_1	8	3	Geotube Structure	0	0.58	0.58
TS10_2	12	3	Geotube Structure	0	0.58	0.70
TS11_1	8	3	Geotube Structure	1.17	0.46	0.52
TS11_2	12	3	Geotube Structure	1.17	0.46	0.63

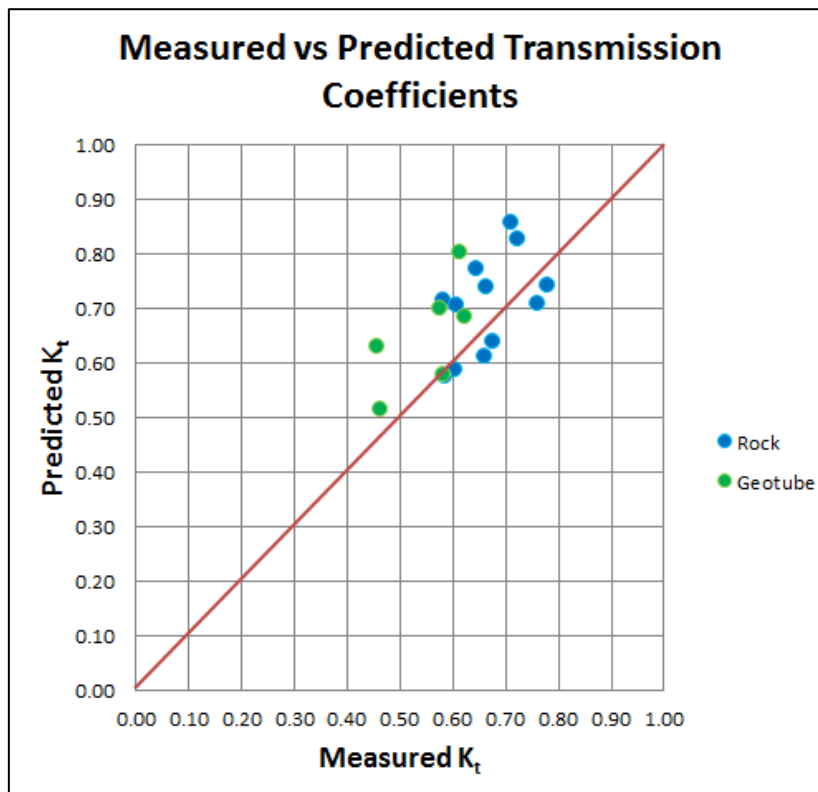


FIGURE 5.27: MEASURED VS PREDICTED TRANSMISSION COEFFICIENTS

From the information in table 5.13 and figure 5.27, it is evident that the proposed model estimates the transmission coefficient reasonably well, with some slight over-predictions. The red line in figure 5.27 shows the ideal case where the measured and predicted values are equal. The data points are clustered tightly around the line. The information given in table 5.13 shows that the transmission coefficient is predicted almost exactly for the tests that were done with an 8 s wave. On the other hand, for the 12 s waves, the model over-predicts the transmission coefficient. The over-prediction is as high as 23% for the rock reef structure and as high as 37% for the geotube structure.

In future studies it is recommended to investigate the influence of the tranquillity zone length on the performance of a tandem breakwater system. Different distances should be considered in order to determine when the optimal amount of sheltering is achieved. If the submerged structure is too far away, its effectiveness is reduced. Say for argument's sake a reef is constructed 1 km away from the main breakwater. In such a case it is highly probable that refracted waves will enter the tranquillity zone from the sides, without ever passing over the reef. Furthermore, if the reef is constructed too close to the main structure, wave oscillation might occur between the two structures, which could possibly result in more damage, instead of less.

5.6 APPLICATION OF RESULTS

This section seeks to provide guidance on how the findings in the physical model study can be applied in future applications of tandem breakwater systems. The results described in section 5.5.5 are applied to the case of Mossel Bay, in order to assess the consequences of the implementation of a tandem breakwater at the site. A basic assessment of the associated costs is also included.

5.6.1 REDUCTION OF DESIGN WAVE HEIGHT

The presence of a submerged reef structure results in smaller waves reaching the main breakwater, as described in section 5.5.5. The amount of wave height reduction is primarily related to the crest elevation of the reef, but also depends on the distance between breakwaters, peak period of the incident waves, and the type of reef structure (rock or geotube).

In this study the design significant wave height for the rubble mound breakwater, as indicated in section 5.3.2, was as follows: 2.6 m for a 16 s wave, 2.7 m for an 8 s and 12 s wave, and 2.8 m for a 10 s and 14 s wave. The maximum of the three significant wave heights was used in the design formula of Burcharth & Liu (1992), as the formulation does not include the peak period. The percentage wave attenuation that can be expected due to the inclusion of a reef does however depend on the peak period, amongst other things. Therefore, the wave attenuation for each of the peak periods has to be calculated first, after which the maximum significant wave height can be selected as input to the design formula.

The amount of reduction to the design wave height is also related to the crest height and type of the reef structure. During the reduction analysis, the same crest elevations as tested in the physical model were used. A comparison is also made between the use of a rock reef and a geotube reef. Table 5.14 and table 5.15 show the predicted design wave height reduction as a result of a rock reef and a geotube reef respectively. The reduction in the significant wave height of the design wave was determined with the aid of figure 5.25 in section 5.5.5. For the design wave conditions of the original design shown in section 5.3.2, the water level was located at 2 m above CD. The same water level was used in reduction analysis of the design wave height. The water level influences the depth of crest submergence of the reef structures.

TABLE 5.14: REDUCED DESIGN HS FOR ROCK REEF

Initial Design Wave [m,s]	Crest Elevation [m above CD]	WAD [-]	Percentage Attenuation [%]	Reduced Design Wave [m,s]
2.7m 8s	-1.17	1.12	31.9	1.8
	0	1.41	34.8	1.8
	1.17	2.19	44.1	1.5
2.8m 10s	-1.17	0.90	29.8	2.0
	0	1.13	32.0	1.9
	1.17	1.75	38.6	1.7
2.7m 12s	-1.17	0.75	28.5	1.9
	0	0.94	30.2	1.9
	1.17	1.46	35.4	1.7
2.8m 14s	-1.17	0.64	27.6	2.0
	0	0.81	29.0	2.0
	1.17	1.25	33.2	1.9
2.6 16s	-1.17	0.56	27.0	1.9
	0	0.71	28.2	1.9
	1.17	1.10	31.7	1.8

TABLE 5.15: REDUCED DESIGN HS FOR GEOTUBE REEF

Initial Design Wave [m,s]	Crest Elevation [m above CD]	WAD [-]	Percentage Attenuation [%]	Reduced Design Wave [m,s]
2.7m 8s	-1.17	1.12	39.6	1.6
	0	1.41	40.4	1.6
	1.17	2.19	42.8	1.5
2.8m 10s	-1.17	0.90	38.9	1.7
	0	1.13	39.6	1.7
	1.17	1.75	41.5	1.6
2.7m 12s	-1.17	0.75	38.5	1.7
	0	0.94	39.1	1.6
	1.17	1.46	40.6	1.6
2.8m 14s	-1.17	0.64	38.2	1.7
	0	0.81	38.7	1.7
	1.17	1.25	40.0	1.7
2.6 16s	-1.17	0.56	38.0	1.6
	0	0.71	38.4	1.6
	1.17	1.10	39.5	1.6

The maximum design significant wave height at the rubble mound breakwater, associated with the implementation of a rock reef for various crest elevations, can be found from table 5.14. A rock reef crest elevation of +1.17 m CD requires the main breakwater to be designed for a significant wave height of 1.9 m. Rock reefs with a crest elevation of 0 m CD and -1.17 m CD both result in a design significant wave height of 2 m. Similarly, from table 5.15, a geotube reef constructed up to crest elevations of +1.17 m, 0 m and -1.17m CD, results in a design H_s of 1.6 m, 1.7 m and 1.7 m respectively.

5.6.2 REDUCTION OF ARMOUR UNIT SIZE

The reduced design significant wave heights associated with the different crest elevations of the submerged reef, as described in the previous section, can be inserted into the design formula of Burcharth & Liu (1992) for dolos armour units, to find the consequent reduction in armour unit size.

From this point on, only the crest elevations of -1.17 m and +1.17 m CD are considered, as the reduction in design wave height provided by the submerged reefs with a crest elevation of -1.17 m and 0 m CD, are the same.

In section 5.3.3, the required armour unit mass on the rubble mound breakwater was determined to be 5.64 tons if no submerged breakwater is in place. To compare the scenarios with and without a reef, all the parameters are kept the same in the dolos design formula, except the design significant wave height.

For a rock reef constructed up to the lower crest elevation (-1.17 m CD), the required armour unit mass is 2.06 ton, while the higher crest elevation (+1.17 m CD) results in 1.76 ton dolos units being required. The corresponding values for the use of a geotube reef are 1.26 ton for the lower crest elevation and 1.05 ton for the higher crest elevation.

5.6.3 COST OF CONSTRUCTION

In this section, the costs associated with various tandem breakwater options to be applied at Mossel Bay are investigated. Note that the cost of the different aspects of construction discussed in this section is subject to change. The presented values are based on current information supplied by one marine construction company. It might be that other companies determine the cost of construction to be slightly different. Over time, the values presented in this section are sure to change. However, it is assumed that the construction costs of the various options will remain the same relative to one another.

The first tandem breakwater implementation option is that of a permanent tandem breakwater system, constructed from scratch. This resembles the scenario where a new breakwater is planned for an area resembling Mossel Bay, and different alternatives are weighed up against each other. The length of the planned breakwater is 200 m, approximately that of the old portion of the current Mossel Bay breakwater.

From the findings in section 5.6.2 it was decided to construct the reef up to a crest elevation of -1.17 m CD, as this seems to be the most cost effective reef structure. This reef requires 2.06 ton dolos units for the primary armour layer. The cost of such a tandem breakwater system has to be compared with the cost of a single rubble mound structure. The armour layer for a rubble mound structure without a reef requires 5.64 ton dolos units on its primary armour layer, as found in section 5.3.3. The armour units used for the port side slope (secondary armour layer) of the breakwater is half of the size of the primary units, i.e. 2.82 tons for the single rubble mound breakwater.

The total cost of construction for a single rubble mound structure, without a reef in place, is estimated to be R76 254 730 (Stefanutti Stocks Marine, 2015). A breakdown of the cost for each of the layers of the rubble mound structure is given in table 5.16. The costs of the various rock layers include the bulk material cost, transport cost and placing cost at the construction site. In the cost estimation, it was assumed that all required rock sizes could be supplied by a quarry in the Mossel Bay area. The total cost includes an additional 35% to allow for preliminary and general (P&G) costs, i.e. overheads, administration and personnel costs, etc.

The breakdown of the cost per unit of the primary 5.64 ton dolos armour units is shown in table 5.17. The cost includes the supply of concrete, formwork, the use of the crane in the precast yard, delivery to construction site, and the use of the crane to place units at the construction site. The precast yard is also assumed to be in the Mossel Bay area. The cost of the secondary dolos armour units is similar, with different rates being applied to crane usage, because units are lighter.

TABLE 5.16: TOTAL COST OF SINGLE RUBBLE MOUND BREAKWATER (STEFANUTTI STOCKS MARINE, 2015)

Layer	Quantity	Unit	Rate [R/unit]	Cost [R]
Core Layer	23200	m ³	633.45	14 696 040.00
Under Layer	6800	m ³	903.00	6 140 400.00
Toe Layer	1426	m ³	913.74	1 302 993.24
Primary Armour Layer	1395	no.	8 791.56	12 260 706.15
Secondary Armour Layer	2214	no.	4 966.05	10 993 747.56
Concrete Topping	2000	m ³	4 847.51	9 695 016.00
Overtopping Wall	288	m ³	4 847.51	1 396 082.30
Total (including 35% for P&G)				76 254 730.09

The construction of the rubble mound structure involves dumping of the bulk rock material with dumper trucks, after which bulk handling equipment such as bulldozers, wheel loaders, and excavators are used to ensure the different layers of the rubble mound structure are formed correctly. The dolos units of the primary and secondary armour layers are placed with the aid of wire-rope cranes. The concrete topping and overtopping wall are cast on site.

TABLE 5.17: COST PER 5.64 TON DOLOS UNIT (STEFANUTTI STOCKS MARINE, 2015)

Production Aspect	Measure	Rate [R/unit]
Supply of Concrete	per unit	5 226.40
Formwork	per unit	717.05
Crane in Precast Yard	per unit	1 893.94
Delivery to Site	per unit	480.68
Crane at Construction Site	per unit	473.48
Total / unit		8 791.56

Next, the cost of the tandem breakwater system with a rock reef constructed to an effective elevation of -1.17 m CD has to be considered. This time a rubble mound breakwater has to be constructed, as well as a reef breakwater. Table 5.18 shows the total cost associated with the construction of the tandem breakwater system, while table 5.19 gives a breakdown of the costs involved in the reef construction.

TABLE 5.18: COST OF TANDEM BREAKWATER SYSTEM (STEFANUTTI STOCKS MARINE, 2015)

Layer	Quantity	Unit	Rate [R/unit]	Cost [R]
Core Layer	23200	m ³	633.45	14 696 040.00
Under Layer	6800	m ³	903.00	6 140 400.00
Toe Layer	1426	m ³	913.74	1 302 993.24
Primary Armour Layer	2729	no.	4 176.46	11 398 937.53
Secondary Armour Layer	3640	m ³	913.74	3 326 013.60
Concrete Topping	2000	m ³	4 847.51	9 695 016.00
Overtopping Wall	288	m ³	4 847.51	1 396 082.30
Reef	21371	m ³	594.51	12 705 213.76
Total (including 35% for P&G)				81 891 940.18

The main rubble mound structure makes use of 2.06 ton dolos units as primary armour layer. Consequently, the secondary armour layer requires units with a mass of approximately 1 ton. It was decided that the required units for the secondary armour layer are light enough that rock material can be used as opposed to dolos units.

The construction of the reef structure is done with the use of a barge with the capacity of 1000 tons. Rock material is loaded onto the barge, after which a pusher boat is used to position the barge at the location of reef construction. From the barge, a pay loader is used to dump the material off of the side of the barge. The MOB/DEMOB of the barge, as referred to in table 5.19, is the costs associated with the preparation of the barge for use, as well as the costs associated with the demobilisation after construction.

TABLE 5.19: COST OF REEF PER CUBIC METRE (STEFANUTTI STOCKS MARINE, 2015)

Production Aspect	Daily Rate [R]	Rate per m³ [R]
MOB/DEMOB of Barge	-	70.19
Barge Hire (with crew)	55000	110.00
Pusher Boat	8455	16.91
Pay loader	2909	5.82
Supervisor	2364	4.73
Total / m³		207.65

From the abovementioned information it can be seen that the cost of the construction of a conventional rubble mound breakwater from scratch is approximately R5.6 million cheaper than the construction of a tandem breakwater system. Thus, a permanent tandem breakwater system to be constructed at Mossel Bay will not be the most cost effective option.

Now, a different option will be considered with regards to a tandem breakwater system in Mossel Bay. The new portion of the Mossel Bay breakwater has recently been replaced with 7.5 ton dolos units due to excessive damage to the original 6 ton units. In the event that the damage extends to the old portion, which still has 6 ton dolos units as armour layer, an option might be to replace the units with 7.5 ton units in a similar manner to the new portion. This method of rehabilitation has been discussed in section 2.4. The cost of replacing the 6 ton armour units with 7.5 ton units is estimated to be R12 845 815 (Stefanutti Stocks Marine, 2015).

Another option is to leave the 6 ton units on the main breakwater and rather construct a rock reef structure a distance in front of the main breakwater. The cost of the reef alone can be seen in table 5.18 to be approximately R12 705 214 (Stefanutti Stocks Marine, 2015).

It can be seen that the reef structure used to provide wave protection to the main structure, provides a cost benefit of approximately R140 601. Therefore, if excessive damage occurs at the old portion of the Mossel Bay breakwater in the future, it might be worth investigating the use of a reef to for a tandem breakwater, instead of replacing the armour units.

5.7 SUMMARY

A physical model was constructed, containing a rubble mound breakwater that resembles the Mossel Bay breakwater. During the testing of the model, the influence of a tandem breakwater's submerged reef crest elevation on the damage level of the main rubble mound structure, as well as the influence of the reef crest elevation on the wave attenuation was investigated. These tests were done for both rock and geotube reefs. The reduction in crest elevation of the dynamically stable rock reefs, due to the action of waves, was taken into account for all tests.

From the test results, two generic graphs, containing non-dimensional parameters, were constructed. These graphs are valid for armour layers made of dolos units. Other types of armour units might not behave in the same manner found in this investigation. The one shows the relationship between the relative reef submergence and the damage level at the main structure, and the other shows the relationship between the relative wave attenuation distance and the wave attenuation. Furthermore, the trend in the data plots of the relative wave attenuation distance versus the percentage wave attenuation was found to be comparable to previous studies conducted by Cox & Clark (1992) and Roa & Shirlal (2003).

The wave transmission coefficient as predicted by the model of Tomasicchio & d'Alessandro (2013) was found to be very accurate for the tests done with 8 s waves and reasonably accurate for the tests done with 12 s waves.

CHAPTER 6: FINDINGS, CONCLUSIONS AND RECOMMENDATIONS

6.1 PHYSICAL MODEL FINDINGS

From the physical model test results, it is evident that the presence of a reef structure, located at a distance of 50 m in front of a rubble mound structure, significantly affects the wave conditions that reach the main structure. When comparing significant wave heights measured at a prototype distance of 20 m in front of the main breakwater, a reduction of as high as 42% can be observed for a reef structure made from rocks. This corresponds to the case where the reef has an initial crest height located at ML, and reduces to a crest elevation located at approximately LAT. The equivalent case for the geotube reef results in a wave height reduction of 54%. In this case, no reduction in crest elevation was observed.

In all the cases, the geotube reef breakwater provides a greater wave reduction compared to the rock reef breakwater. However, it should be noted that the geotube reef's stability was not considered in this study. Therefore, during testing the geotubes were fixed together to form a single unit. This was not the case for the rock reef, which was designed to be dynamically stable. Thus, the rock reef was allowed to deform to a gentler slope, which means that the crest height at the end of the test was not the same as at the beginning. During the interpretation of the results, the reduction in crest elevation of rock reef structure was taken into account. This means that comparisons could be made for structures that effectively have the same crest elevation. It was found that, relative to the rock reef, the geotube reef will provide a greater wave height reduction due to its lower permeability.

Although only one spacing between breakwaters was tested, (50 m prototype), an attempt is made to provide more generic results by using a relative (non-dimensional) parameter called the relative wave attenuation distance. The wave attenuation distance describes the relationship between the reef's crest elevation and the tranquillity zone length. It was found that an increase in the depth of crest submergence, results in a decrease in wave height attenuation. From the trend in the data it is expected that a greater distance between reef and rubble mound breakwaters would result in a higher percentage of wave attenuation, although more tranquillity zone lengths will have to be tested before this can be said for sure.

When considering the influence of the reef structure's crest height on the damage level of the main breakwater, another dimensionless parameter was used. This is the relative reef submergence, which describes the ratio of the depth of crest submergence to the incident significant wave height. It was found that as the relative reef submergence increases, so does the percentage damage level on the main breakwater. Also, it was evident that the geotubes provide better protection against incoming waves than the rock reef. Note that this investigation only considered dolos armour units. Other types of armour units might behave differently.

The damage caused by different wave conditions was also compared. As was expected, the 3 m wave causes more damage than the 2.5 m wave. This is simply due to the 3 m wave having more energy. The comparison between the wave periods is not as straightforward. It was found that the 8 s wave causes more units to displace without being extracted from its location relative to its neighbouring units. However, the 12 s wave causes more units to be extracted than the 8 s wave. In fact, the 8 s wave caused no extractions during testing. The 12 s wave has a larger wave length, which results in a greater uprush and downrush on the structure slope. This enables the 12 s wave to lift the armour unit from its initial position.

6.2 CONCLUSIONS

For either type of reef breakwater (rock or geotube), the crest elevation has a direct influence on the performance of the tandem breakwater as a whole. The smaller the crest submergence, the more wave energy it will dissipate, resulting in less damage on the main breakwater.

The crest level also significantly influences the percentage of wave attenuation that can be observed. A higher crest level results in more wave attenuation. Although it is not a strict conclusion, as only one tranquillity zone length was tested, it is hypothesised that as the length of the tandem breakwater's tranquillity zone increases, so does the wave attenuation. This is said with reference to a 2D situation, but it should be noted that the tranquillity zone length cannot be increased indefinitely in reality, because 3D effects such as refraction and diffraction will also play a role.

The relationship between the relative wave attenuation distance and the percentage wave attenuation, as shown in figure 5.26, can be used to aid future designs that investigate the use of a tandem breakwater system. Once the design wave for the intended site is determined, the abovementioned figure can be used to calculate the wave attenuation that would be caused by the inclusion of a submerged reef. The design wave condition can be altered accordingly to produce the effective design wave condition for which the main breakwater can be designed.

In the physical model setup the geotubes produce better results than the rock in terms of wave attenuation and damage level. Geotubes are also more environmentally friendly with regards to transport emissions. However, the application thereof in the South African context is not likely at present, due to the lack of operational experience and available equipment.

6.3 RECOMMENDATIONS ON FUTURE WORK

Due to the sheer number of parameters involved in the study of the tandem breakwater, it was not possible to vary all of them in this investigation. In order to provide better design guidelines for the implementation of such a system, more variables have to be altered during testing. It is recommended that a greater variety of peak periods be tested, with specific emphasis on longer periods, as they were found to cause greater damage of individual armour units.

This study was designed in such a way that similarities could be drawn between the tested model and the Mossel Bay breakwater. In other words the main breakwater that made up the tandem system was in fact designed to be able to function on its own. The problem with this is that the inclusion of a reef structure means that the breakwater combination that was tested is over-designed. That is also the reason why the crest elevations of LAT and ML reduced the damage level on the main breakwater to zero. As a future study, it is recommended that a tandem breakwater be tested that makes use of a reduced armour unit size as a result of the wave attenuation caused by various crest elevations.

The rock reef structure that was used during the study was designed to be dynamically stable, which meant that the structure's slope was allowed to be altered until an equilibrium profile was reached. Although irregular waves were used to describe the wave conditions in the flume, the majority of the wave energy corresponded to either an 8 s or a 12 s period, depending on which test was performed. This is a somewhat idealised situation in which the tandem breakwater is tested. The reef will reach an equilibrium profile based on the peak period tested at the time. In reality, however, the reef will be exposed to different peak periods that occur after one another. Each of these periods will want to shape the reef into a different equilibrium profile. This means that the reduction in crest levels will in actuality be more than that which was tested in the flume. Therefore, it is recommended that the influence of an alternating peak period on crest level reduction of a dynamically stable reef be tested.

BIBLIOGRAPHY

- Allsop, N. (2009). *Coastal Defense and Harbour Structures (Supporting Notes)*. Wallingford, United Kingdom: HR Wallingford.
- Bancroft, S. (1999). *Performance Monitoring of the Cable Station Artificial Surfing Reef*. Perth, Australia: University of Western Australia.
- Battjes, J., & Janssen, J. (1978). Energy Loss and Set-up due to Breaking of Random Waves. *Proceedings of the 16th International Conference on Coastal Engineering* (pp. 569 - 587). Hamburg: ASCE.
- Bezuijen, A., & Pilarczyk, K. (2012). Geosynthetics in Hydraulic and Coastal Engineering: Filters, Revetments and Sand Filled Structures. *5th European Geosynthetics Congress* (pp. 65 - 80). Valencia, Spain: International Geosynthetics Society.
- Bezuijen, A., Oung, O., Klein Breteler, M., Berendsen, E., & Pilarczyk, K. (2002). Model Tests on Geocontainers, Placing Accuracy and Geotechnical Aspects. *Seventh International Conference on Geosynthetics*. Nice (France): Balkema.
- Bezuijen, M., de Groot, M., Klein Breteler, M., & Berendsen, E. (2004). Placing Accuracy and Stability of Geocontainers. *Third European Geosynthetics Conference* (pp. 1 - 6). Munich, Germany: EUROGEO.
- Brorsen, M., Burcharth, H., & Larsen, T. (1974). Stability of Dolos Slopes. *Proceedings of the 14th International Conference on Coastal Engineering*. Copenhagen: ICCE.
- Bruun, P. (1979). *Common Reasons for Damage or Breakdown of Mound Breakwaters*. Amsterdam: Elsevier Scientific Publishing Company.
- BSI. (2003). *Maritime Structures - Part 1: Code of Practice for General Criteria*. London, United Kingdom: British Standards Institute.
- Buccino, M., & Calabrese, M. (2007). Conceptual Approach for Prediction of Wave Transmission at Low-crested Breakwaters. *Journal of Waterway, Port, Coastal and Ocean Engineering*, 113(3), 213 - 224.
- Burcharth, H., & Brejnegaard-Nielsen, T. (1986). The Influence of Waist Thickness of Dolosse on the Hydraulic Stability of Dolos Armour. *Proceedings of the 20th International Conference on Coastal Engineering*. Taipei: ICCE.
- Burcharth, H., & Liu, Z. (1992). Design of Dolos Armour Units. *Proceedings of the 23rd International Coastal Engineering Conference* (pp. 1053 - 1066). American Society of Civil Engineers.
- CFOO. (2001). *Guidelines: Storm Surge Early Warning System*. Centre for Observational Oceanography. Cape Town: Centre for Observational Oceanography.
- CIRIA CUR CETMEF. (2007). *The Rock Manual. The Use of Rock in Hydraulic Engineering (2nd Edition)*. London: CIRIA.
- Constable, A. (1824). *Supplement to the Fourth, Fifth and Sixth Editions of the Encyclopaedia Britannica, Volume Second*. Edinburgh: Encyclopaedia Britannica Inc.
- Cox, J. (1992). Reef Breakwater Design for Lake Michigan Marina. *Marina Technology: Proceedings of the Second International Conference* (pp. 507 - 516). Southampton: Thomas Telford.

- Cox, J., & Clark, G. (1992). Design Development of a Tandem Breakwater System for Hammond Indiana. *Proceedings of Conference on Coastal Structures and Breakwaters* (pp. 111 - 121). London: Thomas Telford Publishers.
- CSIR. (2008). *Khalifa Port and Industrial Zone: Physical Modelling of Harbour Agitation and Moored Ship Dynamics*. Stellenbosch: CSIR.
- CSIR. (2013). *Procedure for Determining Absorption Gain of Wavemaker Paddle in Hydraulic Flume*. Stellenbosch: CSIR.
- CSIR. (2014). Mossel Bay Bathymetric Data. Stellenbosch: CSIR.
- CSIR. (2014). Mossel Bay Waverider Data (2007/05/22 - 2014/05/31). Stellenbosch: CSIR.
- d'Angremond, K., van der Meer, J., & de Jong, R. (1996). Wave Transmission at Low-crested Breakwaters. *Proceedings of 25th International Conference of Coastal Engineering* (pp. 2418 - 2426). Orlando: ASCE.
- DHI. (2004). *Mike 21 SW - Spectral Waves FM User Guide*. DHI. Horsholm: DHI.
- DHI. (2009). *Mike by DHI Extreme Value Analysis User Guide*. DHI. Horsholm: DHI.
- Fowler, J., Thomas, P., Stephens, C., Santiago, M., & de Bruin, P. (2002). *Amwaj Islands Constructed with Geotubes, Bahrain, CEDA Conference*. Denver, USA: CEDA.
- Goda, Y., & Ahrens, J. (2008). New Formulation of Wave Transmission Over and Through Low-crested Structures. *Proceedings of the 31st International Conference of Coastal Engineering* (pp. 3530 - 3541). Hamburg, Germany: World Scientific.
- Google Inc. (2014). Retrieved from Google Maps: www.google.co.za/maps
- Hirose, N., Watanuki, A., & Saito, M. (2002). New Type Units for Artificial Reef Development of Eco-friendly Artificial Reefs and the Effectiveness Thereof. *Proceedings of 30th International Navigation Congress*. Sydney, Australia: PIANC.
- Holtzhausen, A., & Zwamborn, J. (1990). Stability of Dolosse with Different Waist Thickness for Irregular Waves. *Proceedings of the 22nd International Conference on Coastal Engineering*. Delft: ICCE.
- Hornsey, W. (2009). *Geotextiles in Specialist Marine Applications: An Australia Perspective Over 32 Years*. Gold Coast, Australia: Geofabrics Australasia.
- HR Wallingford. (2014). *Equipment Brochure: Wavemakers for Physical Models*. Retrieved from HR Wallingford: www.hrwallingford.com/_literature_109943/Brochure_-_Wavemakers
- Hughes, S. A. (1995). *Physical Models and Laboratory Techniques in Coastal Engineering*. Singapore: World Scientific.
- Jackson, L., & Hornsey, W. (2003). *An Artificial Reef to Protect Surfers Paradise Beach, Developing & Implementing the Science*. Molendinar, Australia: Soil Filters Australia Pty Ltd.
- Johnson, C. (2009). *The Effect of Artificial Reef Configuration on Wave Breaking Intensity Relating to Recreational Surfing Conditions*. Stellenbosch: Stellenbosch University.
- Juhl, J. (1995). *Berm Breakwater Structures*. Horsholm: DHI.
- Juhl, J., & Jensen, O. (1995). Features of Berm Breakwaters and Practical Experience. *International Conference on Coastal and Port Engineering in Developing Countries* (pp. 1307 - 1320). Rio de Janeiro: COPEDEC.

- Kriel, H. (2012). *Hydraulic Stability of Multi-layered Sand-filled Geotextile Tube Breakwaters Under Wave Attack*. Stellenbosch: Stellenbosch University.
- Liebenberg, N. (2013). *Conceptual Layout and Breakwater Design For a FSRU LNG Import Terminal Off the Coast of Mossel Bay, South Africa*. Stellenbosch: Stellenbosch University.
- Makris, C. V., & Memos, C. D. (2007). Wave Transmission over Submerged Breakwaters: Performance of Formulae and Models. *Proceedings of the Seventeenth (2007) International Offshore and Polar Engineering Conference* (pp. 2613 - 2620). Lisbon, Portugal: The International Society of Offshore and Polar Engineers.
- Miles, M. (1989). The GEDAP Data Analysis Software Package. *Proceedings of IAHR Workshop on Instrumentation for Hydraulics Laboratories* (pp. 325 - 339). Burlington: National Water Research Institute.
- Mitra, A. (2013, May - June). Geotextiles and its Application in Coastal Protection and Off-shore Engineering. *Journal of the Textile Association*, 5 - 11.
- Mol, A., Nieuwenhuys, E., & Groeneveld, R. (1984). Rehabilitation Methods for Damaged Breakwaters. *Proceedings of the 19th International Coastal Engineering Conference*. 3, pp. 2467 - 2486. Houston, Texas: ASCE.
- Oh, Y., & Shin, E. (2006). Using Submerged Geotextile Tubes in the Protection of the E. Korean Shore. *Coastal Engineering*, 53, 879 - 895.
- Phelp, D. (2005). Monitoring and Maintenance of Coastal Structures. *International Conference on Coastlines, Structures and Breakwaters* (pp. 508 - 519). London: Thomas Telford Publishing.
- PIANC. (2003). *State-of-the-Art of Designing and Constructing Berm Breakwaters*. Brussels: PIANC.
- PIANC. (2011). *Report no. 113: The Application of Geosynthetics in Waterfront Areas*. Brussels: PIANC.
- Pilarczyk, K. (2003). Alternative Systems for Coastal Protection: An Overview. *International Conference on Estuaries and Coasts* (pp. 409 - 419). Hangzhou, China: IRTCES.
- Rendle, E., & Davidson, M. (2012). An Evaluation of the Physical Impact and Structural Integrity of a Geotextile Surf Reef. *Proceedings of 33rd Conference on Coastal Engineering*. 4, pp. 3047 - 3060. Santander, Spain: Coastal Engineering Research Council.
- Roa, S., & Shirlal, K. (2003). Laboratory Studies on the Stability of Tandem Breakwater. *ISH Journal of Hydraulic Engineering*, 9(1), 36 - 45.
- Rossouw, M., & Theron, A. K. (2009). *Investigating the Potential Climate Change Impacts on Maritime Operations Around the Southern African Coast*. Stellenbosch: CSIR.
- Ryan, L., & Prehn, J. (2001). Monitoring of Rubble Mound Breakwater Systems. *Proceedings of the 12th Biennial Coastal Zone Conference* (pp. 1 - 4). Cleveland: U.S. National Oceanic and Atmospheric Administration.
- SANHO. (2013). *South African Tide Tables*.
- Seabrook, S., & Hall, K. (1998). Wave Transmission at Submerged Rubble Mound Breakwaters. *Proceedings of the 26th International Conference on Coastal Engineering* (pp. 2000 - 2013). Copenhagen, Denmark: ASCE.
- Seelig, W. (1980). *Two Dimensional Tests of Wave Transmission and Reflection Characteristics of Laboratory Breakwaters*. Washington D.C.: U.S. Army Corps of Engineers.

- Stefanutti Stocks Marine. (2015). *Rubble Mound Breakwater vs Tandem Breakwater Cost Estimation*. Cape Town: Stefanutti Stocks Marine.
- Tanimoto, K., & Goda, Y. (1992). Historical Development of Breakwater Structures in the World. *Proceedings of Conference on Coastal Structures and Breakwaters* (pp. 193 - 206). London: Thomas Telford Publishers.
- TenCate. (2011). *Geotube Debris Shield: Permeable Impact Resistant Composite Technology - Product Description Sheet*. Commerce: TenCate Geosynthetics North America.
- Theron, F. (2014, July 28). Installation of Geotube and Rock Reefs. (E. Thesnaar, Interviewer) Cape Town.
- TNPA. (1967). *Mossel Bay Breakwater Repair*.
- TNPA. (2014). *Mossel Bay Water Depths*.
- TNPA. (2014). *Port of Mossel Bay Current Layout*.
- Tomasicchio, G., & D'Alessandro, F. (2013). Wave Energy Transmission Through and Over Low Crested Breakwaters. *Journal of Coastal Research*(Special Issue No 65), 398 - 403.
- Tulsi, K., & Phelp, D. (2009). Monitoring and Maintenance of Breakwaters which Protect Port Entrances. *Proceedings of the 28th South African Transport Conference (SATC 2009)* (pp. 317 - 325). Pretoria: Document Transformation Technologies cc.
- U.S. Army Corps of Engineers. (1993). *Engineering Design Guidance for Detached Breakwaters as Shoreline Stabilization Structures*. Washington D.C.: U.S. Army Corps of Engineers.
- U.S. Army Corps of Engineers. (2002). *Coastal Engineering Manual (CEM)*. Washington, D.C.: U.S. Army Corps of Engineers.
- van der Meer, J. (1987). Stability of Breakwater Armour Layers - Design Formulae. *Coastal Engineering*, 11, 219 - 239.
- van der Meer, J. (1990). *Data on Wave Transmission due to Overtopping*. Delft: Delft Hydraulics.
- van der Meer, J. (1993). *Conceptual Design of Rubble Mound Breakwaters*. Delft: Delft Hydraulics.
- van der Meer, J., & Daemen, I. (1994). Stability and Wave Transmission at Low Crested Rubble Mound Structures. *Journal of Waterway, Port, Coastal and Ocean Engineering*, 1, 1 - 19.
- van der Meer, J., Briganti, R., Zanuttigh, B., & Wang, B. (2005). Wave Transmission and Reflection at Low-crested Structures: Design Formulae, Oblique Wave Attack and Spectral Change. *Coastal Engineering*, 52, 915 - 929.
- van Gent, M. (1993). *Berm Breakwaters - Hydrodynamics, Forces and Profile-development*. TU Delft. Delft: TU Delft.
- van Gent, M. (1996). Numerical Modelling of Wave Interaction with Dynamically Stable Structures. *Proceedings of the 25th International Conference of Coastal Engineering* (pp. 1930 - 1943). Orlando: ASCE.
- van Gent, M. R. (2013). Rock Stability of Rubble Mound Breakwaters with a Berm. *Coastal Engineering*, 78, 35 - 45.
- van Zijl, P., Vlasblom, W., de Gijt, J., Broos, E., & de Boer, J. (2006, March). Feasibility Study of the Continuous Geotube. *Terra et Aqua*, pp. 19 - 24.

- Vernon-Harcourt, L. F. (1885). *Harbours and Docks: Physical Features, History, Construction Equipment, and Maintenance*. Oxford: Oxford (Clarendon Press).
- Weerakoon, S., Mocke, G., Smit, F., & Al Zahed, K. (2003). Cost Effective Coastal Protection Works Using Sand Filled Geotextile Containers. *Sixth International Conference on Coastal and Port Engineering in Developing Countries (COPEDEC VI)*. Colombo: Lanka Hydraulic Institute.
- Zwamborn, J., Bosman, D., & Moes, J. (1980). Dolosse: Past, Present, Future? *Proceedings of the 17th International Conference on Coastal Engineering*. Sydney: ASCE.

APPENDICES

APPENDIX A: PROCEDURE FOR DETERMINING MASS DENSITY OF MODEL ARMOUR UNITS

Here follows a description of the procedure that was used to determine the mass density of the model armour units.

Acquiring a container of sufficient size was the first step in the procedure. The container had to be large enough that one of the model dolos units can be placed inside of it and be completely submerged under water. The container that was used had relatively coarse calibration markings on the side, i.e. increments of 100 ml.

The next step is to fill the container with enough water to completely submerge the dolos once it is placed inside. In this case, the container was filled up to the 1000 ml mark, as can be seen in figure A.1.

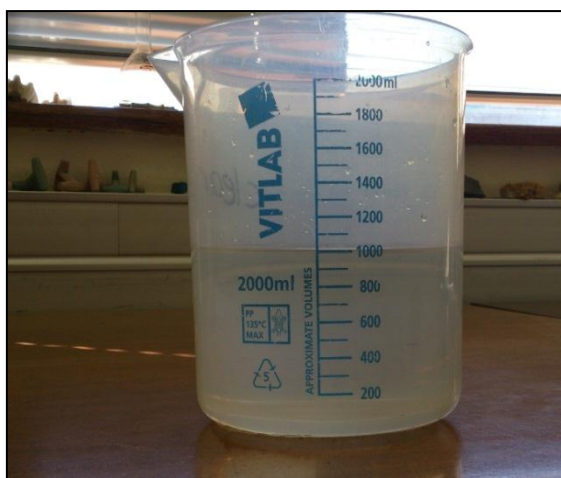


FIGURE A.1: WATER CONTAINER FILLED UP TO 1000ML

After filling the container, a mark was made on one of the sides that do not have writing on it, to indicate the initial water level. Thereafter, the dolos unit was placed in the container, and a rise in water level could be observed. It is indicated in figure A.2.

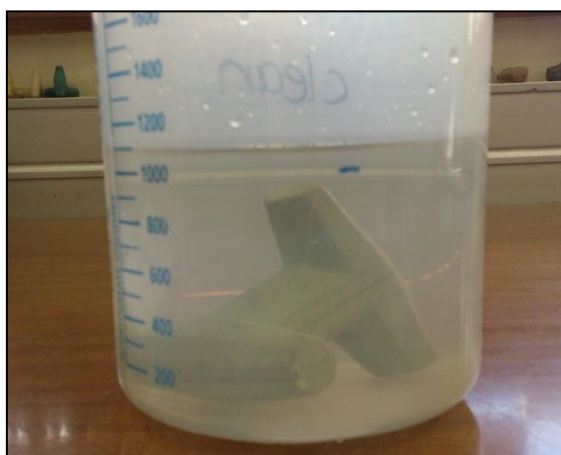


FIGURE A.2: DOLOS UNIT PLACED INSIDE CONTAINER WITH INITIAL WATER LEVEL MARK

Another mark was made on the side of the container to show where the water level is with the dolos unit placed inside. The dolos was then removed, while making sure that practically all of the water on the unit drips back into the container.

A quick check was done to ensure that the water level had indeed dropped back to its initial level.

An additional water measuring container, calibrated in increments of 10 ml, was filled up to 1000 ml. Then, water was carefully poured from the finer calibrated measuring container into the first container until the water level reached the second mark that was made on the container, which indicates the water level in the container when the dolos is placed inside. Figure A.3 shows the filling process and the two water level marks.



FIGURE A.3: FILLING OF CONTAINER UP TO SECOND WATER LEVEL MARK

The water that remained in the second container after filling the first container up to the appropriate mark was subtracted from the initial amount of water that was in the second container. This gives the volume of water that was added to the first container in order to raise the water level to the top mark, which is in fact the volume of the dolos unit.

In an attempt to eliminate any inaccuracies due to human error, the process was repeated five times. The delta volume that was calculated for each of the five iterations is given in table A.1.

TABLE A.1: DELTA VOLUME MEASUREMENTS

Iteration [-]	Initial Volume [ml]	Delta Volume [ml]
1	1000	80
2	1000	81
3	1000	80
4	1000	83
5	1000	84
mean		81.6

The mean value of the delta volumes that were measured is 81.6 ml. This value was used in further calculations regarding the mass density of the armour unit.

The next step was to determine the mass of the model armour unit. This is done quite simply with the aid of a scale. It can be seen in the following figure that the dolos has a mass of 197.7 g.



FIGURE A.4: MEASURING THE MASS OF DOLOS UNIT

After determining the mass of the unit, all the necessary information to calculate the mass density is known. The mass density of an object is the ratio of its mass to its volume. We know that the dolos has a mass of 197.7 g and a volume of 81.6 ml (or $81.6 \times 10^{-6} \text{ m}^3$). The resulting mass density is then calculated to be 2422 kg/m^3 .

APPENDIX B: ROCK GRADING CURVES

The rock grading curves for the various layers of rock used in the physical model are presented here. The mass indicated in these figures shows the prototype value.

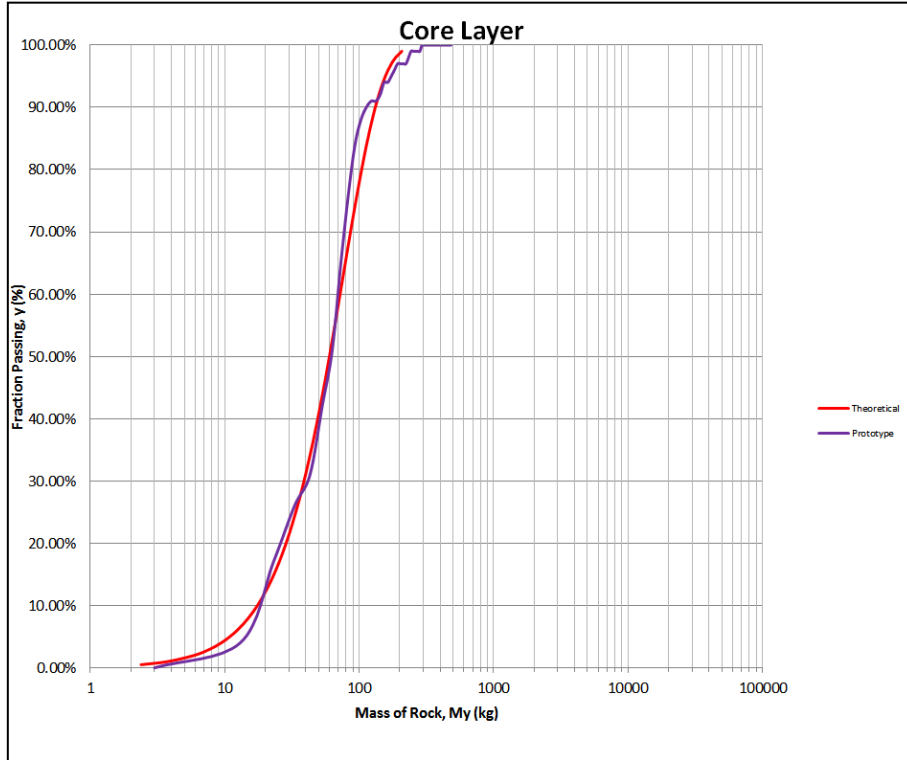


FIGURE B.1: CORE LAYER ROCK GRADING CURVE

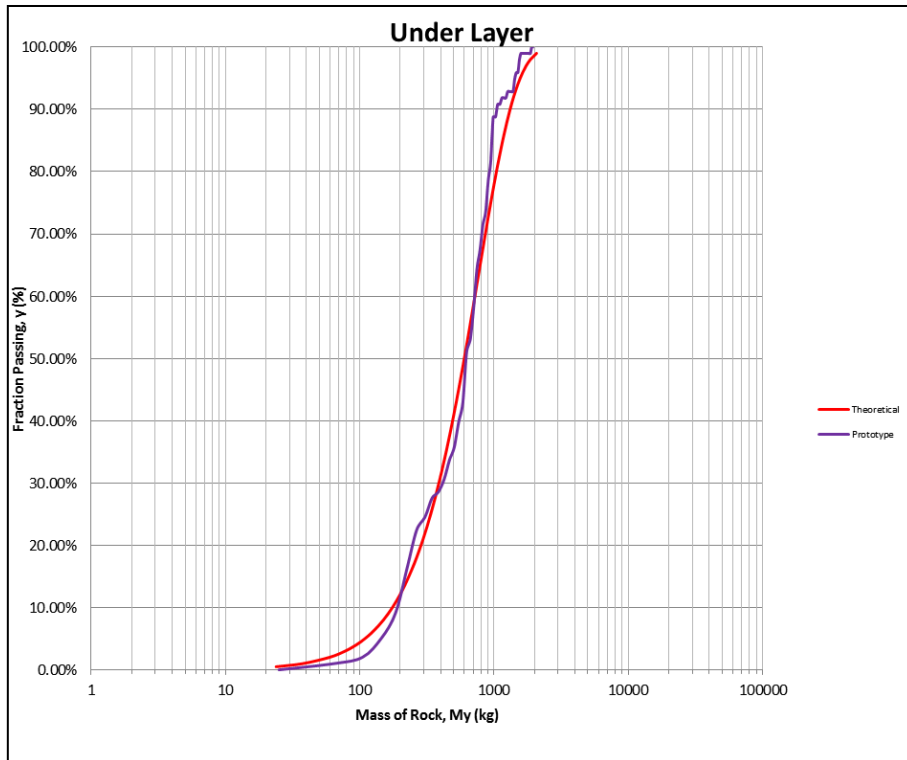


FIGURE B.2: UNDER LAYER ROCK GRADING CURVE

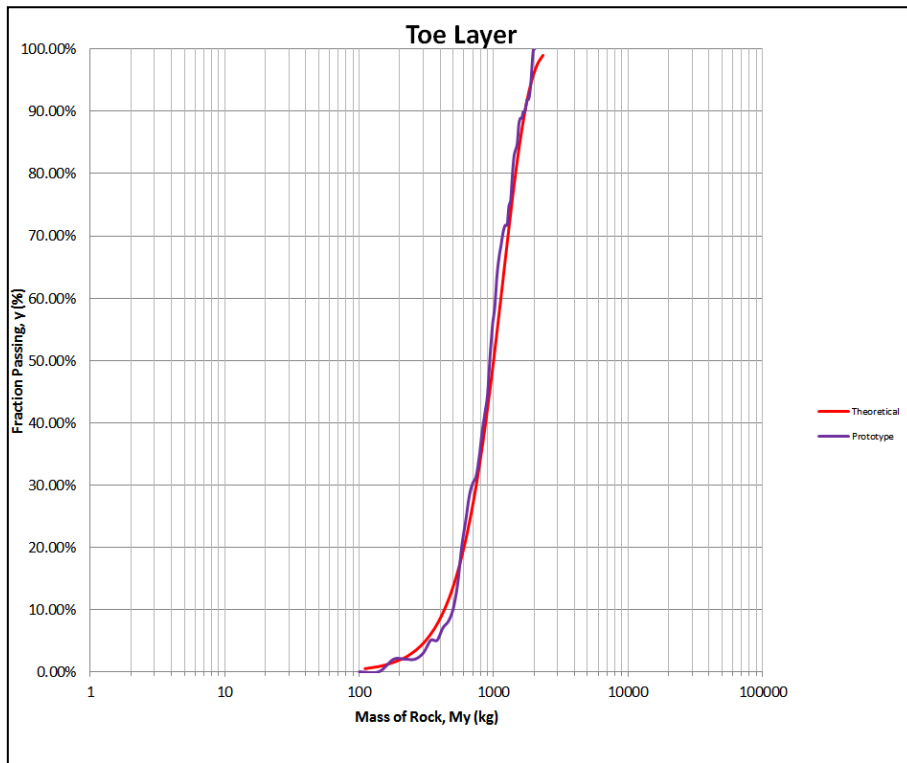


FIGURE B.3: TOE LAYER ROCK GRADING CURVE

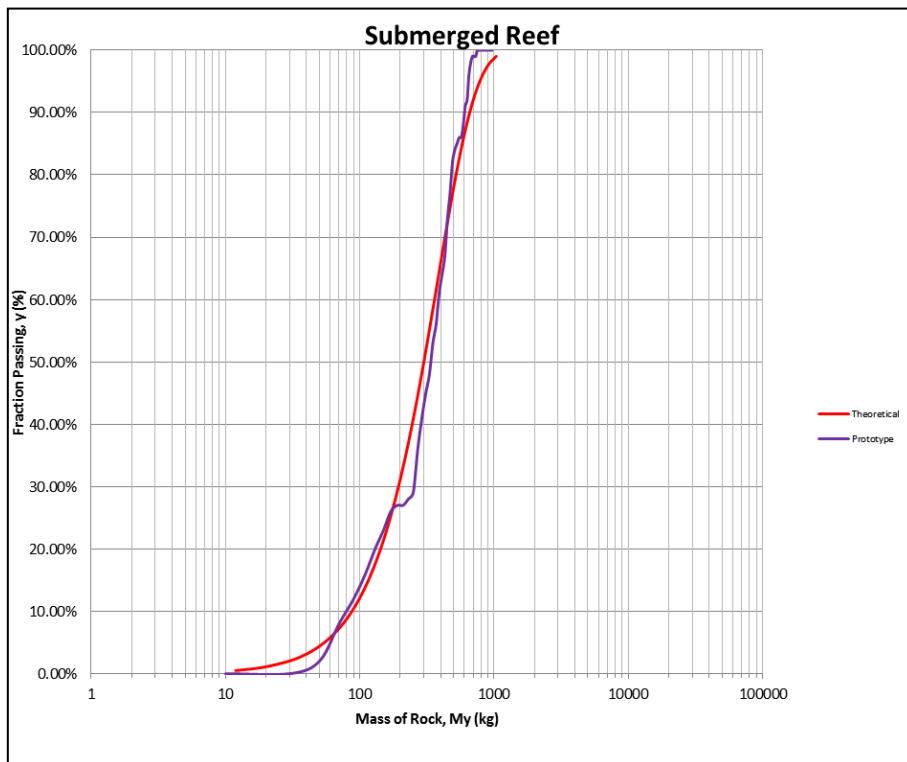


FIGURE B.4: SUBMERGED ROCK REEF GRADING CURVE

APPENDIX C: PHYSICAL MODEL CONSTRUCTION

Model size templates of the cross section of the main breakwater were cut from hardboard and placed in the flume to indicate where the various layers of the breakwater are. The placing of the cross-sectional templates inside the flume was done with the aid of a dumpy level, which allowed the placing accuracy of the templates to be within 1 mm in model scale, or 32 mm in prototype. Figure C.1 shows the cutting process of the templates as well as the core layer as constructed in the flume with the cross-sectional templates installed.



FIGURE C.1: CUTTING OF BREAKWATER TEMPLATES (LEFT) AND CORE CONSTRUCTION (RIGHT)

Before initial construction of the model it was anticipated that the model would have to be reconstructed a few times during the test series due to the fact that damage on the breakwater was to be tested. If the same model breakwater is used for the whole test series, then it might be that more damage is found in the tests just after construction than tests at the end of the test series, when the model breakwater could have reached equilibrium in terms of damage. However, if the breakwater is only reconstructed with similar rock, rather than the exact same rock, then one runs the risk of obtaining results that are not comparable. So, each iteration of breakwater construction had to be done using the same material as the previous construction. This solution gives rise to its own set of difficulties. Having to sort out the different rock layers before reconstructing is a laborious and time consuming activity. Distinguishing between the toe layer and the other layers is not too difficult to perform by eye, but the same cannot be said for the distinction between the under layer and core layer. The solution was to spraypaint the entire under layer rock set. This way, the rock can be separated with significantly less effort if necessary. Figure C.2 shows the spraypainted rock before and after being placed on the model. On the right, the toe layer as constructed is shown as well.



FIGURE C.2: SPRAYPAINTED UNDER LAYER BEFORE (LEFT) AND AFTER (RIGHT) INSTALLATION

For the armour layer, the model dolos units were placed in a double layer with a spacing of 80 mm in both directions. The orientation of the units were kept random, to try and simulate how it would look in prototype. After the armour units were placed, they were spraypainted in three different colour bands, which would aid in the damage analysis process later on. In figure C.3 the spraypainted armour layer can be seen.



FIGURE C.3: SPRAYPAINTED ARMOUR LAYER

The overtopping wall that was used came from a previous project and is made up of a number of Perspex pieces that are glued together. In order to install the wall and prevent it from moving when exposed to the wave attack during a test, it was bolted to a piece of angle iron, which could then be weighed down in place. The edges of the wall, where it meets the side of the concrete flume, were also sealed so that no energy would pass around the wall. The overtopping wall and angle iron setup is shown in figure C.4.



FIGURE C.4: OVERTOPPING WALL ATTACHED TO ANGLE IRON

The construction of the rock reef structure did not involve the use of templates as the main rubble mound breakwater did. Instead, the three reef profiles were drawn on the inside of the flume walls. The crest positions were determined with the aid of a dumpy level to provide sufficient accuracy. The profiles being drawn on the flume walls, as well as the construction of the reef are shown in figure C.5.



FIGURE C.5: SUBMERGED REEF CROSS-SECTION PROFILES (LEFT) AND CONSTRUCTION (RIGHT)

APPENDIX D: DAMAGE ANALYSIS IMAGES

Before and after photographs of the physical model tests are presented here.

TS01_1: 2.5m – 8s (No Structure)



FIGURE D.1: BEFORE (LEFT) AND AFTER (RIGHT) IMAGES OF TEST TS01_1

TS01_2: 2.5m – 12s (No Structure)



FIGURE D.2: BEFORE (LEFT) AND AFTER (RIGHT) IMAGES OF TEST TS01_2

TS02_1: 3m – 8s (No Structure)



FIGURE D.3: BEFORE (LEFT) AND AFTER (RIGHT) IMAGES OF TEST TS02_1

TS02_2: 3m – 12s (No Structure)



FIGURE D.4: BEFORE (LEFT) AND AFTER (RIGHT) IMAGES OF TEST TS02_2

TS03_1: 2.5m – 8s (Below-LAT Rock Structure)



FIGURE D.5: BEFORE (LEFT) AND AFTER (RIGHT) IMAGES OF TEST TS03_1

TS03_2: 2.5m – 12s (Below-LAT Rock Structure)



FIGURE D.6: BEFORE (LEFT) AND AFTER (RIGHT) IMAGES OF TEST TS03_2

TS04_1: 3m – 8s (Below-LAT Rock Structure)



FIGURE D.7: BEFORE (LEFT) AND AFTER (RIGHT) IMAGES OF TEST TS04_1

TS04_2: 3m – 12s (Below-LAT Rock Structure)



FIGURE D.8: BEFORE (LEFT) AND AFTER (RIGHT) IMAGES OF TEST TS04_2

TS05_1: 2.5m – 8s (LAT Rock Structure)



FIGURE D.9: BEFORE (LEFT) AND AFTER (RIGHT) IMAGES OF TEST TS05_1

TS05_2: 2.5 – 12s (LAT Rock Structure)



FIGURE D.10: BEFORE (LEFT) AND AFTER (RIGHT) IMAGES OF TEST TS05_2

TS06_1: 3m – 8s (LAT Rock Structure)



FIGURE D.11: BEFORE (LEFT) AND AFTER (RIGHT) IMAGES OF TEST TS06_1

TS06_2: 3m – 12s (LAT Rock Structure)



FIGURE D.12: BEFORE (LEFT) AND AFTER (RIGHT) IMAGES OF TEST TS06_2

TS07_1: 2.5m – 8s (ML Rock Structure)



FIGURE D.13: BEFORE (LEFT) AND AFTER (RIGHT) IMAGES OF TEST TS07_1

TS07_2: 2.5m – 12s (ML Rock Structure)



FIGURE D.14: BEFORE (LEFT) AND AFTER (RIGHT) IMAGES OF TEST TS07_2

TS08_1: 3m – 8s (ML Rock Structure)



FIGURE D.15: BEFORE (LEFT) AND AFTER (RIGHT) IMAGES OF TEST TS08_1

TS08_2: 3m – 12s (ML Rock Structure)



FIGURE D.16: BEFORE (LEFT) AND AFTER (RIGHT) IMAGES OF TEST TS08_2

TS09_1: 3m – 8s (Below-LAT Geotube Structure)



FIGURE D.17: BEFORE (LEFT) AND AFTER (RIGHT) IMAGES OF TEST TS09_1

TS09_2: 3m – 12 s (Below-LAT Geotube Structure)



FIGURE D.18: BEFORE (LEFT) AND AFTER (RIGHT) IMAGES OF TEST TS09_2

TS10_1: 3m – 8s (LAT Geotube Structure)



FIGURE D.19: BEFORE (LEFT) AND AFTER (RIGHT) IMAGES OF TEST TS10_1

TS10_2: 3m – 12s (LAT Geotube Structure)



FIGURE D.20: BEFORE (LEFT) AND AFTER (RIGHT) IMAGES OF TEST TS10_2

TS11_1: 3m – 8s (ML Geotube Structure)



FIGURE D.21: BEFORE (LEFT) AND AFTER (RIGHT) IMAGES OF TEST TS11_1

TS11_2: 3m – 12s (ML Geotube Structure)



FIGURE D.22: BEFORE (LEFT) AND AFTER (RIGHT) IMAGES OF TEST TS11_2